# Chemistry of Iron Sulfides

David Rickard*,† and George W. Luther III‡

[1]School of Earth, Ocean and Planetary Sciences, Cardiff University, Cardiff CF103YE, Wales, U.K., and College of Marine and Earth Studies, University of Delaware, Lewes, Delaware 19958

Received June 22, 2006

## Contents



* To whom correspondence should be addressed. Phone: +44(0)-2920874284. Fax: +44(0)2920874326. E-mail: rickard@cardiff.ac.uk.
† Cardiff University.
‡ University of Delaware.

## 1. Introduction

The iron sulfides constitute a diverse group of solids and dissolved complexes many of which play key roles in marine systems. The group is particularly complex in the lower temperature environments characterizing much of the Earth's surface where a number of metastable phases become significant in biogeochemical processes. At least seven different solids consisting only of iron and sulfur are known to occur naturally at these temperatures (Table 1). At higher temperatures, the chemistry appears to be simpler although this may be partly a consequence of the experimental difficulties of probing supercritical and often salt-rich aqueous fluids. Certainly the number of iron sulfide products, as seen in the geological record, appears more restricted. This review is concerned with the complex lower temperature chemistry of iron sulfides, which is more directly related to marine systems. There is an interface between this lower temperature regime and the higher temperature regime in the deep ocean hydrothermal vents, where iron sulfide fluids debouch into the deep oceans at temperatures up to 400 °C. We dip our feet tentatively into these waters at the end of this review.

Iron sulfides are an intrinsic and essential part of the global biogeochemical sulfur cycle. They provide evidence for the processes and fluxes occurring in the sulfur cycle. Indeed, because of the relationship between the sulfur cycle and the other key cycles of carbon and oxygen, this evidence is an essential part of what we understand about how the Earth works. The evolution of the global biogeochemical sulfur cycle is a major aspect of the evolution of the Earth because the sulfur cycle is intimately involved in the cycles of a number of key elements including oxygen and carbon, and thus life itself. Because of their role in the iron cycle, iron sulfides also provide information about the biogeochemistry of metals. Iron sulfides are also key indicators of contemporary environmental conditions. The consequence of this is that iron sulfides are central to our understanding of the evolution of the Earth. Many current fundamental concepts about the evolution of the Earth surface environment (e.g., the evolution of atmospheric $O_2$) are mainly based on analyses and interpretations of iron sulfides, particularly pyrite, in ancient sedimentary rocks. As the rocks get older, sedimentary iron sulfides become progressively more central to contemporary debates about Earth history. Indeed, they

10.1021/cr0503658 CCC: $65.00 
Published on Web 01/30/2007

David Rickard trained in geology, chemistry, and microbiology at Imperial College, London, where he obtained his B.Sc. (1965) with first class honours and Ph.D. (1968). He was awarded an ARSM in 1965, DIC in 1968, *Docentur* at Stockholm University in 1975, and C.Eng in 1978. He was awarded Honorary Fellowships of the Geochemical Society, the European Association of Geochemistry, and the Society of Geology Applied to Mineral Deposits in 2003. He was Chair of the Department of Earth Sciences at Cardiff University (1983–2002) having previously worked in Sweden and Australia, and currently holds the Chair in Geochemistry. He has published over 100 scientific papers and books on sulfide chemistry, geochemistry, biogeochemistry, and ore geology. He was an Editor of *Economic Geology* (1975–1980), was an Editor of *Mineralium Deposita* (1982–2000), and has been a Chief Editor of *Chemical Geology* since 2004.

George W. Luther III was born in Philadelphia, Pennsylvania, in 1947. He attended La Salle College where he received an ACS certified B.A. degree in 1968. He received a National Defense Education Act Fellowship from the University of Pittsburgh, where he graduated in 1972 with a Ph.D. in physical–inorganic chemistry. His studies included NMR spectroscopy and boron hydride chemistry with Dr. James C. Carter. Upon graduating from the University of Pittsburgh, he became an assistant professor at Kean College of New Jersey, where he rose through the ranks and became department chair (1976–1984) and helped the program become ACS certified. During this time, he also was active in ACS local section activities and became chair of the New Jersey ACS local section in 1983. In 1986, he moved to the University of Delaware, where he began a research program in marine inorganic chemistry, including studies on trace metal, sulfur, and iodine speciation in environmental waters. His work emphasizes the use of physical chemistry to understand environmental problems. Specific examples include the use of chemical kinetics and frontier molecular orbital approaches to understand redox and metal complexation reactions. In the early 1990s, he began developing *in situ* voltammetric sensors to determine chemical species in sedimentary pore waters and the water column. He has sailed on many cruises studying the chemistry of the major oceans, the hydrothermal vents, the Black Sea, the Arabian Sea, and the Mediterranean Sea. In 1997, he was elected chair of the ACS Division of Geochemistry and in 2004 received the Claire C. Patterson award from the Geochemical Society.

have been associated as catalysts in a number of key biochemical reactions associated with the "iron−sulfur world" hypothesis for the development of life.

This is the third research review on metal sulfides, especially iron sulfides, that the senior author has published over the last 2 years. The first review[1] examined the nature and distribution of HCl-soluble iron sulfides in sediments. The second review[2] summarized current knowledge on the stability, structure, and composition of metal sulfide complexes and clusters in low-temperature aqueous systems. This research review examines Fe and S chemistry in the context of iron sulfide formation processes and their kinetics with particular reference to marine systems. The emphasis is on the chemistry that occurs or can occur within the natural environment but does not emphasize in great detail the distributions of relevant chemical species in the environment. Readers are referred to the other reviews for updates on these aspects of sulfur chemistry in natural systems.

In this review, we have tried to join up the dots of hundreds of recent papers to paint a consistent picture of current knowledge about the chemistry of iron sulfides. However, as with the two previous reviews, it is not merely a compilation of previous data but also presents new information based on (mainly) published observations and measurements. The research themes developed include the following:

- A re-evaluation of the equilibrium thermodynamics of the aqueous iron, sulfide, and iron sulfide systems.
- The importance of carefully distinguishing between kinetics and equilibrium thermodynamics in understanding iron sulfide chemistry.
- The consistency of apparently conflicting reports on iron sulfide chemistry in terms of the equilibrium and kinetics approaches.

This review does not discuss the application of the chemical results to understanding the formation of the extraordinary variety of textures and habits exhibited by pyrite in marine systems. This is a rapidly developing field, which would constitute an equally large review paper. The review focuses on the work on the chemistry of iron sulfides since 1987, when Morse et al.[3] published their benchmark review. Readers interested in the earlier history of the subject are directed to that study, although there are some excursions into the past in the present review as these are required for completion or to explain where some modern ideas originated.

## 1.1. Iron Sulfides in Marine Systems: Background

The biogeochemical sulfur cycle is not well-defined. Pre-1979 and before the discovery of deep sea hydrothermal vents,[4] it was thought that sulfide in the surface environments of the Earth is almost entirely a result of the microbial reduction of sulfate. As discussed below, abiologic sulfate reduction at temperatures below ~150 °C is kinetically extremely slow, even over geologically significant time periods. By contrast, microbial respiration with sulfate is abundant because sulfate is far more soluble in water than dioxygen and therefore it is a more abundant electron acceptor for microbial respiration. Earlier understanding of the biochemical sulfur cycle included a major imbalance in the marine fluxes, which appears to have been largely explained by the influence of deep sea hydrothermal vent activity.[5] However, a number of other processes, including the discoveries of the sulfate-reduction-driven deep bio-

**Table 1. The Solid Phases in the Fe−S System**

| material | composition | structure | properties | natural abundance |
|---|---|---|---|---|
| mackinawite | $FeS_m$ | tetragonal *P*4/*nmm* | metastable material that is the major constituent of the FeS precipitated from aqueous solutions | widespread mineral in low-temperature aqueous environments |
| cubic FeS | $FeS_c$ | cubic $F\bar{4}3m$ | highly unstable phase formed before $FeS_m$ | not found naturally |
| troilite | $FeS_t$ | hexagonal $P\bar{6}2c$ | stoichiometric end member of the $Fe_{1-x}S$ group | mainly found in meteorites |
| pyrrhotite | $Fe_{1-x}S$ | monoclinic, for example, *A*2/*a*; hexagonal *P*6/*mmc* | nonstoichiometric stable group where $x > 0.2$; monoclinic form is approximately $Fe_7S_8$; hexagonal form is approximately $Fe_{10}S_{11}$ | most abundant iron sulfides in the Earth and solar system; rare in marine systems |
| smythite | $Fe_9S_{11s}$ | hexagonal *R*3*m* | metastable phase related to the $Fe_{1-x}S$ group | rare mineral mainly found in hydrothermal systems usually associated with carbonates |
| greigite | $Fe_3S_{4g}$ | cubic *Fd*3*m* | metastable $Fe^{II}Fe^{III}$ sulfide; the thiospinel of iron | fairly widespread mineral particularly associated with fresh water systems |
| pyrite | $FeS_{2p}$ | cubic *Pa*3 | stable iron(II) disulfide known as "fool's gold" | the most abundant mineral on the Earth's surface |
| marcasite | $FeS_{2m}$ | orthorhombic *Pnnm* | metastable iron(II) disulfide | locally common mineral in hydrothermal systems and in sedimentary rocks |

sphere[6] and the sulfate-reduction-driven anaerobic oxidation of methane[7] and a re-appraisal of the significance of organic sulfur burial,[8,9] may also contribute significantly to the global sulfur budget.

The average oceanic sulfate concentration is 0.02824 mol $kg^{-1}$ [10] and, with an oceanic mass of $1.4 \times 10^{24}$ g, the mass of sulfate in the oceans is currently $1.44 \times 10^{21}$ g. The total rate of sulfate reduction is $3 \times 10^{14}$ g of S $a^{-1}$ [11] of which 75−90% is recycled to produce sulfate and intermediate valence sulfur species.[12] The rate of iron sulfide formation (as pyrite) is currently, therefore, at least $5.6 \times 10^{12}$ g $a^{-1}$. That is, about 5 million tons of pyrite are produced every year in the oceans.

Respiration via microbial sulfate reduction is the most important pathway for mineralization of organic matter in marine sediments.[9,13−16] Indeed, sulfate also drives anaerobic methane oxidation in sediments.[7] Since the mineralization and burial of organic matter ultimately determines the oxygen content of the atmosphere, the fixation of pyrite sulfur in sediments is largely responsible for the oxygenated surface environment of the planet at the present and through much of geological time.[17]

Despite the present day oxidized ocean, Fe(II)- and S(−II)-rich environments can be found in sedimentary pore waters and in deep waters of anoxic basins. Permanently anoxic basins (defined operationally as environments with $O_2(aq) < 10^{-6}$ M[18] but also containing tens of micromolar to several millimolar S(−II)) are well represented by the Black Sea,[19] the Cariaco Trench,[20] and fjords such as the Framvaren Fjord in Norway.[21] Seasonally anoxic basins are ubiquitous on all the continents and the upper Chesapeake Bay[22] is a classic example. In these basins, Fe(II) and S(−II) are present during the summer months in the deep water. In all these examples, surface waters contain $O_2$.

It is important not to confuse the chemical terms *oxic*, *suboxic*, and *anoxic* with the biological terms *aerobic*, *dysaerobic*, and *anaerobic*. The chemical terms refer to the concentration of molecular $O_2$ present in the system, whereas the biological terms refer to the characteristics of the organisms inhabiting specific environments. Although there is an obvious overlap, there are significant differences. Thus the chemical terms are operational and based on the limitations of equipment available at the time they were defined. From the point of view of the iron sulfides, for example, $10^{-6}$ M $O_2$ can be a significant amount of dioxygen, especially in open systems. Likewise, many organisms are not obligate in their oxygen sensitivity but are facultative and able to adapt to changing oxygen concentrations.

In the absence of physical forcing, a redox sequence[13] based on the thermodynamics of the decomposition of organic matter by microorganisms using natural oxidants ($O_2$, $NO_3^-$, $MnO_2$, FeOOH, $SO_4^{2-}$) is produced and gives well-defined vertical profiles for $O_2$, $NO_3^-$, Mn(II), Fe(II), $H_2S$, and $SO_4^{2-}$ as shown in Figure 1. The idealized profiles given are dependent on the input of inorganic and organic matter debris from surface waters to bottom waters and sediments via sedimentation. Organic matter brings with it the hard parts of organisms, which include $SiO_2$ and $CaCO_3$, as well as other elements that are important to life processes such as Fe and Mn. The smooth profiles in Figure 1 are governed by diffusion of the soluble species and can be found in sedimentary pore waters[13] and the water column of enclosed anoxic basins.[19] The nonoverlap of $O_2$ with $Mn^{2+}$ is based on voltammetric microelectrode data.[23] Where soluble species overlap or *cross over* as in the Fe and S cycles, redox or precipitation/dissolution reactions or both occur to remove these species from solution. In the ideal case, the gradients of two chemical species that cross over should balance

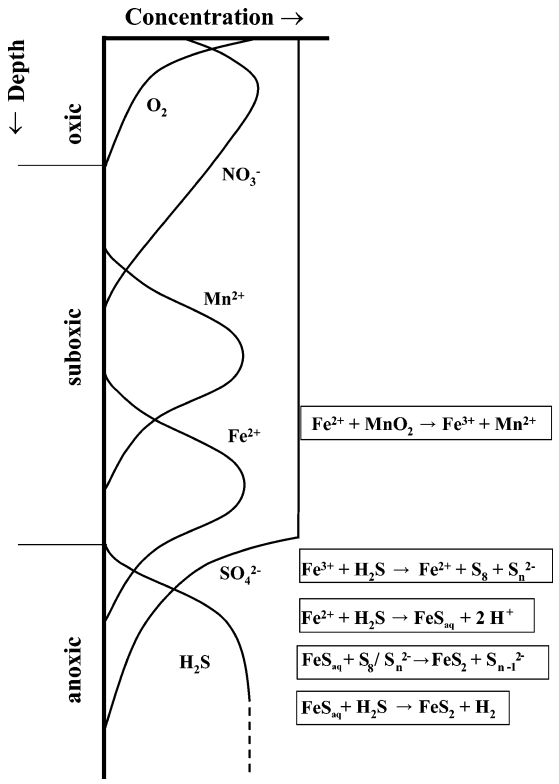


**Figure 1.** Schematic representation of trends in pore water profiles with depth below the sediment−water interface and concentration axes in arbitrary units.

stoichiometrically. If they do not, then other reactions or processes need to be considered.

Figure 1 demonstrates that $O_2$ is depleted before the reduced forms of Fe and S are measurable. The zone between the last detection of $O_2$ and the first detection of S(−II) is called suboxic. The definition is again operational: the limits of detection of dissolved $O_2$ by conventional methods are $>10^{-6}$ M and, of course, much greater in the presence of S(−II). In near-shore sedimentary environments, $O_2$ may be depleted in 1 or 2 mm,[24] whereas in the deep ocean, $O_2$ will be depleted after several centimeters.[25,26] In sediments, the thickness of the suboxic zone can be on the order of a few millimeters to centimeters[27] or several meters.[19] Anoxic basins show a suboxic zone thickness from centimeters (e.g., Framvaren Fjord[21,28]) to a meter (e.g., Bannock Basin[29]) to tens of meters (e.g., Black Sea[19] and Cariaco Basin[30]).

The smooth profiles shown in Figure 1 are disrupted by physical forcing[30−33] and animal/plant activity (bioturbation).[34,35] For suboxic water columns, vertical and lateral mixing of water masses in ocean basins, storms, and seasonal weather patterns affect the idealized profile by forcing $O_2$ deeper into the water column. For sedimentary pore waters, storms and bioturbation mix the upper most sediments. Wave action from storms pounds shallow sediments along the coast and brings $O_2$ and $NO_3^-$ into the reducing sediments. The growth of plants in sediments and the burrowing of organisms into sediments (bioturbation) also mixes oxidized and reduced zones. In addition to dissolved $O_2$ and $NO_3^-$ being forced deeper into reducing environments to oxidize reduced materials, solid-phase iron(III) and manganese(III,IV) (oxy)-hydroxides and oxides are mixed from surface sediments to reduced sediments as sulfide minerals are moved to the surface. These processes disrupt the smooth profiles and allow for significant redox chemistry to occur, for example, the oxidation of sulfide by Fe(III) and Mn(III,IV) phases.

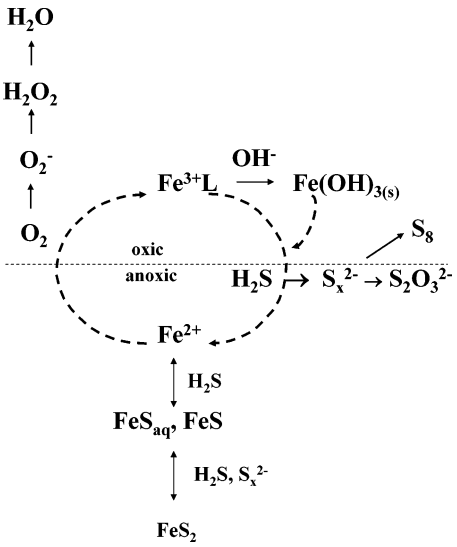


**Figure 2.** Iron catalytic cycle with $O_2$ and $H_2S$ at oxic−anoxic interfaces.

In the case of the reaction of $O_2$ with S(−II), the first electron-transfer step is thermodynamically unfavorable (eq 1)

$$HS^- + O_2 \rightarrow SH + O_2^- \qquad E° = -1.24\ \text{V} \quad (1)$$

and this leads to both the Mn and Fe cycles acting as catalysts to oxidize S(−II). The Mn[36] and Fe[37] catalytic cycles are composed of (1) the reaction of $O_2$ with Mn(II) and Fe(II) to produce Mn(III,IV) and Fe(III) chemical species and (2) the oxidation of S(−II) by the Mn(III,IV) and Fe(III) species, which leads to the re-formation of Mn(II) and Fe-(II) and the creation of electrophilic and nucleophilic sulfur compounds with intermediate oxidation states such as $S_8$, $S_n$(−II), and $S_2O_3$(−II) (Figure 2). Another consequence of one electron-transfer reactions is the possibility of forming reactive oxygen species (ROS) such as $O_2^-$ and $H_2O_2$ at the oxic/anoxic transition zone. Also shown in Figure 1 is the reaction of Fe(II) with $MnO_2$,[38] which can produce Fe(III) compounds and thus transfer oxidation character deeper into the reducing zone.

Once $Fe^{2+}$ forms, it reacts with $S_n$(−II) and S(−II) to form FeS and $FeS_2$ (mainly as pyrite). In environments that experience seasonal oxic conditions, the formation of Fe-(III) species or mixed Fe(II,III) solids (termed "reactive Fe") occurs and can be greater than the formation of $FeS_2$.[39−41] The number of reactive iron solid phases that can form is considerable and their rates of reactivity with sulfide, other reductants, and microbes can vary over several orders of magnitude.[42−44] For example, Fe(III) in silicates is more resistant to reduction and dissolution by sulfide than Fe(III) crystalline materials such as goethite (FeOOH), hematite ($Fe_2O_3$), and magnetite ($Fe_3O_4$), which are less reactive than ferrihydrite (more-or-less $Fe(OH)_3$, see discussion below) and other nanocrystalline materials. The reaction of these solid reactive iron phases with sulfide results in a steady increase of $FeS_2$ (at the expense of any intermediate FeS phases) with depth in the sediments. In the anoxic zone where sulfate decreases toward nondetectible levels, essentially all reactive Fe (and Mn(III,IV)) phases are reduced and the formation of $FeS_2$ reaches a maximum. Once all the Fe is converted to $FeS_2$, $H_2S$ concentrations build up and reach a maximum as sulfate no longer readily diffuses to deeper depths. Where

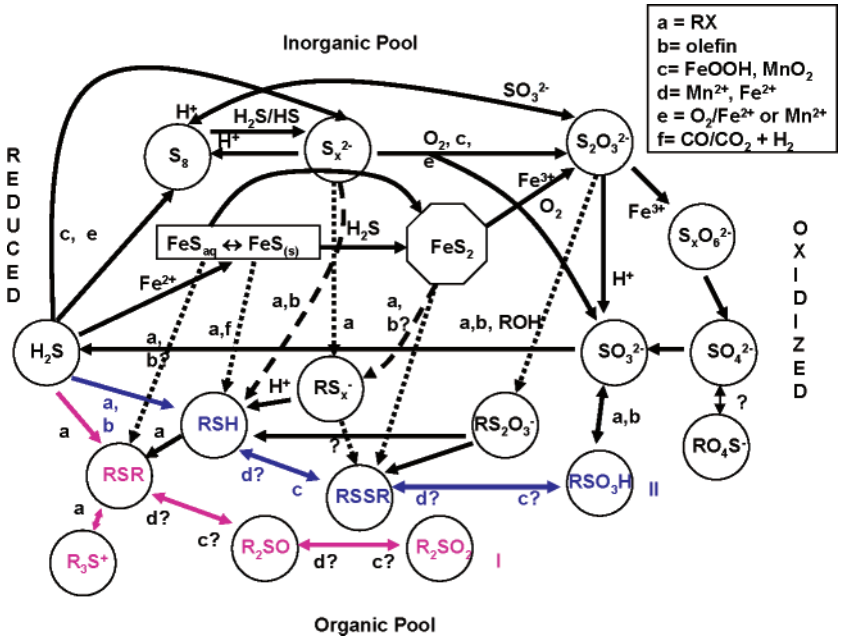


**Figure 3.** The sulfur cycle in the environment. Dashed lines indicate the reaction of inorganic sulfur compounds to form organosulfur compounds. Question marks indicate that the reactant has not been verified for a given sulfur species transformation.

sulfate approaches nondetectible levels, methanogenesis occurs with overlap of sulfate and methane profiles indicating that sulfate is the oxidant for anaerobic methane oxidation.[45] Although sulfate reduction in the deep anoxic zone is limited by the depleted sulfate and metabolizable organic matter contents, sulfate-reducing prokaryotes exist in the deep subsurface and are active.[6]

The burial of $FeS_2$ in sediments has received significant attention (e.g., ref 46). For normal marine sediments with overlying water containing dissolved $O_2$, formation and burial of $FeS_2$ occurs in the sediments and is termed *diagenetic* (formation after reactive Fe deposition). For sediments that have $H_2S$ in the overlying waters, reactive Fe compounds, which sink to the bottom sediments, react with the sulfide and form $FeS_2$ in the water column. This pathway is termed *syngenetic* and has been documented for ancient euxinic sediments, which had no $O_2$ in their overlying waters. The latter pathway also indicates that the sediments are Fe-limited; that is, there is no fresh input of reactive Fe solid phases for diagenetic $FeS_2$ formation. The Black Sea, a modern nearly euxinic system, is an example where $FeS_2$ forms by both pathways.

Figure 3 is a schematic diagram of the sulfur cycle in the environment. Although the Fe−S system can be dominated by $FeS_2$ burial in sediments, organic sulfur burial can equal or exceed $FeS_2$ burial in some saltmarsh and near-shore environments.[47−49] The range and complexity of sulfur compounds and oxidation states are evident in Figure 3 including two pathways for organic sulfur oxidation, as well as the reaction of inorganic sulfur compounds with organic compounds and $CO/CO_2$ to form organosulfur compounds. In this review, we center our efforts primarily on the inorganic chemistry of the sulfur cycle.

## 2. Sulfur Chemistry

### 2.1. Sulfide Chemistry in Aqueous Solutions

Free sulfide, S(−II), exists in aqueous solutions mainly in the form of $H_2S$ and $HS^-$ with minor $S^{2-}$. $HS^-$ is a Lewis base whereas $H_2S$ can act as a Lewis base or acid. The frontier orbitals for the molecule $H_2S$ (S−H−S bond angle 92°) are well-known.[50] Figure 4 shows the molecular orbital energy diagram for $H_2S$, which results from the linear combination of the 1s orbitals of the two hydrogen atoms and 3s and 3p orbitals of the sulfur atom. It also compares the energy level diagrams of $HS^-$ with $H_2S$. The energies of these orbitals are an important feature of their reactivity. The lowest unoccupied molecular orbital (LUMO) for $HS^-$ was calculated to be +8.015 eV[51] with no experimental data available for comparison. However, the high positive energy indicates $HS^-$ cannot be an electron acceptor. The highest occupied molecular orbital (HOMO) for $HS^-$ was calculated to be −2.37 eV, which compares well with the experimental value of −2.31 eV.[52,53] The HOMO for $HS^-$ is less stable than that for $H_2S$ (−10.47 eV) indicating that $HS^-$ is more nucleophilic and basic than $H_2S$, consistent with known reactivity. The HOMO orbital for $H_2S$ was calculated to be

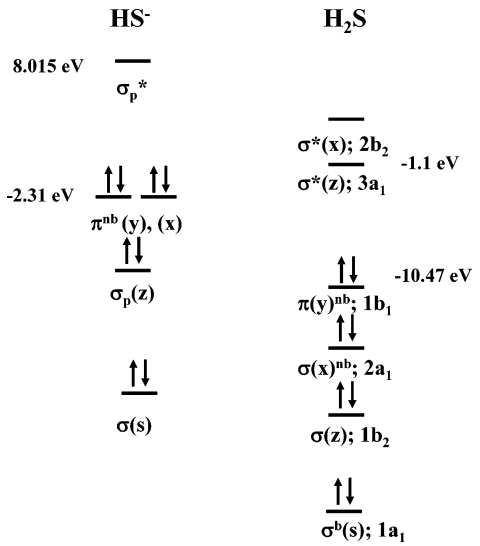


**Figure 4.** Molecular orbital energy diagrams for $HS^-$ and $H_2S$. Modified from Rickard and Luther[2] and reproduced by permission of the Mineralogical Society of America, Copyright 2006.

−9.646 eV, whereas the experimental value from ionization energy data is −10.47 eV.[52,53] Thus, $H_2S$ is not an excellent electron donor because the HOMO is so stable. $H_2S$ can act as an electron donor to Fe(II) because Fe(II) has LUMO orbitals with more stable energies compared with the HOMO of $H_2S$ or has an empty orbital due to water exchange.

The LUMO orbital for $H_2S$ using the semiempirical approach was calculated to be +0.509 eV[51] whereas the experimental value is −1.1 eV based on electron affinity data.[53] These values bracket the LUMO for $O_2$ (−0.47 eV), for example, and suggest that $H_2S$ can be an excellent electron acceptor.[51,54]

The LUMO orbital for $H_2S$ (termed $3a_1$) is made from the combination of 1s orbitals from each hydrogen and the $p_x$ orbital of sulfur, which also mixes with the s orbital of sulfur.[50] The molecular orbital is delocalized across all three atoms since the sign of the wave function encompasses all atomic centers. Figure 5 shows the molecular orbital and the charges from *ab initio* calculations.[55] Because the LUMO is an antibonding orbital in the bent $H_2S$ molecule, it is more destabilized relative to similar molecular orbitals for linear molecules such as $BeH_2$.[50] Because of this destabilization, electrons added to this LUMO orbital cause a weakening of both S−H bonds.

The chemistry of S(−II) in aqueous environmental systems has been fairly well constrained.[3] At infinite dilution, $pK_1(H_2S)$ is 6.98 ± 0.03 at 25 °C and 1 bar,[56] which means that $H_2S$ dominates the system at acid pH values and $HS^-$ is the dominant species in alkaline solutions. In seawater between 5 and 25 °C and salinities of 5 to 40, the value of $pK_1(H_2S)$ in seawater, $pK_1^*(H_2S)$, can be described as a function of both temperature, $T$ (in kelvin), and salinity, $S$.[57]

$$pK_1^* = pK_1 + AS^{1/2} + BS$$

where

$$pK_1 = -98.080 + 5765.4/T + 15.0455 \ln T$$

$$A = -0.1498$$

$$B = 0.0119$$

These data suggest that in standard seawater ($S = 35$) at 25 °C, $pK_1(H_2S)$ is 6.51 ± 0.03, which is 0.47 logarithmic units less than the value at infinite dilution. At 5 °C, $pK_1(H_2S)$ is 7.33 ± 0.03, which compares with 6.86 ± 0.03 in standard seawater.

The $pK_2(H_2S)$ is less precisely constrained but is estimated to be >18.[58,59] The uncertainty stems from the problems of polysulfide contamination in the experimental measurement of $pK_2(H_2S)$. Although it has been reported that the high value of $pK_2$ means that $S^{2-}$ does not have significant concentration in aqueous solutions, this is not actually the case. As shown in Figure 6, the activity of the $S^{2-}$ ion in equilibrium with a total S(−II) activity of $10^{-3}$ varies between approximately $10^{-12}$ at pH = 10 and $10^{-20}$ at pH = 4. In thermodynamic terms, these are significant activities compared with the solubility of many metal sulfide minerals (see ref 2 for example).

The reason why $S^{2-}$ is not considered in low-temperature aqueous sulfide chemistry is not due to its low concentration but due to the *uncertainty* in $pK_2(H_2S)$, which propagates through equilibrium systems. Thus the solubility of metal

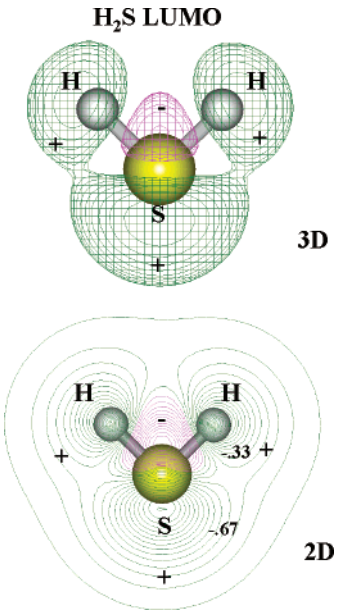


**Figure 5.** LUMO for $H_2S$. Upper panel is a three-dimensional representation; lower panel is a two-dimensional representation with charges from Trsic and Laidlaw.[55] The positive sign indicates the positive part of the orbital's wavefunction and the negative sign the negative part of the orbital's wavefunction.

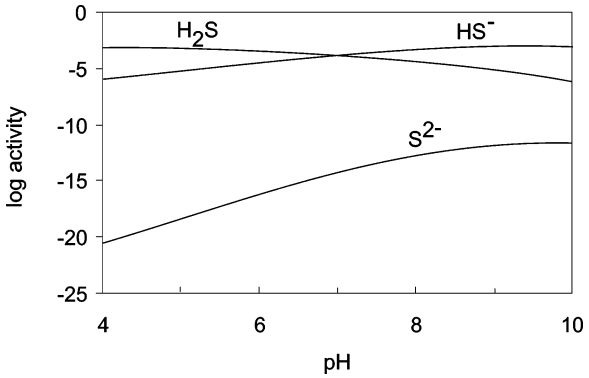


**Figure 6.** Distribution of aqueous sulfide species at $\{S(-II)\}_T = 10^{-3}$ in terms of pH.

sulfides is usually written in terms of the $HS^-$ species, $K_{sp,2}$ for reactions like

$$MS + H^+ = M^{2+} + HS^- \quad (2)$$

rather than in terms of the $S^{2-}$ species, $K_{sp}$,

$$MS = M^{2+} + S^{2-} \quad (3)$$

The problem is that some compilations of stability constants still include older $pK_2(H_2S)$ values around 12 or 14 or include sulfide solubility constants that are based on these older values. These still slip readily into the literature since thermodynamic databases may include these intrinsic errors as pointed out originally by Schoonen and Barnes.[59]

Microbial sulfate reduction is carried out by a number of prokaryotes, including bacteria and archaea, and we refer to these collectively as sulfate-reducing prokaryotes (SRPs) and the process as prokaryotic sulfate reduction (PSR). The process, which involves an eight-electron reduction, proceeds through a number of stages. $SO_4^{2-}$ is attached to the phosphate of ATP forming adenosine phosphosulfate (APS) catalyzed by ATP sulfurylase. The APS $SO_4(-II)$ moiety is

reduced to $SO_3(-II)$ with the release of AMP. The subsequent reduction of the $SO_3(-II)$ moiety is relatively facile.

The process involves a considerable fractionation of the S isotopes, conventionally measured in terms of the $^{34}S/^{32}S$ ratio. The measurements are present in terms of the per thousand deviation of the $^{34}S/^{32}S$ ratio from that of a meteoritic standard, $\delta^{34}S$ ‰. Fractionations of the order of −30‰ are common in PSR and are used as proxies for identifying PSR in ancient and modern environments. The main part of the fractionation takes place at the initial reduction of APS.

The abiologic reduction of sulfate is kinetically extremely slow at low temperatures (e.g., less than *ca.* 150 °C) except in the most extreme conditions with powerful reductants and relatively high concentrations, such as HI and acidified $Cr^{2+}$. The reason is the high symmetry of the sulfate ion, and this is demonstrated by the observation that $SO_3^{2-}$ is readily reduced. In contrast the oxidation of S(−II) to $SO_4^{-2}$ is kinetically more amenable. The result is that the interchange

$$SO_4^{2-} \leftrightarrow S(-II) \quad (4)$$

is abiologically irreversible in low-temperature natural environments. The predominance of PSR in sulfide formation means that in reality the reduction of $SO_4^{2-}$ to S(−II) in natural systems is kinetically fast and equilibrium may be approached. It is also important for theoretical equilibrium computations involving sulfate and sulfide: in the absence of microorganisms, the sulfate−sulfide couple is not reversible and the equilibrium approximation is invalid.

A Pourbaix[60] or pH−Eh diagram of the stable phases in the S− $H_2O$ system at 25 °C and 1 bar total pressure is shown in Figure 7. This diagram has several interesting features. The boundary between the dominance fields of $SO_4^{2-}$ and S(−II) is widely assumed to be co-incident with the boundary between oxic and anoxic sulfide-bearing systems. In fact, of course, this is not actually true as is shown in Figure 1. The boundary is merely a convenient way of expressing redox in the S−$H_2O$ system. It denotes the locus of points where $\{SO_4^{2-}\} = \{S(-II)\}$. Sulfide occurs on both sides of the boundary. At pH = 8, for example, the relationship between $\{SO_4^{2-}\}$ and $\{S(-II)\}$ is given by the reaction

$$HS^- + 4H_2O = SO_4^{2-} + 9H^+ + 8e^- \quad (5)$$

where

$$\log \{SO_4^{2-}\}/\{HS^-\} = (135.14)Eh - 33.52 \quad (6)$$

The $\{SO_4^{2-}\}/\{HS^-\}$ boundary is then at Eh = −0.247 V. But at $\{S\}_T = 10^{-3}$, $\{S(-II)\}$ is still present at $10^{-6}$, a significant activity, at Eh = +0.022 V. Likewise, $SO_4^{2-}$ is still present at significant activities deep into the sulfide zone. The latter is, of course, important for SRPs, which require a supply of $SO_4^{2-}$.

Mass-dependent S isotope fractionation as it variously impinges on the sedimentary sulfur system has recently been widely reviewed.[9,61,62] Much of the information regarding the sulfur isotope systematics in natural systems is based on the sulfur isotopic composition of pyrite. Earlier work was limited by the analytical considerations, in particular, the need to collect sulfur from bulk sediments in order to obtain enough sulfur for the isotopic composition to be measured precisely. Bulk analyses give the average isotopic composition of the pyrite. Technical advances have enabled the sulfur

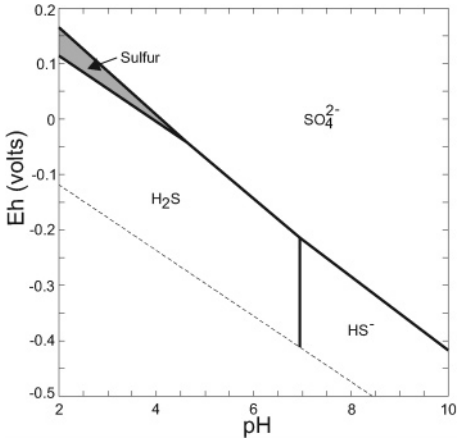


**Figure 7.** pH−Eh diagram for stable sulfur species in aqueous solution (25 °C, 1 bar total pressure, $\sum\{S\} = 10^{-3}$).

isotopic composition of single pyrite grains to be analyzed, and these measurements have revealed considerable variations in isotopic compositions between individual sedimentary pyrite grains and even within single pyrite grains.[63] The variation in the sulfur isotopic compositions between and within pyrite grains can encompass a large fraction of the total variation in bulk sulfur isotope in the sediment. Intragrain analyses show that sulfur isotopes normally become heavier toward the outside of the pyrite grain.

The degree of S isotope fractionation is related to the concentration of $SO_4^{2-}$, which limits the rate of PSR at <200 $\mu$M $SO_4^{2-}$.[64,65] Halbicht et al.[66] showed that $\delta^{34}S$ decreased discontinuously from an average 22.6‰ ± 10.3‰ above 200 $\mu$M $SO_4^{2-}$ to less than 0.7‰ ± 5.7‰ at <200 $\mu$M $SO_4^{2-}$. The uppermost sedimentary layers, adjacent to the sediment−water interface, are affected by physical processes such as bioirrigation and current action. Thus the sulfate reservoir in these layers can be regarded as effectively infinite since it is open to continued recharge from seawater sulfate. In this zone, oxidation may also be widespread due to the abundance of iron and mangenese oxides, as well as molecular oxygen ingress. The result is microbially powered oxidation−reduction cycles, which may produce large fractionations.[67,68]

At lower levels in the sediment, the availability of $SO_4^{2-}$ is determined by diffusion. The recharge of the sediment pore waters with $SO_4^{2-}$ from the overlying depleted zones is therefore limited and the concentration reduced. Since $SO_4^{2-}$ is present at these low concentrations deep (>0.5 km) into the sediments,[6] this means that PSR will produce S(−II) with a spectrum of sulfur isotopic compositions. The initial rapid $SO_4^{2-}$ reduction will give rise to relatively light S(−II) whereas later, slower $SO_4^{2-}$ reduction at low $SO_4^{2-}$ concentrations will produce smaller fractionations. The interesting aspect of this conclusion is that changes in sulfur isotopic composition of pyrite in sediments are not necessarily related to any separate fluid or sulfate source. Nor are changes necessarily a result of deeper burial. The variations can occur at the same level, at closely related times, through changes in $SO_4^{2-}$ concentration.

## 2.2. Polysulfide Chemistry

Pyrite, the most abundant terrestrial iron sulfide mineral in Earth surface conditions, is an iron(II) disulfide, $FeS_2$. This suggests that somewhere in the formation of this material, disulfide species, $S_2(-II)$, should be involved.

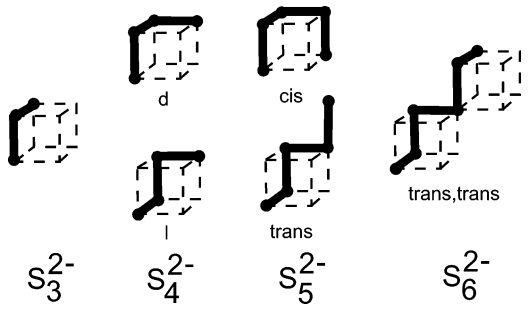


**Figure 8.** Figurative representation of polysulfide geometries. Modified from ref 70, Copyright 1987, with permission from Elsevier.

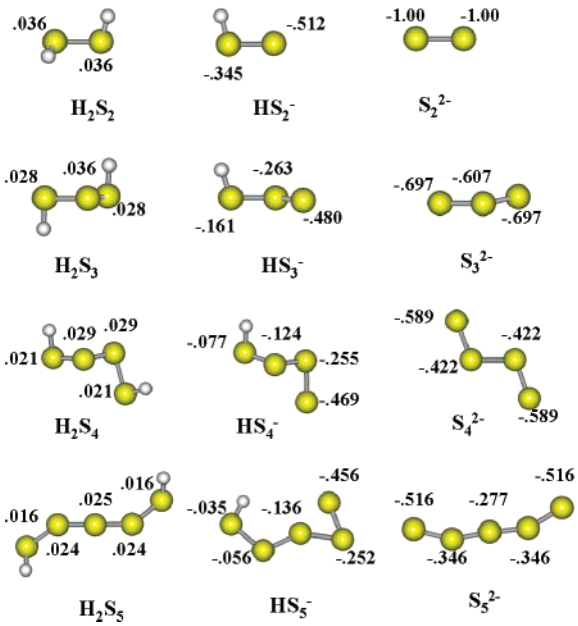


**Figure 9.** Molecular models of aqueous inorganic polysulfide structures.

Disulfides are end members of a series of sulfanes, usually referred to as polysulfides, which occur as discrete species in aqueous solutions. The shorter chain polysulfides ($S_n(-II)$ where $n < 4$) and the longer chain polysulfides ($n \geq 4$) have actually never been individually isolated in aqueous solutions. They occur as part of a spectrum of polysulfide species. The evidence for their existence is based on an arithmetic analysis of spectroscopic or mass data for total polysulfide solutions under varying conditions.[3,69]

Polysulfide ions consist of chains of sulfur atoms. For polysulfides, the dihedral angles vary between 60° and 110°. In Figure 8, the angle is schematically fixed at 90°.[70] The $S_3^{2-}$ ion is coplanar, but adding a further S atom leads to two possible forms for $S_4^{2-}$, the *d*- and *l*-isomers. $S_5^{2-}$ also displays *cis* and *trans* forms. The $S_6^{2-}$ ion can form three enantiomers *cis,cis*, *trans,trans*, and *cis,trans*, each *d* and *l*, respectively. The *cis*-$S_5^{2-}$ and the *cis,cis*-$S_6^{2-}$ ions effectively constitute fragments of an $S_8$ ring. In contrast, the *trans*-$S_5^{2-}$ and the *trans,trans*-$S_6^{2-}$ really correspond to parts of an infinite helical chain, as in fibrous sulfur. In complexes, the normal arrangement is *all-trans* conformations, although the *cis*-conformation has been detected in α-$Na_2S_5$. Molecular calculations of the structures and charges for the $S_2$, $S_3$, $S_4$, and $S_5$ systems are given in Figure 9. The charges indicated on the S atoms are from the extended Hückel calculations[71] for $S_n$ where $n = 2-8$. They are in reasonable agreement with the charges from the *ab initio* calculations[55] for $n = 1-4$.

**Table 2. Stability Data for Polysulfide Ions and Their Conjugate Acids at 25 °C**[a]

| $n$ | $\Delta G_f^\circ(S_n^{2-})$ | $\Delta G_r^\circ(S_n^{2-})$ | log $K(S_n^{2-})$ |
|---|---|---|---|
| 2 | 77.41 | 65.36 | −11.46 |
| 3 | 71.63 | 59.58 | −10.44 |
| 4 | 67.41 | 55.36 | −9.70 |
| 5 | 66.05 | 54.00 | −9.47 |
| 6 | 67.15 | 55.10 | −9.66 |
| 7 | 70.45 | 58.40 | −10.24 |
| 8 | 73.58 | 61.53 | −10.79 |
| $n$ | $\Delta G_f^\circ(HS_n^-)$ | $\Delta G_r^\circ(HS_n^-)$ | log $K(HS_n^-)$ |
| 2 | 22.07 | 10.02 | −1.76 |
| 3 | 28.84 | 16.79 | −2.94 |
| 4 | 31.47 | 19.42 | −3.40 |
| 5 | 33.53 | 21.48 | −3.76 |
| 6 | 37.31 | 25.26 | −4.43 |
| 7 | 42.44 | 30.39 | −5.33 |
| 8 | 46.94 | 34.89 | −6.11 |
| $n$ | $\Delta G_f^\circ(H_2S_n)$ | $\Delta G_r^\circ(H_2S_n)$ | log $K(H_2S_n)$ |
| 2 | −6.46 | −18.51 | 3.24 |
| 3 | 4.88 | −7.17 | 1.26 |
| 4 | 9.79 | −2.26 | 0.40 |
| 5 | 13.56 | 1.51 | −0.26 |
| 6 | 18.14 | 6.09 | −1.07 |
| 7 | 23.90 | 11.85 | −2.08 |
| 8 | 28.91 | 16.86 | −2.95 |

[a] The log $K$ values are for the formation constants for the reactions $((n-1)/8)S_8(s) + HS^- = Sn^{2-} + H^+$, $((n-1)/8)S_8(s) + HS^- = HS_n^-$, and $((n-1)/8)S_8(s) + HS^- + H^+ = H_2S_n$ and are of the type used in the databases for speciation programs such as MINEQL+. $\Delta G_f^\circ(HS^-) = 12.05$ kJ mol$^{-1}$,[81] and $\Delta G_f^\circ(S_n^{2-})$, $\Delta G_f^\circ(HS_n^-)$, and $\Delta G_f^\circ(H_2S_n)$ were taken from Kamyshny et al.[78]

Much of the earlier published work on the geochemistry of the short chain ($n \leq 5$) polysulfides in low-temperature aqueous conditions uses free energy data for these species[72−77] that have considerable uncertainties.[1] Kamyshny et al.[78] collected what appears to be a more accurate data set for the stability of polysulfides up to $n \leq 8$ (Table 2). They trapped aqueous polysulfides with methyl trifluoromethanesulfonate and determined the dimethylpolysulfides formed with HPLC methods. They used the Schwarzenbach and Fischer[79] data set in combination with measured data to derive their stability constants. They employed a linear algorithm similar to that originally derived by Cloke,[73,74] Schoonen and Barnes,[59] and Williamson and Rimstidt[80] to determine protonation constants.

In their classical study, Schwarzenbach and Fischer[79] only actually measured protonation constants for $S_4^{2-}$ and $S_5^{2-}$ and then extrapolated data for $S_3^{2-}$ and $S_2^{2-}$. So these linear extrapolations are based on two experimental points. Independent measurements of p$K_2$ for $S_4^{2-}$ and $S_5^{2-}$ were reported by Chadwell et al.[82,83] Chadwell et al.[83] found a p$K_2(S_4^{2-})$ of 6.6, and Chadwell et al.[82] found that p$K_2(S_5^{2-})$ varied between 6.0 and 6.1 These values are in reasonable agreement with those of Schwarzenbach and Fischer.[80]

Stability data for the polysulfides are listed in Tables 2 and 3. Kamyshny et al.[78] presented polysulfide speciation versus pH (Figure 10) in the presence of excess S(0). The calculations based on these data show that polysulfides become the dominant species in alkaline solutions relative to S(−II). In the model solution chosen, for example, polysulfides become the dominant species at pH > 9. The

**Table 3. Stability Data for Polysulfide Ions and Their Conjugate Acids for the Dissociation Reactions Written in Terms of $HS^-$, $SO_4^{2-}$, and $H^+$ of the Type Used in the Database of Equilibrium Calculation Programs Like GWB[a]**

| $S_n^-$ | reaction | $\Delta G_f^\circ(S_n^{2-})$ | $\Delta G_r^\circ(S_n^{2-})$ | $\log K(S_n^{2-})$ |
|---|---|---|---|---|
| 2 | $S_2^{2-} + H_2O = 1.75HS^- + 0.25SO_4^{2-} + 0.25H^+$ | 77.41 | −5.13154 | 0.8993 |
| 3 | $S_3^{2-} + 2H_2O = 2.50HS^- + 0.50SO_4^{2-} + 1.50H^+$ | 71.63 | 60.8769 | −10.6689 |
| 4 | $S_4^{2-} + 3H_2O = 3.25HS^- + 0.75SO_4^{2-} + 2.75H^+$ | 67.41 | 125.3254 | −21.9638 |
| 5 | $S_5^{2-} + 4H_2O = 4.00HS^- + 1.00SO_4^{2-} + 4.00H^+$ | 66.05 | 186.9138 | −32.7574 |
| 6 | $S_6^{2-} + 5H_2O = 4.75HS^- + 1.25SO_4^{2-} + 5.25H^+$ | 67.15 | 246.0423 | −43.1199 |
| 7 | $S_7^{2-} + 6H_2O = 5.50HS^- + 1.50SO_4^{2-} + 6.50H^+$ | 70.45 | 302.9708 | −53.0969 |
| 8 | $S_8^{2-} + 7H_2O = 6.25HS^- + 1.75SO_4^{2-} + 7.75H^+$ | 73.58 | 360.0692 | −63.1036 |
| $HS_n^-$ | reaction | $\Delta G_f^\circ(HS_n^-)$ | $\Delta G_r^\circ(HS_n^-)$ | $\log K(HS_n^-)$ |
| 2 | $HS_2^- + H_2O = 1.75HS^4 + 0.25SO_4^{2-} + 1.25H^+$ | 22.07 | 50.20846 | −8.7992 |
| 3 | $HS_3^- + 2H_2O = 2.50HS^- + 0.50SO_4^{2-} + 2.50H^+$ | 28.84 | 103.6669 | −18.1681 |
| 4 | $HS_4^- + 3H_2O = 3.25HS^- + 0.75SO_4^{2-} + 3.75H^+$ | 31.47 | 161.2654 | −28.2624 |
| 5 | $HS_5^- + 4H_2O = 4.00HS^- + 1.00SO_4^{2-} + 5.00H^+$ | 33.53 | 219.4338 | −38.4567 |
| 6 | $HS_6^- + 5H_2O = 4.75HS^- + 1.25SO_4^{2-} + 6.25H^+$ | 37.31 | 275.8823 | −48.3495 |
| 7 | $HS_7^- + 6H_2O = 5.50HS^- + 1.50SO_4^{2-} + 7.50H^+$ | 42.44 | 330.9808 | −58.0057 |
| 8 | $HS_8^- + 7H_2O = 6.25HS^- + 1.75SO_4^{2-} + 8.75H^+$ | 46.94 | 386.7092 | −67.7724 |
| $H_2S_n$ | reaction | $\Delta G_f^\circ(H_2S_n)$ | $\Delta G_r^\circ(H_2S_n)$ | $\log K(H_2S_n)$ |
| 2 | $H_2S_2 + H_2O = 1.75HS^- + 0.25SO_4^{2-} + 2.25H^+$ | −6.46 | 78.73846 | −13.7992 |
| 3 | $H_2S_3 + 2H_2O = 2.50HS^- + 0.50SO_4^{2-} + 3.50H^+$ | 4.88 | 127.6269 | −22.3671 |
| 4 | $H_2S_4 + 3H_2O = 3.25HS^- + 0.75SO_4^{2-} + 4.75H^+$ | 9.79 | 182.9454 | −32.0619 |
| 5 | $H_2S_5 + 4H_2O = 4.00HS^- + 1.00SO_4^{2-} + 6.00H^+$ | 13.56 | 239.4038 | −41.9565 |
| 6 | $H_2S_6 + 5H_2O = 4.75HS^- + 1.25SO_4^{2-} + 7.25H^+$ | 18.14 | 295.0523 | −51.7091 |
| 7 | $H_2S_7 + 6H_2O = 5.50HS^- + 1.50SO_4^{2-} + 8.50H^+$ | 23.9 | 349.5208 | −61.2550 |
| 8 | $H_2S_8 + 7H_2O = 6.25HS^- + 1.75SO_4^{2-} + 9.75H^+$ | 28.91 | 404.7392 | −70.9322 |

[a] $\Delta G_f^\circ(HS^-) = 12.05$ kJ mol$^{-1}$,[81] $\Delta G_f^\circ(H_2O) = -237.14$ kJ mol$^{-1}$,[84] $\Delta G_f^\circ(SO_4^{2-}) = -744.0$ kJ mol$^{-1}$,[84] and $\Delta G_f^\circ(S_n^{2-})$, $\Delta G_f^\circ(HS_n^-)$, and $\Delta G_f^\circ(H_2S_n)$ were taken from Kamyshny et al.[78]

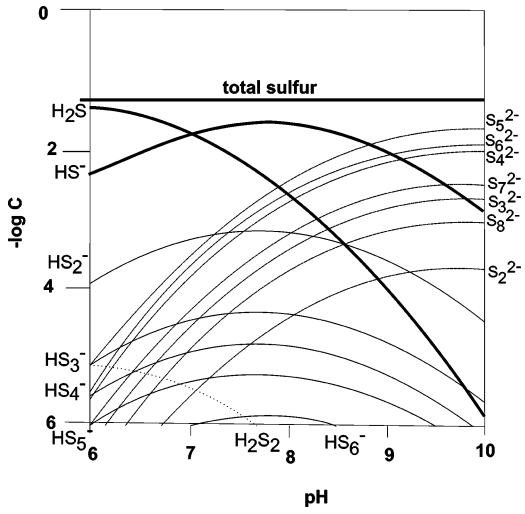


**Figure 10.** Polysulfide distribution in terms of pH in the presence of excess S(0) calculated according to the Kamyshny et al.[78] data set. Modified from ref 1, Copyright 2005, with permission from Elsevier.

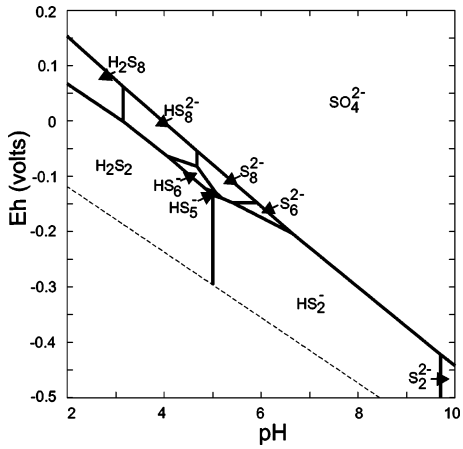


**Figure 11.** Figure 7 with stable phases removed, showing polysulfide distribution in terms of pH and Eh.

most important species in this pH range in this system are $S_4^{2-}$, $S_5^{2-}$, and $S_6^{2-}$. Removing stable sulfide species and rhombic sulfur from the pH−Eh diagram in Figure 7 reveals the underlying metastable polysulfide distribution (Figure 11). The data show the surprising result that disulfide species, $S_2$(−II), dominate much of the pH−Eh space, which would otherwise be occupied by stable S(−II) species. Higher order $S_n$(−II) species shadow but extend the stability space of rhombic sulfur. In a key area for natural environmental systems, around the $SO_4^{2-}$/S(−II) redox boundary at pH 5−9, the dominant polysulfide species are $S_8^{2-}$, $S_6^{2-}$ and $HS_2^-$. Rickard and Morse[1] commented that one of the features of the Kamyshny et al.[78] data set is the remarkable relative stability of the hydrodisulfide ion, $HS_2^-$, over the environmentally significant pH range of 6−8. It is the dominant polysulfide at pH < 7 and contributes to ca. 1% of the total dissolved sulfide in much of the system.

The Kamyshny data set can be used to determine the equilibrium distribution of polysulfides in the absence of S(0), using reactions like

$$S_2^{2-} + H_2O = 1.75HS^- + 0.25SO_4^{2-} + 0.25H^+ \quad (7)$$

This approach is useful for both determining the distribution of polysulfides in much of the natural environment where sulfur is not present or measured and using commercial equilibrium speciation programmes, such as Geochemist's Workbench (GWB), where reactions are written in terms of the basis species $SO_4^{2-}$. Equilibrium constants for polysulfides in terms of reactions like eq 7 are listed in Table 3. The data are calculated via $\Delta G_f^\circ$ values since the uncertainties in the transformations of measured equilibrium constants to $\Delta G_f^\circ$ is of the same magnitude as the uncertainty in summing the logarithm of the equilibrium constants for the series

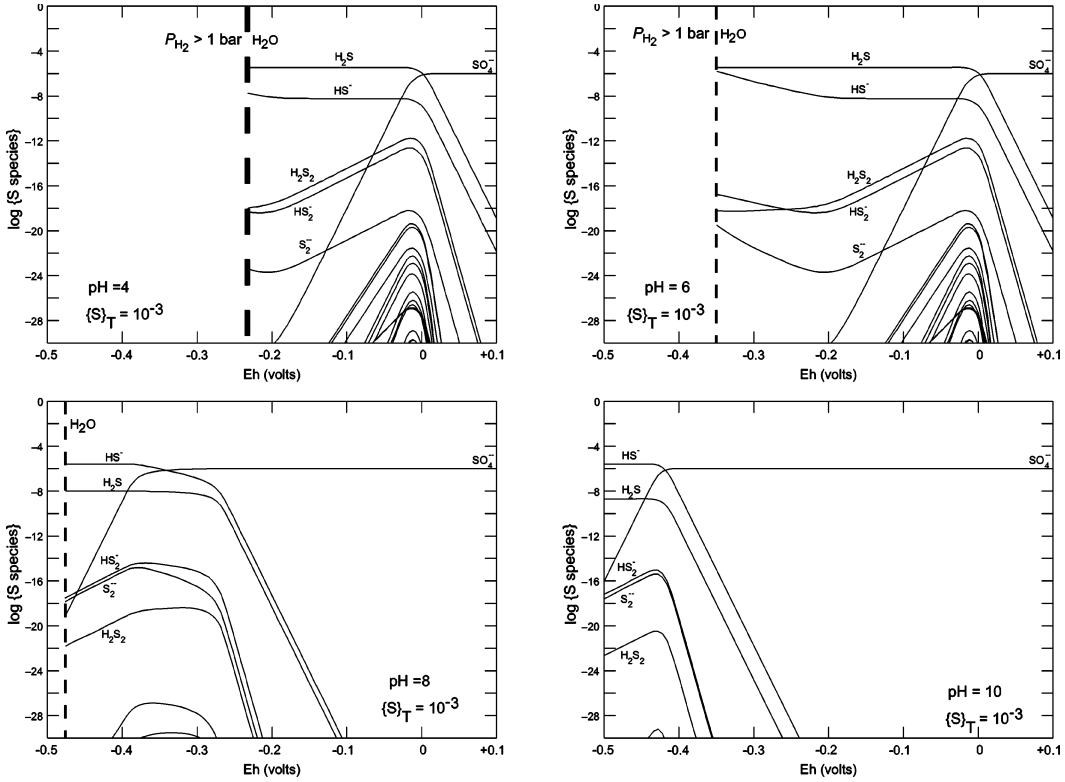


**Figure 12.** Polysulfide distribution for various pH values at $\sum\{S\} = 10^{-3}$.

of reactions involving $SO_4^{2-}$, $S^0$, and $HS^-$. The $\Delta G_f^\circ$ values for polysulfides are taken from Kamyshny et al.;[78] $\Delta G_f^\circ(SO_4^{2-}) = -744$ kJ mol$^{-1}$; $\Delta G_f^\circ(HS^-) = 12.05$kJ mol$^{-1}$.

The distribution of polysulfides in terms of Eh for pH values between 4 and 10 and $10^{-3}$ total sulfur activity is shown in Figure 12. These diagrams are calculated using the REACT algorithms of the GWB suite. Sulfate is reduced by titrating electrons at fixed pH values. As the electron activity increases, the partial pressure of $H_2$ in equilibrium with $H_2O$ increases until it reaches 1 bar pressure. Although disequilibrium in water reduction is common, with the formation of considerable overpotentials, this is conventionally regarded as the lowermost potential at which water can remain stable in Earth surface environments for any meaningful period.[85] Obviously as these high $H_2$ pressures are approached, the system becomes progressively more difficult to balance and no solution to the equilibrium matrix is possible. Figure 12 essentially shows sections through Figure 11 at constant pH. The diagrams show that the total activity of polysulfide species approaches $10^{-12}$ at pH < 7 and constitutes about 10 parts per million of the total sulfide activity. The polysulfide activity reaches a maximum close to where $SO_4^{2-}$/S(−II) approaches 1 which, in the environmental literature, appears to be often assumed to approximate the anoxic−oxic (or, more vaguely, oxidized/reduced) boundary zone in low-temperature natural systems. At pH > 7, the polysulfide activity reaches around $10^{-15}$ and the polysulfides make up about 0.1 parts per billion of the total sulfide.

As shown in Figure 12, the dominant polysulfides are the disulfides, $H_2S_2$, $HS_2^-$, and $S_2^{2-}$. A significant aspect of these computations is that these disulfides display significant equilibrium activities even in the absence of elemental or rhombic sulfur. In the presence of sulfur, the higher polysulfides become the dominant species near to the $SO_4^{2-}$/S(−II) boundary, as was shown in Figure 11.

The activities of the polysulfide species are directly proportional to the activities of the sulfide species. For example, we can write

$$S^0 + HS^- = HS_2^- \quad (8)$$

for which the equilibrium constant, log $K = -11.46$, is a direct measurement of $\{HS_2^-\}/\{HS^-\}$. In terms of concentrations in solutions with ionic strengths up to around 0.7, this would still be a reasonable guide. The activity coefficient, computed through Debye−Hückel-based algorithms, of −1 species is around 0.7 at this ionic strength and about twice that of −2 species. The conversion of activities to concentrations would mean that $[HS_2^-]/[HS^-] \approx 0.5\{HS_2^-\}/\{HS^-\}$ at $I \approx 0.7$.

Solutions of polysulfides are mixtures of $S_n$(−II), S(−II), and S(0) species and their protonated forms. Kamyshny et al.[86] showed that polysulfides exchange sulfur isotopes with other sulfur species in the system in characteristic times of <10 s. This means that polysulfides retain no isotopic memory. Amrani et al.[87] showed that the heavier polysulfides ($4 \le n \le 7$) are $^{34}S$ enriched as a function of chain length. The fractionation varies up to $\delta^{34}S = 3.4‰$ for $n = 7$ relative to the $\delta^{34}S$ value of the total S in the system. As discussed below, polysulfide S is directly incorporated into pyrite and thus S isotopic measurements of sedimentary pyrite will retain this fractionated S. However, the degree of fractionation through this process is relatively small compared with the fractionation of $SO_4$ S through PSR.

## 3. Iron Chemistry

The formation, dissolution, and transformations of iron sulfides in natural aqueous systems involve reactions with non-sulfide iron species. The nature and distribution of non-sulfide iron species in natural systems has been the subject

of much recent study. The problems have included analytical uncertainties due to the subnanomolar concentration of dissolved iron in most marine systems, the nanoparticulate nature of dispersed iron solids, and the lack of knowledge about organic Fe.

Conventionally, the ferrous ion in aqueous solution is written as $Fe^{2+}$. This is essentially a shorthand notation for the hexaqua species, $[Fe(H_2O)_6]^{2+}$, which eliminates the need for balancing the water molecules in chemical equations used in equilibrium computations. For example,

$$Fe^{2+} + HS^- = FeS\downarrow + H^+ \quad (9)$$

is equivalent thermodynamically to the overall reaction (eq 10)

$$[Fe(H_2O)_6]^{2+} + HS^- = FeS\downarrow + H^+ + 6H_2O \quad (10)$$

ignoring for the moment the fact that the proton is likely to be in the form of $H_3O^+$ and $HS^-$ may be surrounded by coordinated $H_2O$ molecules. As discussed below, the complete formulation (eq 10) is important in the real world since the formation of iron sulfides is a ligand substitution reaction, where the sulfide species replaces the water in the first coordination sphere of a hexaqua Fe(II) ion.

$[Fe(H_2O)_6]^{2+}$, $d^6$ ($t_{2g}^4e_g^2$), shows coordination number 6 and displays octahedral geometry. The arrangement also produces a cavity of appropriate size such that the $Fe^{2+}$ ion can be contained while providing enough space for significant $Fe-OH_2$ bonding interaction. Ligand-field effects determine the $Fe-OH_2$ distance and the lability. In the crystal field model, the electrons in the $d_{x^2-y^2}$ and $d_{z^2}$ orbitals point directly at the electron density on the ligands. They are then regarded as experiencing a greater electrostatic repulsion than those residing in the $d_{xy}$, $d_{yz}$, and $d_{xz}$ orbitals. Thus in an octahedral $[Fe(OH_2)_6]^{2+}$ ion, three degenerate orbitals (the $t_{2g}$ set) are at a lower energy than the two degenerate orbitals in the $e_g$ set. For a tetrahedral arrangement, none of the orbitals would be pointing directly at the ligands and the resultant tetrahedral ligand-field stabilization energy (LFSE) is lower than $\Delta_0$ so that $\Delta_t \approx {}^4/_9\Delta_0$.

Both $[Fe(OH_2)_6]^{2+}$ and $[Fe(OH_2)_6]^{3+}$ are high spin. Ligand-field theory uses a molecular orbital approach (MO) to arrive at a similar picture of the bonding orbitals for octahedral complexes except that the repulsive doubly degenerate $e_g$ set is interpreted as antibonding ($e_g$*). However, the LFSE accounts for less than 10% of the total hydration energy of $[Fe(OH)_2)_6]^{2+}$, despite its effect on $Fe-OH_2$ bond distance, hydration number, and the kinetic lability of the primary shell. The hydration enthalpy is closely correlated with the degree of hydration or hydration radius.

Wagman et al.[88,89] listed a widely used series of stability constants, which were based on the National Bureau of Standards (NBS) value for the Gibbs free energy of formation for the hexaqua $Fe^{2+}$ ion at 25 °C and 1 atm total pressure, $\Delta G_f^\circ(Fe^{2+}(aq))$, of $-78.9$ kJ mol$^{-1}$. This value was used in compilations in some very influential textbooks.[90] It was derived from the measurements collected by Randall and Frandsen[91] ($\Delta G_f^\circ(Fe^{2+}) = 84.9$ kJ mol$^{-1}$), Patrick and Thompson[92] ($\Delta G_f^\circ(Fe^{2+}) = -78.8$ kJ mol$^{-1}$), and Whittemore and Langmuir[93] ($\Delta G_f^\circ(Fe^{2+}) = -74.3$ kJ mol$^{-1}$). In contrast, Hoar and Hurlen[94] found $-90.0$ kJ mol$^{-1}$, Larson et al.[95] found $-91.1$ kJ mol$^{-1}$, Cobble and Murray[96] found $-91.5$ kJ mol$^{-1}$, Sweeton and Baes[97] found $-91.8$ kJ mol$^{-1}$, and Tremaine and LeBlanc[98] found $-88.92 \pm 2$ kJ mol$^{-1}$.

**Table 4. Log $\beta_1$ Values for $Fe^{3+} + H_2O = [FeOH]^{2+} + H^+$ Obtained in $NaClO_4$ at 25 °C and $I = 0.7$**

| log $\beta_1$ | method | refs |
|---|---|---|
| −2.73 | spectrophotometry | 102 |
| −2.77 | potentiometry | 109 |
| −2.72 | spectrophotometry | 110 |
| −2.75 | potentiometry | 103 |
| −2.75 | potentiometry | 104 |
| −2.68 | assessment of literature data | 111 |
| −2.62 | reanalysis of literature data | 105 |
| −2.74 | potentiometry | 113 |

The whole matter was critically reviewed in 1995 on behalf of the CODATA Task Force on Chemical Thermodynamic Tables by Parker and Khodakovskii[99] who recommended the lower value of $-90.53 \pm 1$ kJ mol$^{-1}$. They also reviewed the experimental problems encountered in measurements of this value and showed how the various values had been obtained. The higher values had come about through errors in the measurements of the standard potential of the $Fe^{2+}$/Fe couple using Fe electrodes. Latimer[90] had warned about the problems this method involved, and Hoar and Hurlen[94] demonstrated how these problems could be overcome with a kinetic approach. The experimental problems involved in the use of Fe electrodes were avoided by Larson et al.[95] by using measurements of the specific heat of hydrous iron(II) sulfate. Cobble and Murray[96] achieved a similar result by measuring the specific heat of ferrous chloride, and Sweeton and Baes[97] and Tremaine and LeBlanc[98] measured the solubility of magnetite.

The value for $\Delta G_f^\circ(Fe^{2+}(aq))$ is fundamental to all computations based on Fe species in complex natural systems. The difference between the NBS network $\Delta G_f^\circ(Fe^{2+}(aq))$ value of $-78.9$ kJ mol$^{-1}$ and the modern IUPAC value of $-90.53 \pm 1$ kJ mol$^{-1}$ is substantial. $Fe^{2+}(aq)$ is far more stable in computations using the IUPAC value than with the old NBS value. The result is that the relative distribution of dissolved species and solids in Fe-bearing systems based on the older NBS value is erroneous. The problem is more extensive since the compatibility between networks of different cation species is required to determine the relative stabilities of Fe and other cation species. For example, Langmuir[100] produced an excellent set of Fe stability data, which is internally consistent but which is based on the higher NBS $\Delta G_f^\circ(Fe^{2+}(aq))$ value. It cannot therefore be used for considerations of the stability of Fe species in systems containing components from other networks. This is not entirely a historical problem. As recently as 2000, workers[101] were still publishing data (and some referees were still not picking it up) on the iron sulfide system based on the erroneous NBS $\Delta G_f^\circ(Fe^{2+}(aq))$ value.

The dominant inorganic species in normal seawater are the Fe(III) hydroxyl complexes and the hexaqua Fe(II) ion.[106] Stability constants for the mononuclear Fe(III) hydroxyl complexes are generally presented in the form of cumulative constants, log $\beta_j$, for reactions like

$$Fe^{3+} + jH_2O = [Fe(OH)_j]^{(3-j)+} + jH^+ \quad (11)$$

Stability constants for $[FeOH]^{2+}$ at $I = 0.7$ are listed in Table 4, and Byrne et al.[107] tabulated stability constants for $[FeOH]^{2+}$ over the ionic strength range 0.01−6.00 *m*. The data at $I = 0.7$ show good reproducibility mainly because the experimental conditions used are such that only mononuclear species are formed, high Fe concentrations and high

**Table 5. Hydrolysis Constants for Fe(III) at 25 °C and $I = 0.7$ M**

| species | medium | log $\beta_j$ | ref |
|---|---|---|---|
| $FeOH^{2+}$ | NaCl | −2.52 | 116 |
| | $NaClO_4$ | −2.68 | 111 |
| | | −2.75 | 103 |
| | | −2.71 | 112 |
| | | −2.62 | 105 |
| | | −2.71 | 113 |
| $Fe(OH)_2^+$ | NaCl | −6.5 | 116 |
| | $NaClO_4$ | −6.29 | 111 |
| | | < −6.97 | 103 |
| | | −6.0 | 112 |
| | | ≤ −7.0 | 113 |
| $Fe(OH)_3^0$ | NaCl | −15.0 | 116 |
| | $NaClO_4$ | < −12.54 | 111 |
| | | ≤ −13.6 | 113 |
| $Fe(OH)_4^-$ | NaCl | −22.8 | 116 |
| | $NaClO_4$ | −21.86 | 111 |
| $Fe(OH)_3$ | NaCl | 4.2 | 116 |

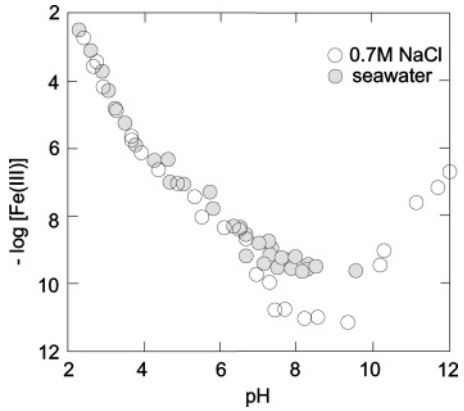


**Figure 13.** Graphical representation of experimentally determined iron(III) hydroxy complex stability. Based on data collected by Liu and Millero.[154] Reproduced from ref 154, Copyright 2002, with permission from Elsevier.

acidities[108] or Fe concentrations ≤ $10^{-44}$ M.[109,110] Table 5 lists stability constants for the common Fe(III) hydroxyl species. As the pH and iron concentration increase, polynuclear species like $[Fe_2(OH)_2]^{4+}$ and $[Fe_3(OH)_5]^{4+}$ and higher order polymers become important,[111,112] and $[FeOH]^{2+}$ becomes a relatively minor species. Measurements of the stability of $[Fe(OH)_2]^+$ are relatively scarce.[111] $[Fe(OH)_2]^+$, if it exists, is insensitive spectrophotometrically and is within the uncertainty of halide potentiometric studies.[113] Certainly, the stability is much lower than is widely cited in the older literature. $[Fe(OH)_3]^0$ stability has been measured by solubility methods, which are prone to considerable uncertainties because of the changing nature of the reactant and the problems of separation of the dissolved species. Byrne at al.[113] suggested that the solubility constant for $Fe(OH)_3$ is not a constant but is pH dependent. They interpreted the pH dependency in terms of changing particle size for the $Fe(OH)_3$ precipitate with pH rather than due to the reactant containing $Cl^-$ or $NO_3^-$.[114,115] Workers in this field tend to present Fe solubility results in terms of the ideal iron(III) hydroxide, $Fe(OH)_3$. As mentioned above, the composition of this phase is not well-known and may vary, thus further contributing to uncertainties in the measurement of its solubility.

Figure 13 shows the experimental measurements of the Fe(III) hydroxy complex stability data collected by Liu and Millero.[116] These are probably the most precise data obtained

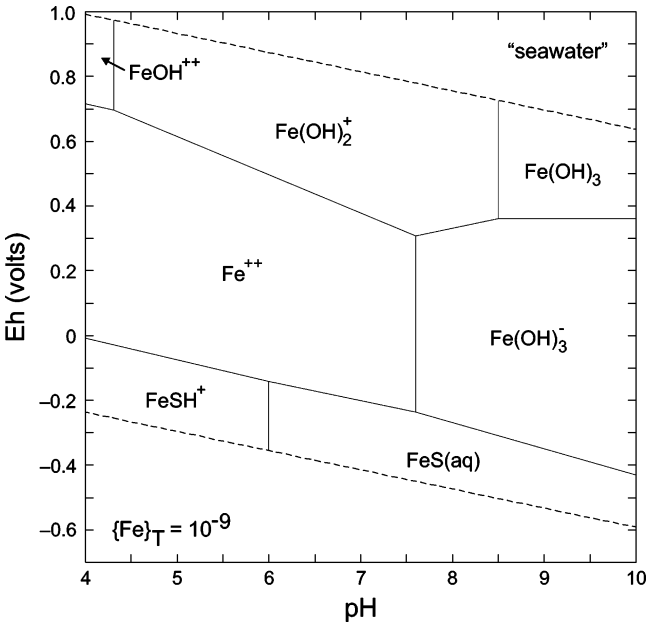


**Figure 14.** pH−Eh diagram of the relative stability of the inorganic dissolved Fe species in an inorganic solution with an average seawater composition and a total dissolved Fe(II) activity of $10^{-9}$.

to date. They used an $^{59}Fe$ isotope tracer analytical method for dissolved Fe(III). Previous methods have been subject to various technical problems. Total dissolved Fe(III) here is defined as the Fe(III) that passes through a 20 nm filter after 1 week aging. Nanoparticulate iron (oxy)hydroxides would pass through this filter, of course, unless sufficiently concentrated Fe(III) was used so that the particles coagulated into larger masses. Even so, Byrne et al.'s[113] finding that the particle size of $Fe(OH)_3$ varies with pH might affect the filtration procedure. The 1 week aging is also significant because the kinetics of Fe(III) precipitation, especially at low Fe(III) concentrations, are relatively slow. Liu and Millero[116] explain the data in terms of four straight lines, reflecting four iron hydroxide complexes ($[FeOH]^{2+}$, $[Fe(OH)_2]^+$, $[Fe(OH)_3]^0$, and $[Fe(OH)_4]^-$). Their values for these four constants are compared with previous measurements in Table 4. Although the interpretation produces a fair description of the experimental data, there is actually limited independent evidence for the existence of complexes with these compositions, as mentioned above.

The relatively stability of the inorganic dissolved Fe species in an inorganic solution with an average seawater composition is shown in Figure 14. All these diagrams are for 25 °C and 1 bar total pressure, mainly because the availability of data for other conditions is limited. The "seawater" conditions are an approximation. We used the following free ion activities: log $\{Cl^-\} = -0.4462$, log $\{Na^+\} = -0.4958$, log $\{Mg^{2+}\} = -1.901$, log $\{SO_4^{2-}\} = -2.566$, log $\{K^+\} = -2.213$, log $\{Ca^{2+}\} = -2.833$, and log $\{HCO_3^-\} = -2.98$. These were computed by GWB from average surface seawater conditions with thermodynamic constants from the standard database incorporated with the program, which is based, in turn, on the Lawrence Livermore National Laboratory (LLNL) thermodynamic database of Delany and Lundeen.[117] In fact, the speciation is not overly sensitive to the precise value of these major ion activities since the Fe complexes with inorganic anions like $Cl^-$, $NO_3^-$, $SO_4^{2-}$, and $HCO_3^-$, are relatively weak. All mineral phases are suppressed. At pH ≈ 8, $Fe^{2+}$ and $[Fe(OH)_3]^-$ appear to be the dominant species, with $Fe^{2+}$ becoming more important

at acid pH values as suggested by Turner et al.[106] The Fe(III) hydroxyl complexes become significant in systems with high Eh value. Note that sulfide complexes dominate in the sulfide zone, where $S(-II) > SO_4^{2-}$, and are discussed below.

The difference between the Fe(III) solubility in inorganic media such as NaCl or $NaClO_4$ at seawater ionic strength ($I = 0.7$) and seawater itself is shown by inspection of the measured stability constants for the proposed complexes in Table 5. The values of log $\beta_1$ and log $\beta_2$ are similar to those in inorganic media, but the value of log $\beta_3$ is higher. The result is due to the formation of Fe(III) organic compounds. The result is significant because the experimentally measured solubility of Fe(III) in inorganic media (Figure 13) reaches a minimum around seawater pH, where $Fe(OH)_3^0$ may be a dominant Fe(III) hydroxy species. The formation of organic Fe(III) complexes therefore becomes particularly important in ocean water Fe chemistry. As shown in Figure 13, the measured concentration of dissolved Fe(III), or at least that fraction that is <20 nm in size, is some 2 orders of magnitude higher in normal surface seawater (pH $\approx$ 8) than in an inorganic solvent of similar ionic strength.

Van den Berg,[118] Rue and Bruland,[119] and Wu and Luther[120] provided the first evidence that dissolved Fe(III) in seawater is strongly chelated by 0.4−2.0 nmol $kg^{-1}$ Fe(III)-binding ligands. Rue and Bruland[119] divided these into two classes: 0.3−0.4 nmol $kg^{-1}$ of a strong ligand ($L_1$) with a conditional solubility constant on the Fe scale (not accounting for the side reaction coefficients of inorganic Fe(III)) of $10^{12.5}-10^{13}$ $M^{-1}$ and 0.2−1.5 nmol $kg^{-1}$ of a weak ligand ($L_2$) with a conditional stability constant of $10^{11.5}-10^{11.8}$ $M^{-1}$. The detailed nature of the organic ligands is unknown, and the data obtained by a variety of workers in different waters show that the range of conditional stability constants is $10^{8.6}-10^{13}$ $M^{-1}$, indicating that the division of ligands into two classes is artificial.

Witter et al.[121] used both a kinetic and a thermodynamic approach to measure the binding of unknown natural ligands to Fe(III) in seawater and then compared those data with the data obtained from three porphyrin compounds and five siderophores. The kinetic data provided an assessment of both $k_f$ and $k_d$ for Fe(III)−ligand binding from which $K$ could be calculated. $K$ data from both kinetic and thermodynamic experimental approaches gave similar results. Interestingly both porphyrins and siderophores gave a wide range of kinetic constants, so it was not possible to indicate which ligand may be present in any given natural sample. Microbial siderophores and porphyrins gave conditional stability constants within the range found for the Fe(III) binding ligands in seawater samples, but the range is $10^{11}-10^{13}$ $M^{-1}$ for porphyrins and $10^{10}-10^{13}$ $M^{-1}$ for siderophores. Rose and Waite[122] found similar kinetic and thermodynamic data for unknown Fe(III) binding ligands in coastal waters. Barbeau et al.[123] reported photodegradation of Fe(III) binding ligands and reduction to Fe(II) in laboratory experiments with a known α-hydroxy siderophore (aquachelin) and a lowering of the conditional stability constant by 0.7 log units for the photodegraded byproduct. Using samples from the Gulf of Mexico, Powell and Wilson-Fineli[124] showed similar photodegradation behavior, but Rijkenberg et al.,[125] who studied estuarine water samples, did not.

Bruland and Lohan[126] note that in the ocean, where Fe is biologically limiting, an individual Fe atom might be in a different form each day: an iron(III)−siderophore, intracellular photosynthetic proteins, an iron−porphyrin cell lysis product, or assimilated by diatoms. If the diatom is then digested by a copepod and excreted as part of a fecal pellet, it would enter the marine sediment reservoir[126] and be a source of Fe for iron sulfides. Of course, the siderophore and other biological activity are also ongoing in this environment, too. The role of organic complexes and colloids in the bioinorganic chemistry of acid volatile sulfide (AVS) environments is not well understood. Luther et al.[127] examined organic ligands in saltmarsh sediments and concluded that organic ligands were involved in seasonal iron cycling. They suggested that multidentate organic chelates containing oxygen, such as carboxylate and catecholate groups, complex Fe(III).

The concentration of particulate Fe in ocean waters can be as high as 5 nmol $kg^{-1}$ in continental shelf waters but is generally 0.1−0.3 nmol $kg^{-1}$.[128,129] The concentrations increase from 0.1 nmol $kg^{-1}$ at the surface to 0.4 nmol $kg^{-1}$ at depth.[126] In inshore and estuarine environments, extreme total Fe concentrations can be measured, such as up to 40 μM in the waters of Galveston Bay.[130] In these Fe-rich systems, it would appear that the solubility of inorganic Fe species controls the dissolved Fe concentration since the total Fe is likely to exceed the total concentration of Fe(III) chelating organic compounds.

A listing of stability constants for iron oxide solids is shown in Table 6. The stable mineral phases in the Fe−$H_2O$ system at 25 °C and 1 bar pressure are hematite (α-$Fe_2O_3$), magnetite (α-$Fe_3O_4$), and wüstite (FeO). However, in these low-temperature aqueous systems, formation of these phases is kinetically hindered, and the major observed phase appears to be nanoparticulate goethite, α-FeOOH.[141] This is in accord with the stability diagram for Fe−$H_2O$ at nanomolar $\{Fe\}_T$ with the stable phases kinetically suppressed (Figure 15d).

Experimentally, the initial inorganic precipitate in oxic aqueous systems usually appears to be ferrihydrite, whose composition is uncertain. It was thought to be equivalent to ferric hydroxide, $Fe(OH)_3$, but this is now questioned. Its approximate composition appears to be more like $5Fe_2O_3 \cdot 9H_2O$.[142] Other formulations include $Fe_5O_7(OH) \cdot 4H_2O$, $Fe_5O_3(OH)_9$, and $Fe_4O_5(OH)_2 \cdot 2.6H_2O$.[143,144] It appears in two structural forms related to the degree of crystallinity known as two- and six-line ferrihydrite although the differences are more likely to result from differences in the dimensions in their coherence domains.[145] Ferrihydrite is metastable and transforms to goethite, α-FeOOH, and hematite, α-$Fe_2O_3$. Suppression of goethite in the stability diagram at nanomolar $\{Fe\}_T$ reveals that six-line ferrihydrite appears with a somewhat reduced stability region compared with goethite (Figure 15e). Also, two-line ferrihydrite appears if six-line ferrihydrite is suppressed (Figure 15f).

Obviously, in the natural system the nature of the iron(III) (oxy)(hydr)oxide reactant will depend on its history, particularly how long the material has been exposed to the aqueous solution. The transformation of ferrihydrite in solution is highly dependent on pH,[146,147] but even in the relatively alkaline oceanic environments, the major observed phases appear to be more stable nanoparticulate goethite. Alternatively, it has been suggested that iron-reducing bacteria preferentially utilize the more metastable phases and this contributes to the persistence of the more stable phases.[148,149] The net result is that a spectrum of iron(III)

**Table 6. Solubility Products of Iron Oxides and Green Rusts at 298.15 K, 1 bar[a]**

| composition | mineral name | $\Delta G_f^\circ$ (kJ mol$^{-1}$) | reaction | log $K$ |
|---|---|---|---|---|
| $Fe_3O_4$ | magnetite | −1015.5 | $Fe_3O_4 + 8H^+ = 2Fe^{3+} + Fe^{2+} + 4H_2O$ | 10.0[b] |
| $\alpha$-$Fe_2O_3$ | hematite | −755.5 | $\alpha$-$Fe_2O_3 + 6H^+ = 2Fe^{3+} + 3H_2O$ | −1.7[c] |
| $\gamma$-$Fe_2O_3$ | maghemite | −727.9 | $\gamma$-$Fe_2O_3 + 6H^+ = 2Fe^{3+} + 3H_2O$ | 3.5[d] |
| $\epsilon$-$Fe_2O_3$ | | −717.8 | $\epsilon$-$Fe_2O_3 + 6H^+ = 2Fe^{3+} + 3H_2O$ | 4.7[e] |
| $\alpha$-FeOOH | goethite | −488.8 | $\alpha$-FeOOH + $3H^+ = Fe^{3+} + 2H_2O$ | 0.4[f] |
| $\gamma$-FeOOH | lepidocrocite | −469.7 | $\gamma$-FeOOH + $3H^+ = Fe^{3+} + 2H_2O$ | 3.7[g] |
| $Fe(OH)_2$ | | −489.8 | $Fe(OH)_2 + 2H^+ = Fe^{2+} + 2H_2O$ | 12.8[h] |
| $Fe(OH)_3$ | two-line ferrihydrite | −708.5 | $Fe(OH)_3 + 3H^+ = Fe^{3+} + 3H_2O$ | 3.4[d] |
| $Fe(OH)_3$ | six-line ferrihydrite | −711.0 | $Fe(OH)_3 + 3H^+ = Fe^{3+} + 3H_2O$ | 3.0[d] |
| $Fe^{II}_3Fe^{III}(OH)_8Cl$ | GR1($Cl^-$) | −2145.0 | $Fe_4(OH)_8Cl + 8H^+ = 3Fe^{2+} + Fe^{3+} + Cl^- + 8H_2O$ | 28.3[i] |
| $Fe^{II}_4Fe^{III}_2(OH)_{12}CO_3$ | GR1($CO_3^{2-}$) | −3588.0 | $Fe_6(OH)_{12}CO_3 + 13H^+ = 4Fe^{2+} + 2Fe^{3+} + HCO_3^- + 12H_2O$ | 39.1[j] |
| $Fe^{II}_4Fe^{III}_2(OH)_{12}SO_4$ | GR2($SO_4^{2-}$) | −3785.0 | $Fe_6(OH)_{12}SO_4 + 12H^+ = 4Fe^{2+} + 2Fe^{3+} + SO_4^{2-} + 12H_2O$ | 3.9[h] |
| $Fe^{III}_2Fe^{II}(OH)_8$ | ferrosoferric hydroxide | −1681.0 | $Fe_3(OH)_8 + 8H^+ = 2Fe^{3+} + Fe^{2+} + 8H_2O$ | 59.4[j] |
| $Fe^{II}_2Fe^{III}(OH)_7$ | fougerite | −1770.0 | $Fe_3(OH)_7 + e^- + 7H^+ = 3Fe^{2+} + 7H_2O$ | 28.2[l] |
| $Fe^{II}Fe^{III}(OH)_5$ | hydroxy GR1 | −1244.1 | $Fe_2(OH)_5 + e^- + 5H^+ = 2Fe^{2+} + 5H_2O$ | 25.4[l] |
| $Fe^{III}_2Fe^{II}(OH)_8$ | hydroxy GR2 | −1944.3 | $Fe_3(OH)_8 + 2e^- + 8H^+ = 3Fe^{2+} + 8H_2O$ | 45.8[l] |
| $FeO(OH)_{0.74}(SO_4)_{0.13}$ | schwertmannite | −518.0 | $FeO(OH)_{0.74}(SO_4)_{0.13} + 2.74H^+ = Fe^{3+} + 0.13SO_4^{2-} + 1.74H_2O$ | 0.9[m] |

[a] All values are consistent with $\Delta G_f^\circ(H_2O) = -237.13$ kJ mol$^{-1}$,[88] $\Delta G_f^\circ(Fe^{2+}) = -90.5 \pm 1$ kJ mol$^{-1}$,[99] and $\Delta G_f^\circ(Fe^{3+}) = -16.8 \pm 1$ kJ mol$^{-1}$.[99] [b] Reference 131. [c] From $E^\circ = 0.72$ V for the reaction hematite + $6H^+ + 2e^- = 2Fe^{2+} + 3H_2O$.[132] [d] Reference 140. Ferrihydrite has various compositions (see text), and the stability data are given for the formulation $Fe(OH)_3$. [e] Ref 133 as calculated by Majzlan et al..[140] [f] Reference 99. [g] Reference 134. [h] Reference 135. [i] Reference 136. [j] Reference 137 with $CO_3^{2-} + H^+ = HCO_3^-$, log $K = 10.35$. [k] From $E^\circ = 51.373$ V for the reaction $Fe_3(OH)_8 + 8H^+ + 2e^- = 3Fe^{2+} + 8H_2O$.[138] [l] Reference 155. [m] Reference 139 and $\Delta G_f^\circ$ for ideal $FeO(OH)_{0.75}(SO_4)_{0.125}$.[140] Majzlan et al.[140] used $\Delta G_f^\circ$ values for $Fe^{3+}$ (−16.7 kJ mol$^{-1}$), $H_2O$ (−237.1 kJ mol$^{-1}$), and $SO_4^{2-}$ (−744.0 kJ mol$^{-1}$).

oxides, oxyhydroxides, and hydroxides occur in the environment with different stabilities and reactivities.[150,151]

There has been considerable interest by the soil chemists in a series of mixed Fe(II)/Fe(III) compounds collectively know as the green rusts (GR).[152] These compounds are readily prepared in the laboratory: precipitated $Fe(OH)_2$ is white, but it rapidly turns blue and blue−green in water with the evolution of $H_2$ gas as the GRs develop. They are believed to be responsible for the blue−green color of waterlogged soils, which turn ochrous when exposed to the atmosphere.[150] A GR-type mineral, with the suggested name "fougerite", was first observed in soils by Trolard et al.[153] The GRs included compounds with $Cl^-$, $CO_3^{2-}$, or $SO_4^{2-}$ as their dominant anion. Ponnamperuma et al.[138] proposed ferrosoferric hydroxide, which appears to be analogous to the end-member hydroxyl GRs defined by Bourrie et al.[155] Schwertmannite, an iron(III) oxyhydroxysulfate with a structure related to that of $\beta$-FeOOH, was first defined by Bigham et al.[156] and occurs mainly in environments affected by acid mine drainage. The stability of these phases has been studied, and the estimated values of their solubility constants and free energies of formation are listed in Table 6, together with simple oxides and oxyhydroxides.

Even at nanomolar $\{Fe\}_T$, fougerite, the mixed Fe(II)Fe(III) hydroxide, $Fe^{II}_2Fe^{III}(OH)_7$, appears in the stability diagrams where goethite is suppressed. The phase appears in the important pH zone around 7.5−8.0, and these data would suggest that even in normal ocean water, fougerite is an additional possible precursor to goethite. However, in inshore and estuarine waters where $\{Fe\}_T$ may reach micromolar values, fougerite appears to occupy a major stability region (Figure 15a−c.). Even in the presence of goethite, fougerite appears to be stable (Figure 15a). And, if goethite is suppressed, fougerite appears to dominate the major seawater environment at Eh < +300 mV at pH 7−8. These calculations are instructive because Fe(II) is formed by photodegradation processes[123,125] and has been measured as a dissolved entity in seawater.[122,157] The data suggest that a mixed oxidation state iron hydroxide phase may be a significant precursor to the iron sulfides.

Figure 16 shows the Fe phases involved in the theoretical "seawater" described above. The surprising thing is the appearance of the sulfate green rust 2 ($GR2SO_4$), the mixed iron hydroxide with sulfate, $Fe^{II}_4Fe^{III}_2(OH)_{12}SO_4$. Again goethite dominates the more oxidized water systems, but $GR2SO_4$ replaces the pure mixed iron hydroxide, fougerite, and displays an increased stability region. Indeed, it is stable in the presence of goethite at nanomolar $\{Fe\}_T$ (Figure 16d), and its stability region becomes even more extensive at micromolar $\{Fe\}_T$ (Figure 16a). In these systems, we have included pyrite to show the relationships between goethite and the ferrihydrites, $GR2SO_4$, and the iron sulfides. At nanomolar $\{Fe\}_T$, there is no direct relationship between the iron(oxy)hydroxides and pyrite. None of the phases have any stability in the intermediate zone, and pyrite is separated from the iron (oxy)hydroxides by the solution species $Fe^{2+}$ and $Fe(OH)_3^-$. Note that these species are Fe(II) species and not Fe(III) species, which are limited to far more oxidized systems. It has been widely noted that microorganisms do not perform any chemical transformation that is thermodynamically impossible (e.g., ref 158), and the presence of organisms that make a living from the reduction of Fe(III) to Fe(II) in this region is consistent with the thermodynamics.

At micromolar $\{Fe\}_T$ values, $GR2SO_4$ has a wide stability region and forms a direct link between goethite and pyrite (Figure 16a). In the presence of the less stable ferrihydrites, $GR2SO_4$ becomes even more significant (Figure 16b,c). Note that $\{Cl^-\}$ and $\{HCO_3^-\}$ in normal seawater are insufficient for the other GR2s with Cl and $CO_3$ to form. Note also the absence of $FeCO_3$, siderite, which, although a stable phase, is limited to sulfide-free waters. The other surprising aspect of the numbers in Table 6 is the relative stability of schwertmannite, $FeO(OH)_{0.74}(SO_4)_{0.13}$. It is unstable with respect to goethite (Figures 16a,d) but displays a significant stability zone relative to the ferrihydrites (Figure 16b,c,e,f). The schwertmannite stability zone is generally limited to acid

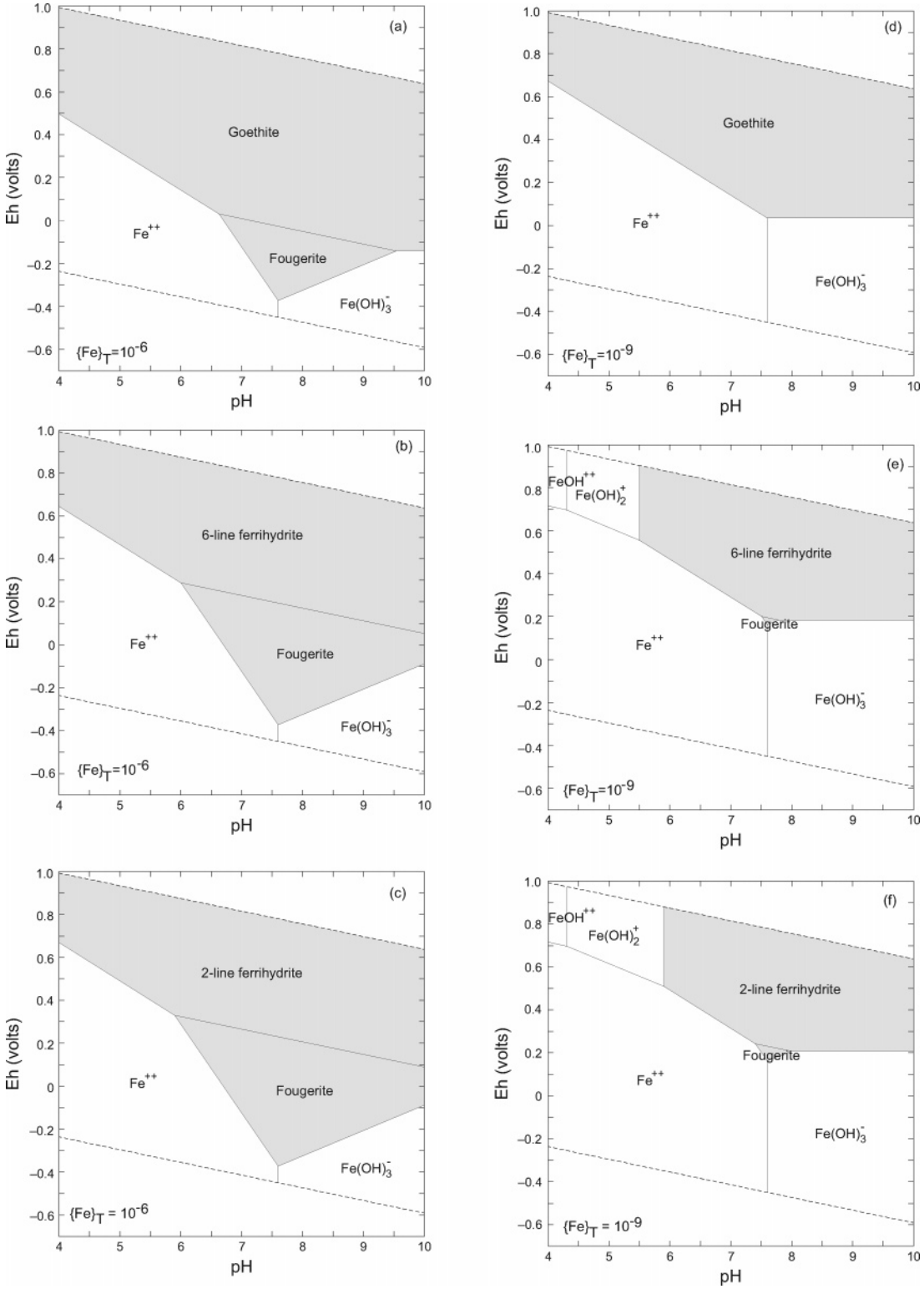


**Figure 15.** Distribution of species and phases in the $Fe-H_2O$ system at nanomolar and micromolar $\sum\{Fe\}_T$, 25 °C, and 1 bar total pressure. The diagrams show the successive distribution of metastables phases as more stable phases are sequentially removed (see text).

oxic environments, as suggested by its discovery in acid mine water systems. However, if the supposed relative stability of the ferrihydrites and goethite reflects a sequence of transformations in the iron (oxy)hydroxides from two-line ferrihydrite to six-line ferrihydrite to goethite, then schwertmannite must be considered as a possible early contributor, even at pH 8, in micromolar $\{Fe\}_T$ systems (Figure 16c).

If the reported estimates of the stabilities of the mixed Fe(II)/Fe(III) hydroxides are correct, they appear to have the potential for a far wider spread in the marine environment than previously supposed. Schwertmannite is metastable with respect to goethite but has a more extensive region of stability in seawater than two-line ferrihydrite. Fougerite appears to be a potential stable phase, but $GR2SO_4$ is noticeably stable in marine conditions. It took over 30 years for a GR mineral phase to be identified and isolated from soil environments after their occurrence was first mooted. The reason was their relatively low concentration and nanoparticulate size.

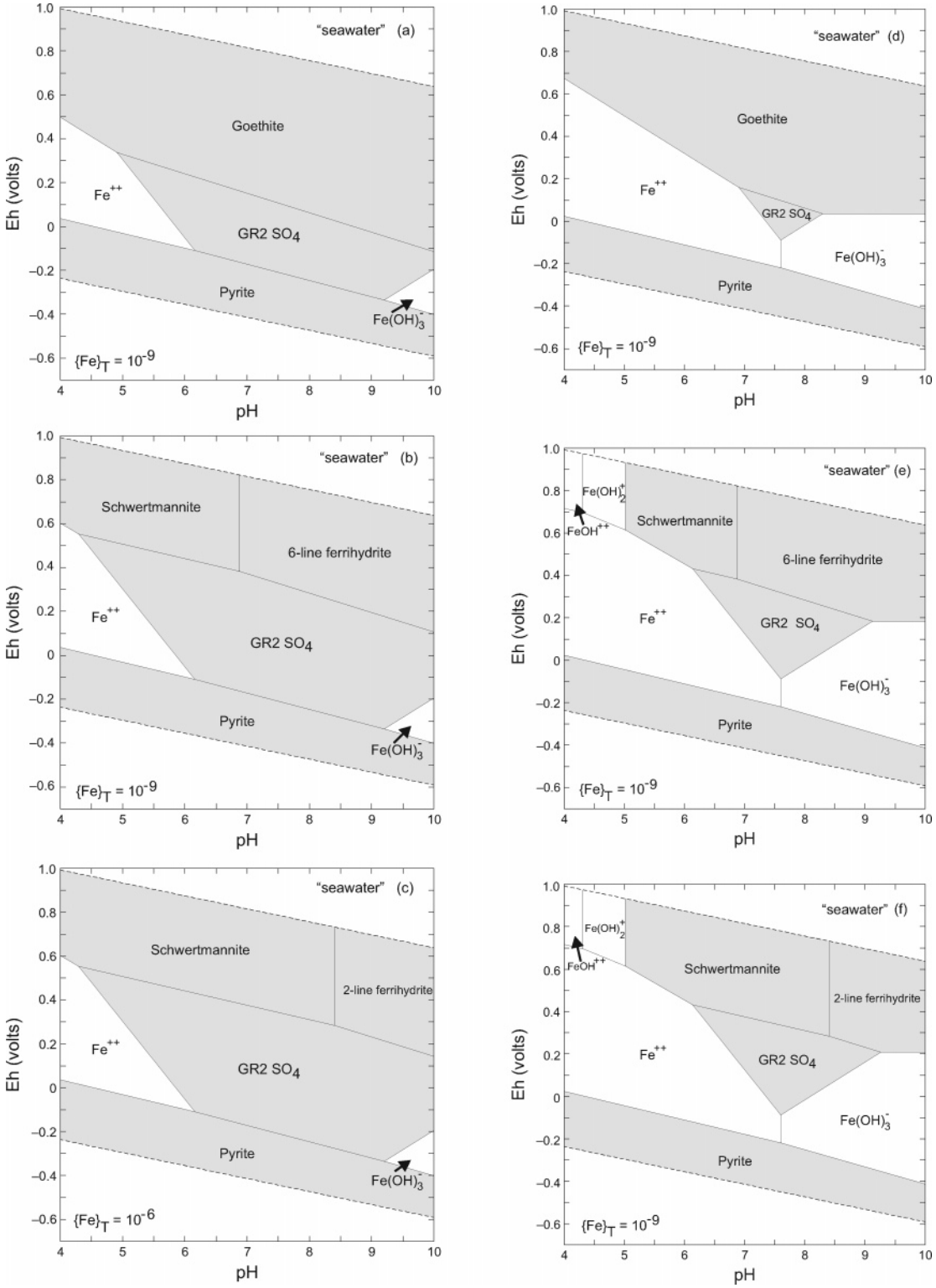


**Figure 16.** Distribution of species and phases in the iron−seawater system at nanomolar and micromolar $\sum\{Fe\}_T$, 25 °C, and 1 bar total pressure. The diagrams show the successive distribution of metastables phases as more stable phases are sequentially removed (see text).

However, the reported thermodynamic data imply that these phases could occur in marine environments especially where oxygen minimum zones occur in the water column (e.g., the Arabian Sea and the equatorial Pacific Ocean). In addition to the production of Fe(II) by photochemical processes in the surface ocean and the release of ferredoxins on lysis of planktonic material, these phases may also be found in marine snow aggregates or particles, which have been shown to contain low oxygen and elevated trace metals.[159,160] If mixed Fe(II)/Fe(III) material is present in particles formed in the oxic or suboxic ocean, then the chemistry and dynamics of the Fe supply to sulfidic zones in marine systems will need to be revisited.

Further support for the presence of Fe(II) species and other reduced material in oxic waters comes from the determination of (sub)nanomolar levels of sulfide in oxic oceanic waters,[161,162] even though sulfate is the thermodynamically stable form of sulfur under oxic conditions (section 2.1). The

**Table 7. Formation Constants for $FeSH^+$**

| $\log \beta_1$ | medium | method | ref |
|---|---|---|---|
| 1.4 | $I = 0$ | linear free energy | 168 |
| $5.5 \pm 0.24$ | $I = 0.7$ | voltammetry | 182 |
| $5.3 \pm 0.1$ | $I = 0.7$ | voltammetry | 169 |
| $5.07 \pm 0.12$ | $I = 0.7$ | voltammetry | 172 |
| $4.34 \pm 0.15$ | $I = 0$ | spectrophotometry | 171 |
| <3 | $I = 0$ | FeS solubility | 174 |
| 5.94 | seawater | voltammetry | 175 |

presence of sulfide at such low levels has been linked to decomposition processes related to marine snow,[159,160] to decomposition of OCS,[163] and to production by phytoplankton when exposed to elevated metal concentrations.[164] Although the form(s) has not been identified conclusively, manipulations of samples and laboratory solutions indicate that the sulfide is bound to trace metals such as Cu and Zn but not Fe.[163,164,165] Luther and Rickard[166] suggested that cluster species such as $M_3S_3$ and $M_4S_6^{4-}$ and nanoparticles, which can come through 0.2 and 0.4 $\mu$m filters, most likely stabilize the sulfide in oxic waters.

## 4. Iron Sulfide Complexes and Clusters

Several studies of sulfide complexation of Fe(II) have been reported using both solubility and voltammetric approaches.[82,83,167−178] Earlier work was reviewed by Emerson et al.,[179] Davison,[180,181] and Morse et al.,[3] and recent reviews are included in Rickard and Morse[1] and in Rickard and Luther.[2]

Aqueous iron−sulfide complexes play a potentially important role in the chemistry of iron sulfides in marine systems.[1,168−170,174,175,181−183] Reported measurements for the constants for the reaction

$$Fe^{2+} + HS^- = FeSH^+ \qquad (12)$$

are listed in Table 7.

Dyrssen's[168] estimate was made using an isovalent−isostructural analogue approach and is obviously out of line with the later measurements. Since the method involved using linear interpolation, Dyrssen's values for $Fe(SH)_2^0$ and $FeHS_2^-$ must also be uncertain. The independent measurements for the stability of $Fe(SH)^+$ [169,172] show a degree of congruency, which suggests some confidence in a log $\beta_1$ value close to 5.2. The value for seawater measured by Al-Farawati and van den Berg[175] incorporates a measured side reaction coefficient of 0.16. Luther et al.[172] also provided experimental evidence for the stoichiometry of this complex. They demonstrated that the Fe/S ratio is 1:1 and that the complex includes one proton. Wei and Osseo-Asare[171] measured a lower stability constant of $\log K = 4.34 \pm 0.15$ at 25 °C ($I = 0$) for $[Fe(SH)]^+$ by using a stopped-flow spectrophotometric technique. They monitored the peak at 500 nm, which they attributed to the first formed transient intermediate, $[Fe(SH)]^+$, when Fe(II) and sulfide react at pH > 7. This species is metastable and eventually decomposes to FeS via several possible pathways. However, curve fitting from solubility studies[174] shows that the $[Fe(SH)]^+$ stability constant does not fit the measured solubility. Davison et al.[174] found that the solubility of mackinawite, $FeS_m$, could be partially explained by $[Fe(SH)]^+$ using a constant at least two logarithmic units smaller than the measured values. This result has been confirmed by Rickard.[178]

**Table 8. Summary of Stability Constants for Proposed Iron Sulfide Complexes and the Methods Used**

| species | $\log K$ | $I$ | method | ref |
|---|---|---|---|---|
| $[Fe(SH)]^+$ | 5.94 | 0.7 | sulfide titration | 175 |
| | 5.3 | 0.7 | sulfide titration | 169 |
| | 4.34 | 0.0 | spectrophotometry | 171 |
| | 5.07 | 0.7 | sulfide titration | 172 |
| | 1.4 | 0.0 | linear free energy | 168 |
| | 5.5 | 0.7 | voltammetry | 182 |
| $[Fe(SH)_2]^0$ | 8.9 | 0.0 | linear free energy | 168 |
| | 6.45 | 0.0 | solubility | 174[a] |
| | 6.0 | 0.11 | solubility | 184 |
| $[Fe(SH)_3]^-$ | 9.28 | 0.18 | solubility | 184 |
| $[Fe_2(SH)]^{3+}$ | 10.07 | 0.7 | sulfide titration | 172 |
| $[Fe_3(SH)]^{5+}$ | 16.15 | 0.7 | sulfide titration | 172 |
| $[Fe(S_4)]^0$ | 5.97 | 0.55 | sulfide titration | 83 |
| $[Fe_2(S_4)]^{2+}$ | 11.34 | 0.55 | sulfide titration | 83 |
| $[Fe(S_5)]$ | 5.69 | 0.55 | sulfide titration | 82 |
| $[Fe_2(S_5)]^{2+}$ | 11.30 | 0.55 | sulfide titration | 82 |
| $FeS^0$ | −0.6 | 0 | linear free energy | 168 |
| | −2.2 | 0 | solubility | 178[b] |
| $Fe_2S_2$ | −0.48 | 0.01 | voltammetry | 185 |

[a] Davison et al.[174] suggests that the species is probably polymeric $Fe_x(SH)_{2x}$ with $x \geq 2$. [b] $Fe_xS_x^0$ ($x \geq 1$) modeled as the monomer.

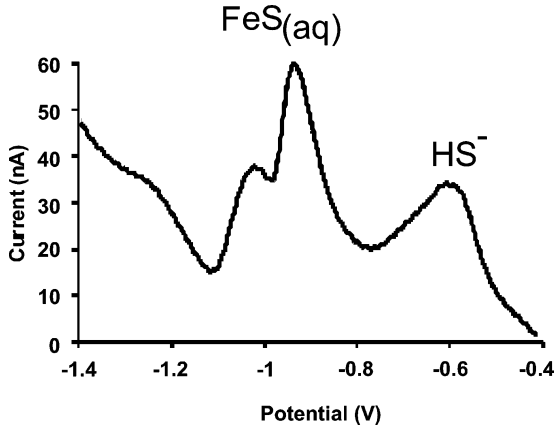


**Figure 17.** Conventional square wave voltammetric scan of an Fe−S solution showing the typical split peak at around −1.1 V, which is assigned to FeS(aq). Reprinted from ref 1, Copyright 2005, with permission from Elsevier.

Table 8 lists all the iron sulfide complexes that have been suggested and their proposed stability constants. The stability of further bisulfide complexes, such as $[Fe(SH)_2]^0$ and $[Fe(SH)_3]^-$, is controversial.[172,174,175] The results of voltammetric titrations provide evidence for $[Fe(SH)]^+$ but no evidence for $[Fe(SH)_2]^0$ as was found in measurements of $FeS_m$ solubility.[178]

FeS clusters, termed here as FeS(aq), are well-known in biochemistry where they constitute the active centers of FeS proteins, such as ferredoxins, and occur in all organisms where they are responsible for basic electron transfer in many key biochemical pathways. Aqueous FeS clusters, in which various numbers of FeS molecules are ligated directly to $H_2O$ molecules, were first observed by Buffle et al.[186] in lake waters. They were characterized by Theberge and Luther[173] and Theberge[187] and are routinely probed electrochemically (Figure 17). Theberge and Luther[173] analyzed the characteristic wave form from the FeS clusters and showed that the 0.2 V split is consistent with the splitting of Fe(II) in tetrahedral geometries (Figure 18).

The stoichiometry of this $FeS_{aq}$ cluster species is presently unknown, although it has been suggested to include an $Fe_2S_2$ form[173,186] or, possibly, a $Fe_2(SH)_4$ composition.[188] These studies agree than it includes dominantly neutral species.

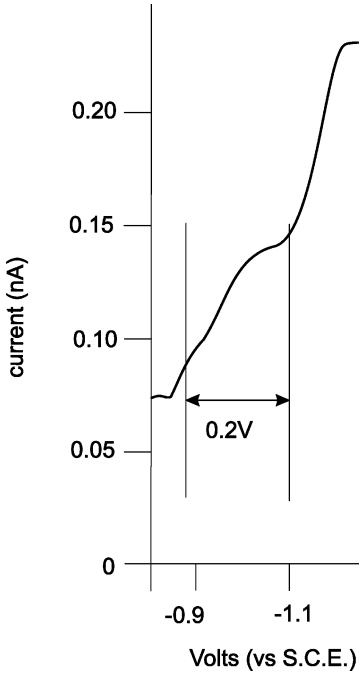


**Figure 18.** Sampled DC polarogram of an FeS cluster showing two waves with 0.2 V center−center distance, which reflect two single-electron transfers at the Hg electrode: $Fe^{2+} + 2e^- \rightarrow Fe^0$.[173,187] Reprinted from ref 1, Copyright 2005, with permission from Elsevier.

However, Theberge and Luther[173] pointed out that the data could actually fit any FeS phase with a 1:1 stoichiometry. Rickard[178] showed that the solutions developing from $FeS_m$ solubilization in neutral−alkaline systems showed the characteristic voltammetric signature of the aqueous FeS cluster and modeled the solubility using the monomer $FeS^0$ with a stability constant of $10^{2.2}$ for the acid dissociation reaction (eq 13).

$$FeS^0 + H^+ \rightarrow Fe^{2+} + HS^- \qquad (13)$$

The molecular form of the FeS clusters has been modeled by Luther and Rickard[166] with the HYPERCHEM program, using molecular mechanical calculations with the Polak−Ribiere algorithm where lone pair electrons are considered and the most stable configuration is computed (Figure 19). The interesting feature of these model structures is that they are very similar in form to the structure of the FeS centers in ferredoxins and show planar and cubane geometries. Since these are neutral species, the molecules are liganded directly with water. The structure of $Fe_2S_2$ is similar to the basic structural component of mackinawite (Figure 20, Table 9), which is the first condensed phase in the system.[189] Similar structural homologies for aqueous zinc and copper sulfide clusters and the first condensed phases in those systems led Luther et al.[190,191] to the suggestion that the form of the first condensed phase was determined in solution by the structure of the clusters. Other FeS cluster stoichiometries have been suggested.[192] These include sulfur-rich varieties, such as $[Fe_2S_4]^{4-}$, and metal-rich species, like $[Fe_nS_m]^{(n-m)+}$. These are consistent with the sulfide titrations of Luther et al.[172] (Table 8). It is important to note that these species will probably incorporate a counterion in natural systems to neutralize the charge. It appears that these counterions may be organic molecules.

The FeS(aq) cluster stoichiometry could range from $Fe_2S_2$ to $Fe_{150}S_{150}$, where the first condensed phase appears. The

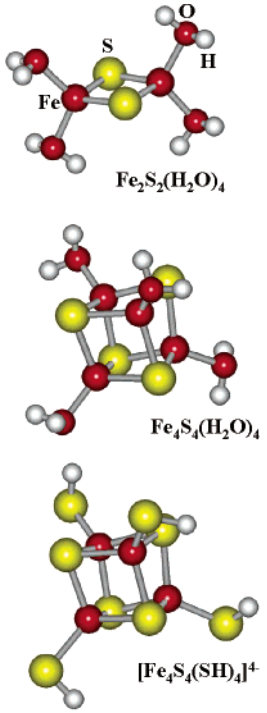


**Figure 19.** Molecular models of aqueous $Fe_2S_2$ and $Fe_4S_4$ clusters and the $Fe_4S_4(SH)_4^{4-}$ cluster prepared in nonaqueous solvents.[193]

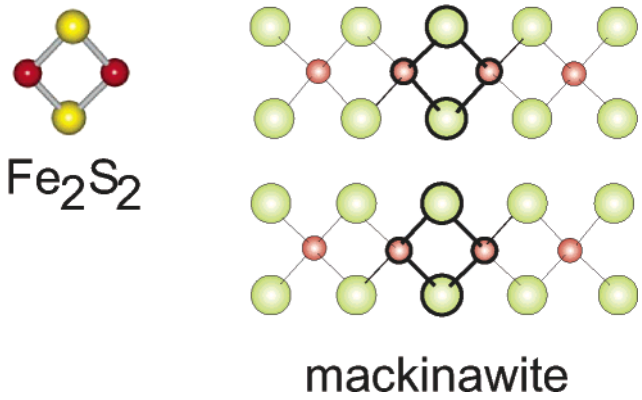


**Figure 20.** Homology between the structure of the aqueous $Fe_2S_2$ cluster and mackinawite. Similar structural congruities between aqueous clusters and the first condensed phase were found in the Cu−S and Zn−S systems and led to the theory that the form of the first condensed phase is controlled by the structure of the cluster in solution. Modified from ref 1, Copyright 2005, with permission from Elsevier.

**Table 9. Homology between the Structure of the Aqueous Iron Sulfide Clusters, $Fe_2S_2 \cdot 4H_2O$ and $Fe_4S_4 \cdot 4H_2O$, and Mackinawite in Terms of Bond Lengths and Bond Angles**[a]

| | $Fe_2S_2 \cdot 4H_2O$ | $Fe_4S_4 \cdot 4H_2O$ | mackinawite |
|---|---|---|---|
| Fe−S | 2.201 Å | 2.217 Å | 2.256 Å |
| Fe−Fe | 2.833 Å | 2.800 Å | 2.560 Å |
| Fe−S−Fe | 80.10° | 78.33° | 70.31° |
| S−Fe−S | 99.85° | 100.62° | 109.02° |

[a] The longer bond lengths of the aqueous forms are consistent with the ligation with $H_2O$ and the subsequent contraction in the continuous solid (from ref 1).

first condensed $FeS_m$ phase is 2 nm in size[194] and is thus potentially electroactive at voltammetric electrodes.[167] Luther and Rickard[166] discussed the problem of differentiating between classical dissolved complexes and nanoparticles at the scale of the first condensed phase in the FeS system.

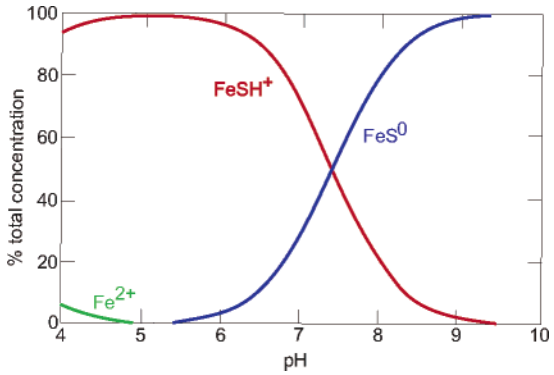


**Figure 21.** Distribution of iron sulfide complexes and clusters.

The first condensed phase has a size of around 2 nm and a volume on the order of 10 $nm^3$.[194] This compares with the smallest aqueous FeS cluster, $Fe_2S_2 \cdot 4H_2O$, which is about 0.5 nm in size and has a volume of around 0.125 $nm^3$. The variation is only about 100-fold in volume and 4-fold in length. The significant difference between the first condensed phase and the solution species is the density increase, which is on the order of $>10^6$, depending on the configuration of $H_2O$ around the FeS nanoparticle. This density discontinuity should provide a means of discriminating between dissolved species and nanoparticles, but this has not been achieved yet in the FeS system. Thus, aqueous FeS clusters are defined operationally in terms of their voltammetric characteristics.[166] Rickard[178] measured the intrinsic solubility of mackinawite in aqueous systems, and this led to the determination of the stability constant of the monomer, $FeS^0$. However, the maximum concentration of FeS(aq) in equilibrium with mackinawite is $10^{-5.88}$ M, in terms of the monomer, and this is at or below the detection limit of most physical−chemical probes available at present.

Aqueous FeS clusters, defined operationally in terms of their voltammetric characteristics, may make up a substantial fraction of the sulfide budget of many natural aqueous and sedimentary environments, including lakes,[177,180,186,195] river waters,[192] wetlands,[196] estuarine sediments,[2,183,197] marine sediments,[196,198,199] and deep ocean hydrothermal vents.[200]

The distribution of iron sulfide complexes and clusters in terms of the most probable species, $FeSH^+$, $FeS^0$, $Fe^{2+}$, and the iron hydroxy species described above and using the listed stability constants, is shown in Figure 21. This MINEQL+ computation shows that, with these figures and in the presence of excess S(−II), $FeS^0$ becomes the dominant species above pH = 7.5 and $FeHS^+$ in more acid solutions. The hexaqua $Fe^{2+}$ has a minor importance in sulfidic systems and becomes more significant at very acid pH values. The significance of $FeS^0$ in these pH regions is consistent with the electrochemical observation of the widespread distribution of FeS(aq) in marine systems noted above. Even with these limited data for iron sulfide complexes, we would predict that Fe-rich, polynuclear clusters should occur in systems where iron is enriched relative to sulfide, such as some fluvial or lacustrine systems, which again is consistent with observed natural data.

The distribution of iron sulfide complexes in the seawater-like matrix defined above is shown in Figure 22. In this system, we have used high S(−II) activities of $10^{-3}$ and high Fe(II) of $10^{-6}$, approaching millimolar sulfide and micromolar total iron. The computation is made with the GWB REACT algorithm with all minerals suppressed and with the $HS^-/SO_4^{2-}$ redox couple disabled. Figure 22a shows that

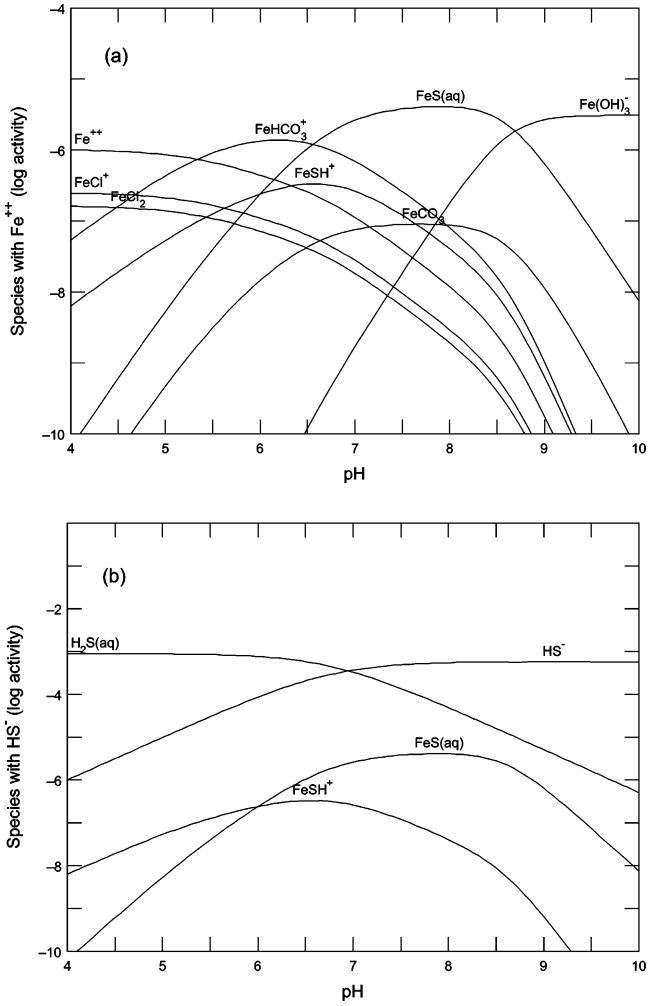


**Figure 22.** The distribution of iron sulfide complexes in the seawater-like matrix. In this system with high $\sum\{S(-II)\} = 10^{-3}$ and high $\sum\{Fe(II)\} = 10^{-6}$, FeS(aq) dominates Fe speciation and constitutes ca. 1% of the total S activity in the environmentally important pH range around neutral.

FeS(aq), calculated as the monomer $FeS^0$, is the dominant Fe species in the important marine pH region of 6.5−8.5. At higher pH, iron(II) hydroxyl species become important. At lower pH, the $FeHCO_3^+$ species is more significant than $FeSH^+$ or $Fe^{2+}$. This is interesting since sulfate-reducing prokaryotes, which provide the sulfide in these systems, produce 2 mol of carbonate for each mole of sulfide. So a significant $HCO_3^-$ concentration with consequent Fe complexation is not surprising. The close relationship of microbially produced carbonates and sulfides in these systems has been widely described.[201] $Fe^{2+}$(aq) becomes the dominant Fe species at pH < 5.5 and constitutes <1% of the total dissolved Fe at pH = 8. The lack of abundance of the free hexaqua Fe(II) in sulfidic systems may have considerable effects on the ecology of sulfidic environments.[200]

Of course, the iron sulfide complexes constitute a significant fraction of the dissolved sulfide budget in these systems (Figure 22b). With $10^{-3}$ $\{S\}_T$ and $10^{-6}$ $\{Fe\}_T$, FeS(aq) constitutes around 1% of the total S(−II) at pH = 8. However, if $\{S\}_T = \{Fe\}_T$, then this species will dominate the sulfide speciation. Rickard[178] noted that FeS(aq) would not form at $\{S\}_T < 10^{-6}$ in the presence of mackinawite, for example.

Pyrite is a low-spin ($d^6$, $t_{2g}^6$) iron(II) disulfide. Thus it is to be expected that Fe(II) should have significant polysulfide

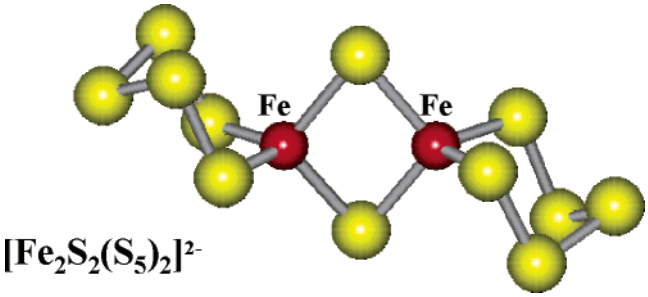


**Figure 23.** Molecular model for the tetrahedral $[Fe_2S_2(S_5)_2]^{4-}$ complex.

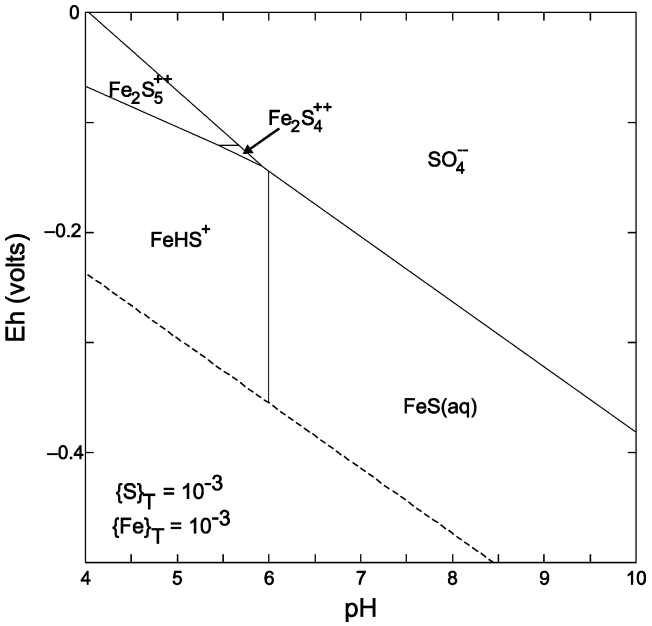


**Figure 24.** pH−Eh diagram showing the distribution of the iron polysulfide complexes (25 °C, 1 bar total pressure, $\sum\{Fe\} = \sum\{S\} = 10^{-3}$).

chemistry. Chadwell et al.[82,83] showed iron polysulfide complexes analogous to the manganese species with compositions $[Fe(\eta^1\text{-}S_4)]$, $[Fe(\eta^1\text{-}S_5)]$, $[Fe_2(\mu\text{-}S_4)]^{2+}$, and $[Fe_2(\mu\text{-}S_5)]^{2+}$. The formation of these iron(II) polysulfide complexes is interesting since they further suggest that non-protonated iron sulfide complexes could have a significant stability. Coucouvanis et al.[202] synthesized an interesting bidentate pentasulfido complex, $[Fe_2S_2(S_5)]^{4-}$, which has a $Fe_2S_2$ core similar to rubredoxin (Figure 23). Table 8 lists the iron sulfide complexes reported in aqueous solution.

The distribution of the iron polysulfide complexes in terms of a conventional pH−Eh diagram is shown in Figure 24. In this computation, all minerals are suppressed and the stable species $H_2S(aq)$ and $HS^-$ are removed. Even then, for the iron polysulfide to display a significant stability field, exceptionally high $\{Fe\}_T$ values are required ($10^{-3}$ in the case of Figure 24), as well as high $\{S\}_T$. The computations show that, under these conditions, the polynuclear forms $Fe_2S_4^{2+}$ and $Fe_2S_5^{2+}$ replace the simple aqueous polysulfide ions in pH−Eh space where sulfur is stable. The monomeric forms, $FeS_4$ and $FeS_5$, have no significant stability region.

Although an iron(III) sulfide with the composition $Fe_2S_3$ appears widely in the earlier literature,[203] the sulfide analog of hematite has not been isolated. However, the sulfide analog of magnetite, the cubic thiospinel greigite, $Fe_3S_{4g}$, is a well-established mineral phase, which can be readily synthesized at low temperatures. The synthesis always involves the precursor phase, mackinawite, and proceeds via a solid-state transformation.[1,204] The solid-state transformation would seem to preclude the formation of iron(III)-bearing sulfide complexes, and no such complexes have been isolated in aqueous solutions. However, the active centers of some FeS proteins are Fe(III)-bearing units and the Fe(II)−Fe(III) transition in these moieties are key to the biological electron-transfer processes. These clusters have similar cubane forms to the basic structural unit of greigite, and the occurrence of iron(III)-bearing sulfide clusters in aqueous solutions stabilized by organic ligands is possible.

## 5. Iron(II) Monosulfide: Mackinawite

The synthetic brownish black iron(II) monosulfide resulting from the reaction between aqueous S(−II) and Fe(II) at ambient temperatures has been described as *precipitated FeS* and *amorphous FeS*. The mineral equivalent was thought to have been a major constituent of *hydrotroilite*, an older term for the black iron sulfide material of sediments. Meyer et al.[205] reported it as a corrosion product of steel pipes and called it *kansite*. Berner[206] demonstrated that this material had a tetragonal structure. He identified this phase as *mackinawite*. We refer to this phase as $FeS_m$.

X-ray powder diffraction (XRPD) methods routinely used to examine the material give no pattern or show a broad peak around 5 Å. This has led to the uncertain identification of the phase in the literature. In fact, as shown through the recent work discussed below, this material always displays a mackinawite structure. Truly amorphous FeS has not been identified.

### 5.1. Mackinawite Structure

Kuovo et al.[207] described a tetragonal iron sulfide from the Outokumpu Mine, Finland. Evans et al.[208] defined this tetragonal iron sulfide as mackinawite, named from the type locality at the Mackinaw Mine, Washington. Much of the original information about the structure and composition of $FeS_m$ derives from this well-crystalline material from high-temperature monosulfide solid solution (mss) ore associations. The black iron(II) monosulfide precipitate formed at ambient temperatures in aqueous solution turned out to be identical to $FeS_m$ as defined by Evans et al.[208] Rickard[209] showed that long-range mackinawite ordering in precipitated iron(II) monosulfide developed within 1 h, and Lennie and Vaughan[210] were able to detect long-range mackinawite ordering in $FeS_m$ precipitates within 1 s of formation. Current work using extended X-ray absorption fine structure (EXAFS) and rapid flow techniques by Rickard and Vaughan's groups shows that the material develops between 1 and 10 ms after mixing Fe(II) and S(−II) solutions.

The tetragonal layer structure of mackinawite is shown in Figure 25. The cell parameters are $a = b = 3.6735$ Å and $c = 5.0329$ Å.[211] The iron atoms are linked in a tetrahedral coordination to four equidistant sulfur atoms. The Fe atoms form sheets with Fe in perfect square planar coordination and with an Fe−Fe distance of 2.5967 Å,[211] which is similar to the Fe−Fe distance in α-iron. Fe−Fe bonding is obviously substantial in this material. Vaughan and Ridout[212] originally suggested that the d electrons of mackinawite are extremely delocalized in this plane forming metallic bonds. The Fe sheets are stacked along the *c*-axis, with van der Waals forces between S atoms holding the sheets together.[213] The char-

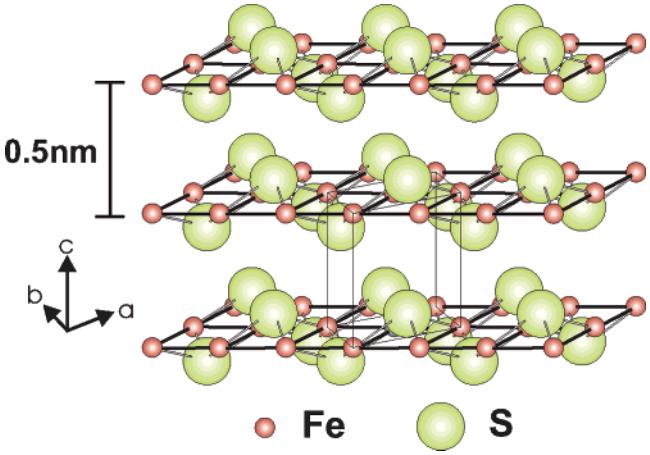


**Figure 25.** Mackinawite, $FeS_m$, structure. Modified from ref 1, Copyright 2005, with permission from Elsevier.

acteristic broad peak at around 5 Å, which is observed in conventional XRPD analyses of the fine-grained precipitates derives from the spacing of these layers. Lennie et al.[211] investigated the detailed structure of synthetic mackinawite using Rietveld analysis. They did not detect any crystallographic evidence for vacancy occupancy or surplus Fe occupancy. They found that the structure is almost perfectly regular, with a much smaller distortion than had been previously reported.

Wolthers et al.[189] used low-angle XRPD to show that synthetic $FeS_m$ is nanocrystalline and displays a tetragonal mackinawite structure. According to Wolthers et al.[189] the first-formed precipitate has an average particle size of 2.2 ± 1.7 nm and lattice parameters $a = b = 4.0$ Å and $c = 6.7$ ± 0.1 Å. Lattice expansion relative to bulk mackinawite was interpreted by Wolthers et al.[189] as being caused by either intercalation of water molecules between the tetrahedral sheets of the mackinawite structure or lattice relaxation due to small crystallite size. Neutron scattering analysis[214] of a synthetic mixture of greigite and mackinawite also showed the presence of 2 nm nanoparticles. Theoretically, the neutron scattering results could be explained equally well by nanoparticles or holes. However, Watson et al.[214] suggested that this material contained 2 nm nanoparticles rather than holes since this better explained the difference between the surface areas suggested by the measurements of trapped magnetic flux and those measured by Brunauer−Emmett−Teller (BET) methods. Michel et al.[215] used paired distribution function analysis of XRD collected at the Advanced Photon Source and concluded that the initial precipitate showed only minor relaxation compared with the bulk material. They also found that drying did not induce significant structural changes. Ohfuji and Rickard[194] showed that the first precipitated $FeS_m$ was in the form of plates elongated along the *c*-axis ranging in length from 3 to 10.8 nm and in thickness from 2 to 5.7 nm with a mean size of 5.6 nm × 3 nm. The smallest particles are more equidimensional, 3 nm × 2 nm in size (Figure 26). They measured the structure with high-resolution transmission electron microscopy (HR-TEM) and showed that the precipitated material showed a 3% relaxation in the *c*-axis ($d = 5.19$ Å) compared with the bulk and the freeze-dried material a 1% relaxation. They also showed that the material displayed various structural flaws consequent on its nanoparticulate size.

Independent confirmation of the $FeS_m$ nanoparticle size by HR-TEM is important because the Wolthers et al.[189]

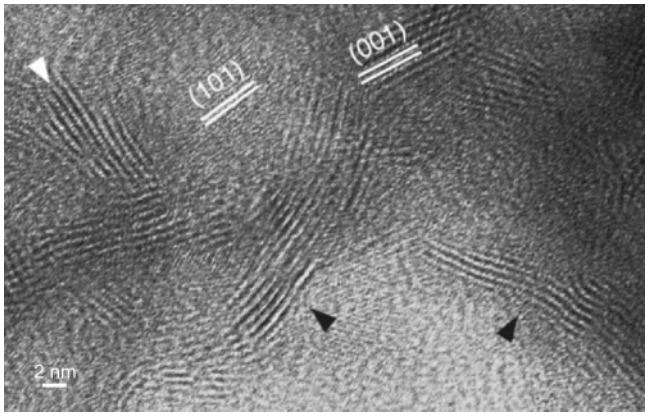


**Figure 26.** High-resolution transmission electron microscope image of $FeS_m$ nanoparticles. Modified from ref 194, Copyright 2006, with permission from Elsevier.

XRPD results in themselves are surprising. The classical Bragg approach to XRD assumes the presence of an infinite periodic lattice, which is a reasonable approximation in large crystalline solids. However, for nanoparticles, an infinite periodic structure cannot be assumed as a reasonable approximation. The 2 nm $FeS_m$ particles, for example, contain just 75 mackinawite unit cells or around 150 FeS molecules. The limiting size for the breakdown of the classical approach is not well understood. However, it would be intuitively assumed that 75 unit cells cannot be modeled accurately as an infinite periodic lattice. The Scherrer equation, which is conventionally used for determining particle sizes in crystalline material, is based on measuring XRD peak broadening. It assumes that the peak broadening is entirely derived from coherence length of the structural domains. For normal particles, this may be a close approximation to the effective situation. However, it may not be applicable in nanoparticulate materials since intraparticle disorder can also contribute significantly to the apparent coherence length. It may be that the extreme platelike form of $FeS_m$ lies behind the reason why the classical XRPD approach provided a reasonable approximation to the real properties of the material.

## 5.2. Mackinawite Composition

The problem of the composition of mackinawite has been resolved by Rickard et al.[216] Textbooks state that mackinawite is nonstoichiometric with excess Fe and is formulated $Fe_{1+x}S$. Rickard et al.[216] showed that mackinawite is stoichiometric FeS. The textbook nonstoichiometry derives from electron probe microanalyses of mackinawites from the high-temperature mss (monosulfide solid solution) ore association, which include large concentrations of other metals such as Cu, Ni, and Cr. These observations have led to the intuitive conclusion that low-temperature aqueous mackinawite in marine systems should sequester significant amounts of often more toxic metal ions. In fact, this does not seem to be the case.[1]

Previous results on mackinawite composition have tended to present only the Fe/S ratio and not the total analysis in terms of measured weight percent of each component. Berner[217] and Rickard[209] found $Fe_{0.91}S$. Sweeney and Kaplan[218] reported compositions between $Fe_{1.09}S$ and $Fe_{1.15}S$. Ward[219] reported a range between $Fe_{0.995}$ S and $Fe_{1.023}S$. Rickard[54] reported $Fe_{1.04}S$. The largest crystals of synthetic mackinawite are prepared by reaction of α-Fe (in the form

of iron wire) with bisulfide solutions. Lennie and Vaughan[210] reported an average Fe/S ratio of 0.99 ± 0.02 for three crystals using energy dispersive X-ray analysis (EDAX) measurements in a TEM.

However, analyses of mackinawite have not normally been presented in published reports and total analyses have been lacking (e.g., refs 101, 174, 189, 211, and 220) Mackinawite tends to have been identified solely on the basis of its XRPD characteristics. This has somewhat increased the uncertainty surrounding understanding of the properties of mackinawite.

Morse et al.[3] suggested that mackinawite was hydrated. This was based on the observation that drying changes the physical properties of mackinawite.[221] The idea is attractive by analogy with the iron oxides and oxyhydroxides. The fundamental mechanism of the formation of $FeS_m$ from aqueous solution involves the expulsion of $H_2O$,[220] and intuitively, one might expect some part of this $H_2O$ to be trapped in the rapidly forming initial precipitate. Rickard et al.[216] used solid-state NMR, thermogravimetric analysis (TGA), and TGA-MS to demonstrate that no water was contained in the mackinawite structure. They also showed that apparent hydration was due to low and erratic analytical totals.

## 5.3. Mackinawite Solubility

The dissolution of $FeS_m$ in mineral acids has been a basic means of analyzing the material in experimental and natural systems. Those older readers will remember the Kipp's apparatus of their school days, where $H_2S$ was conventionally generated for analysis by dissolving FeS (usually in the form of commercial pyrrhotite) in HCl. The lives of older chemistry teachers were consequently short but healthy. The reaction gave rise to the idea that $FeS_m$ was readily soluble in mineral acids. However, closely related transition metal sulfides, such as CoS and NiS, are not readily soluble in HCl. So $FeS_m$ may not dissolve in HCl as readily as might be supposed.

The main reason why the composition of mackinawite was previously uncertain appears to have been mainly a problem with digestion procedures. Cornwell and Morse[222] analyzed the S content of wet $FeS_m$ and corrected for water contents by weight loss on drying at 65 °C overnight. They reported 100% ± 4% recovery in hot and cold HCl between 1.0 and 6.0 N for $FeS_m$ S, except for cold 1 N HCl, which only recovered 92%. However, the Fe content was not reported, and the recovery efficiency appears to have been measured against a theoretical stoichiometric composition of FeS. Allen and Parkes[223] and Polushkina and Sidorenko[224] found that only 81% ± 3% of $FeS_m$ was recovered in hot 6 M HCl digestions over 1 h and 104% ± 14% was recovered in cold 6 M HCl digestions over 1 h. In the case of the cold acid digestions, the ±14% standard deviation of the recovery suggests a range between 90% and 118% recovery. The result is a spread of analyses over 28%, which means a lack of reproducibility of the analyses.

Cornwell and Morse[222] noted that the recovery efficiency of $FeS_m$ S from dried $FeS_m$ was less than that of wet $FeS_m$. This seems to be a general observation. The reasons are unknown. Dried $FeS_m$ has a strong static charge, and it may be that this contributes to a difficulty in wetting the sample. Dried $FeS_m$ also tends to flocculate into hard cakes with limited pore space,[214] and this may reduce the surface area to such a degree that dissolution is less efficient.

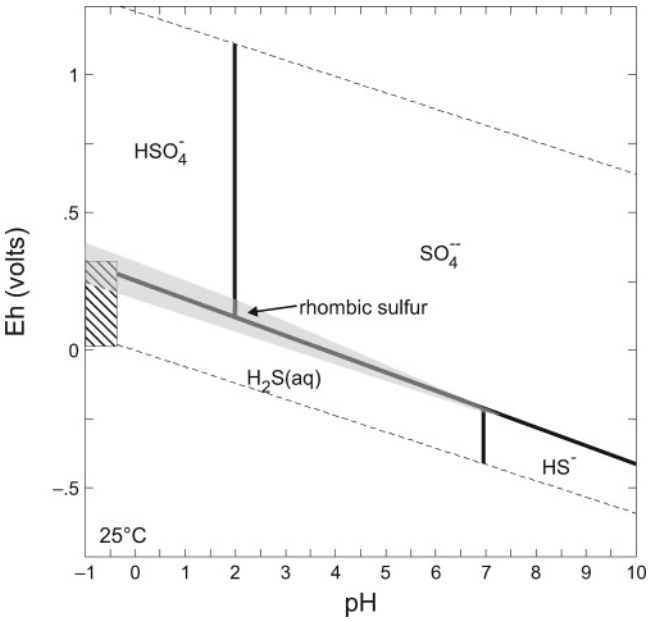


**Figure 27.** Conventional pH−Eh equilibrium diagram for sulfur species at 25 °C and 1 atm pressure. The conditions of the $FeS_m$ dissolution environment are hatched (total S = 0.03 M, HCl = 6 M) and range down to the presence of titanium(III) citrate with Eh approaching 0 V at pH < 0. Reprinted from ref 216, Copyright 2006, with permission from Elsevier.

Frequently a black residue is left after reaction of $FeS_m$ with HCl indicating incomplete dissolution. Rickard et al.[216] showed that this residue is black rhombic sulfur. The cause of its formation is shown with respect to a pH−Eh diagram (Figure 27). In acid solutions, $S^0$ has a significant stability area, especially at high $\{S(-II)\}_T$ values. Once formed $S^0$ is difficult to redissolve inorganically. Rickard et al.[216] overcame this problem by adding the reducing agent titanium(III) citrate to the system before dissolution, ensuring that the dissolution occurred in conditions where $S^0$ was not stable and did not form.

Earlier results of measurements of the solubility of $FeS_m$ have been reviewed by Davison.[181] In more recent times, there have been two contrasting approaches to solubility measurements. In the classical approach, $FeS_m$ is precipitated in solution and then dissolved in acid.[174] In an alternative approach, $FeS_m$ is dissolved and then reprecipitated.[101] In both cases, the concentrations of dissolved Fe(II) and S(−II) are measured at fixed pH values. Since the value of $pK_2(H_2S)$ is very uncertain, the solubility cannot be calculated from eq 14.

$$FeS = Fe^{2+} + S^{2-} \quad (14)$$

The solubility product measured is a secondary product, designated $K^*_{1,sp}(FeS_m)$, given by eq 15.

$$FeS_m + 2H^+ = Fe^{2+} + H_2S \quad (15)$$

Davison et al.[174] made an extensive series of measurements using a precipitation system in an automatic titrator under a fixed partial pressure of $H_2S$ gas. Aliquots of the equilibrated solution were taken and filtered through a 0.45 $\mu$m filter and analyzed for total iron colorimetrically. From the known $P(H_2S)$, the total iron in solution, and the pH, the solubility of the iron(II) monosulfide solid was determined. The results were interpreted in terms of the dissolved iron species $Fe^{2+}$

and the bisulfide complexes $FeSH^+$ and $Fe(SH)_2$. In acid solutions (pH < 6), the results provided a straight line plot of log $[Fe(II)]_T$ versus pH with a slope of −2. The result was consistent with the equilibrium shown in reaction 16

$$\log K^*_{1,sp}(FeS_m) = \log\{Fe^{2+}\} + \log\{H_2S\} + 2pH \quad (16)$$

At constant log$\{H_2S\}$, a plot of log$\{Fe^{2+}\}$ vs pH will give a straight line with a slope of −2. The results demonstrated that log $K^*_{1,sp}$ is 4.442 ± 0.175.

Just two measurements of the solubility of iron(II) monosulfide at 25 °C in acid solutions have been reported earlier using the inverse methods,[101] and these gave values for log $K^*_{1,sp}(FeS_m)$ of 3.10 and 3.20, about an order of magnitude less than that of Davison et al.,[174] although a series of measurements were made up to 95 °C and the derived solubilities were consistent.

These differences in log $K^*_{1,sp}(FeS_m)$ are quite significant. In a solution at pH = 5 and with $\{H_2S\} = 10^{-4}$, this would mean that $\{Fe^{2+}\} = 10^{-1.6}$ or 0.025[174] and $10^{-2.9}$ or 0.00125.[101] Using a molar scale for activities, this variation would be between 25 and about 1 mM. The difference in the availability of aqueous Fe(II) in the two measurements is around 20.

As previously discussed, since the $S^{2-}$ ion is insignificant in most aqueous solutions and log $K_2(H_2S)$ is highly uncertain, it has been popular to present sulfide solubilities, $K^*_{2,sp}$, in terms of the bisulfide ion, $HS^-$. That is

$$FeS_m + H^+ = Fe^{2+} + HS^- \quad (17)$$

Since the dissociation constant $K_1(H_2S)$ for the reaction

$$H_2S = HS^- + H^+$$

is well defined, often with precisions within 0.02 log units[56] in a variety of media, the conversion is justified. The results suggest that log $K^*_{2,sp}(FeS_m)$ is −3.00 ± 0.12[174] or between −3.88 and −3.98.[101]

Rickard[178] revisited the solubility of $FeS_m$ and found a value of log $K^*_{1,sp}(FeS_m) = 3.5 \pm 0.25$ ($n = 84$) for the pH-dependent reaction 15. This is equivalent to log $K^*_{2,sp}(FeS_m)$ being −3.5 ± 0.25 ($\pm 1\sigma$, $n = 84$) between pH 3 and 10 and at $\sum[S(-II)]$ concentrations between $3.27 \times 10^{-5}$ and $1.76 \times 10^{-1}$ M. This compares with values of −3.00 ± 0.12 (20 °C),[174] −2.95 (25 °C),[225] −2.94 (25 °C),[173] and −3.9 (25 °C).[101] It is similar to the the recalculated value for "mackinawite" of −3.55 ± 0.09[174] originally provided by Berner,[225] which is related to a more crystalline variety of synthetic $FeS_m$. The Gibbs free energy of formation for $FeS_m$ is then −98.2 kJ mol$^{-1}$ using $\Delta G^\circ_f(Fe^{2+})$ = −90.53 kJ mol$^{-1}$ [99] and $\Delta G^\circ_f(HS^-)$ = 12.2 kJ mol$^{-1}$ [84]. This compares with recalculated values for $\Delta G^\circ_f(FeS_m)$ of −96.4 ("precipitated FeS"),[225] −100.4 ("mackinawite"),[225] and −101.09 kJ mol$^{-1}$.[101]

However, the solubility of $FeS_m$ in solutions above pH 6 does not show a dependence on pH. In this pH-independent area, reproducible results have been difficult to collect. Davison et al.[174] and Wolthers[226] reported that the dissolved Fe(II) concentration appears to be pH independent above pH ≈ 6, and therefore reaction 17 is not controlling the solubility in this environmentally important region. Earlier measurements[101] showed variations of up to 6 orders of magnitude in this region! Davison et al.[174] reported that a neutral iron bisulfide complex became the dominant dissolved species above pH 6. The significance of these results is that neither the value nor the process controlling the solubility of $FeS_m$, in the important marine environmental pH range of 6−8, was known until recently. The interpolation of the process described for acid pH values is wrong, since the process changes.

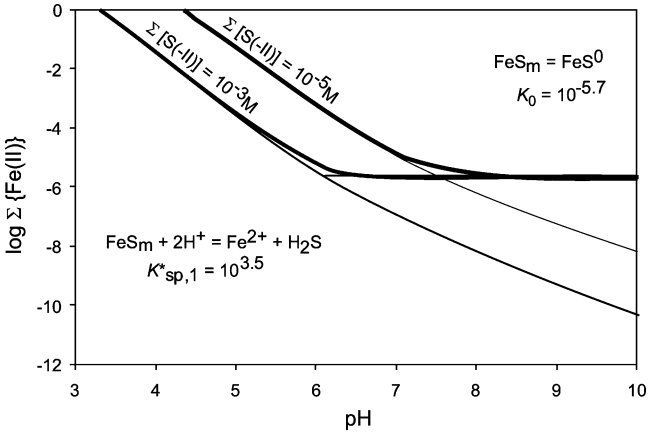


**Figure 28.** Solubility of $FeS_m$ at 23 °C and 1 atm total pressure according to ref 178. The total solubility in terms of the logarithm of the total activity of Fe(II) is plotted against pH for total sulfide concentrations of $10^{-3}$ M and $10^{-5}$ M. The thick lines denote the experimentally measured total solubility and the thin lines the solubility of the hexaqua $Fe^{2+}$ in equilibrium with $FeS_m$. Reprinted from ref 178, Copyright 2006, with permission from Elsevier.

Rickard[178] showed voltammetrically that the dominant dissolved species in the pH-independent area was the FeS(aq) cluster. The stoichiometry of this cluster is unknown, but it can be represented mathematically by the monomer $FeS^0$, which then provides the intrinsic solubility, $K_0$, for $FeS_m$ in the pH-independent regime:

$$FeS_m = FeS^0 \quad (18)$$

For which log $K_0(FeS_m) = -5.7$.

The overall equation for $FeS_m$ solubility is described by the relationship[178]

$$\log [Fe(II)]_T = \log K_0(FeS_m) + \log K^*_{1,sp} - \log\{H_2S\} - 2pH \quad (19)$$

where $[Fe(II)]_T$ is the total dissolved Fe(II) concentration. The model closely describes the solubility of $FeS_m$ at 23 °C for pH 3−10 and total dissolved S(−II) concentrations, $[S(-II)]_T = 10^{-1}-10^{-6}$ M.

The solubility of $FeS_m$ is shown in Figure 28 from Rickard's study. These results show that in neutral to alkaline environments with greater than micromolar $[S(-II)]_T$, the total solubility of Fe(II) in equilibrium with $FeS_m$ approaches 1 $\mu$M and the dominant species is FeS(aq). Relative to oxic ocean water, Fe(II) is transportable in solution at quite significant concentrations in sulfidic sediments in the presence of $FeS_m$. However, the availability of the hexaqua Fe(II) ion, which may be significant biologically, is correspondingly reduced in these environments although it dominates in all systems with $<10^{-6}$ M $[S(-II)]_T$. At pH = 8, which is near the normal seawater value, the concentration for dissolved Fe(II), in the form of FeS(aq), is some 3 magnitudes greater than the concentration of free hexaqua Fe(II) at millimolar concentrations of S(−II). Since

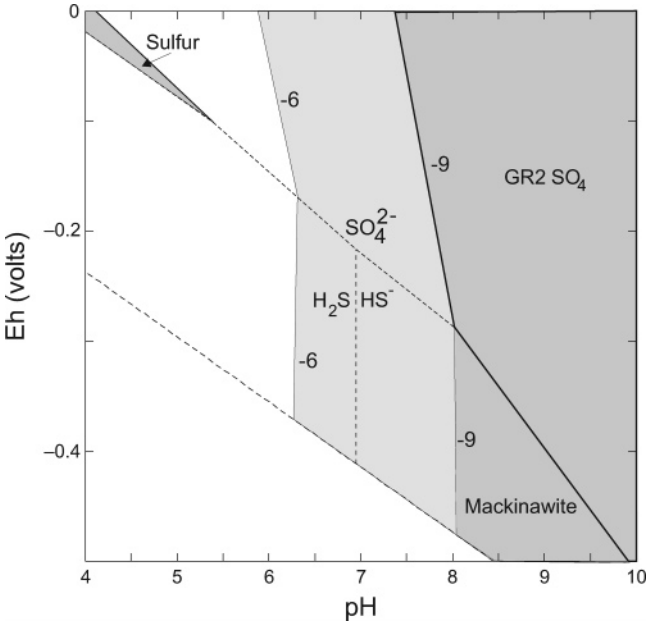


**Figure 29.** Stability of mackinawite in seawater in terms of Eh and pH at 25 °C and 1 atm total pressure. Dashed boundaries are lines of equal activity of dissolved species. Boundaries for mackinawite (and green rust 2 sulfate, $GR2SO_4$) are drawn for total Fe activities of $10^{-6}$ and $10^{-9}$ (indicated by $-6$ and $-9$ on diagram). Darker shading indicates stability areas at $\{Fe\}_T = 10^{-9}$ and lighter areas at $\{Fe\}_T = 10^{-6}$.

$[S(-II)]_T = [H_2S] + [HS^-] + [FeS^0]$, $FeS_m$ dissolves at $[S(-II)]_T \leq 10^{-5.7}$ M to form $Fe^{2+}$. FeS(aq) as a dominant dissolved Fe(II) species is limited to environments with greater than micromolar total dissolved S(−II) concentrations. Note that as the $[S(-II)]_T$ approaches $10^{-5.7}$ M, a progressively more significant part of the total dissolved sulfide is in the form of FeS(aq) rather than free $H_2S$ or $HS^-$.

The equilibrium solubility of $FeS_m$ is a good indicator of the {Fe{II)}{S(−II)} product where $FeS_m$ precipitates, since the precipitation reaction is kinetically fast[220] and significant supersaturations are not expected in the marine environment. In most environments with $\{S(-II)\} > 10^{-5.7}$ (i.e., a total sulfide concentration of ca. 1 $\mu$M), the {Fe{II)}{S(−II)} product is pH independent. Thus at a relatively high S(−II) concentration of 1 mM, the Fe(II) concentration required to precipitate $FeS_m$ is ca. 1 mM. This is at the extreme end of the range of Fe(II) concentrations observed in marine systems. The stability of $FeS_m$ in seawater (as defined above) is shown in Figure 29. Two total Fe activities are defined: $10^{-9}$, which approximates to a nanomolar total Fe concentration, which is the upper limit of normal ocean water, and $10^{-6}$, which approximates to the micromolar total Fe concentrations found in some marginal environments. The thermodynamic database includes the values for iron complexes and solids described above. Note that at seawater sulfate concentrations ($\log \{SO_4^{2-}\} = -2.536$), the mixed $Fe^{II}Fe^{III}$ hydroxide $GR2SO_4$ is stable relative to goethite, if the thermodynamic estimates discussed above are accurate. The substitution of goethite for $GR2SO_4$ makes little difference to the diagram except that the closure errors are improved. The program reduces the total sulfate to sulfide providing a maximum total sulfide concentration at millimolar levels, which appears to be near to the normal natural limit in areas with high organic matter contents and high SRP activities. Under these conditions, $FeS_m$ does not precipitate at pH < 8 at normal marine total Fe concentrations, which is within the pH range of normal marine sediments. $FeS_m$ does have a significant stability at micromolar total Fe concentrations at pH > 6. The results explain the observation by Rickard and Morse[1] that $FeS_m$ has not often been reported from direct observations of normal marine sediments, although pyrite is widely distributed. Most observations of $FeS_m$ in sediments are from marginal environments where the total concentration of Fe(II) is high. In contrast, as noted above, the $FeS_{aq}$ cluster has been widely observed, which is in accord with these solubility observations.

The idea that $FeS_m$ is relatively insoluble in sulfidic sedimentary environments is an oversimplification. Compared with Fe solubility in oxic ocean water, the concentration of dissolved Fe(II) in sulfidic systems in equilibrium with $FeS_m$ is substantial. The data suggest that Fe(II) is transportable in solution at quite significant concentrations in sulfidic sediments in the presence of $FeS_m$, mainly in the form of an aqueous FeS species. This means that in the global Fe cycle, the transfer of Fe from a normal oxic oceanic environment to an anoxic sulfidic system with $FeS_m$ may result in a sharp increase in the dissolved Fe concentration and a consequent increase in the transport of Fe within the system. The result contributes to the understanding of the formation of pyrite concretions in sediments[227] and also suggests a flux of Fe from sulfidic sediments with $FeS_m$ to more oxic overlying systems. However, the availability of the hexaqua Fe(II) ion itself, which may be significant biologically, may be correspondingly reduced in high sulfide systems.[200]

## 5.6. Kinetics and Mechanism of Mackinawite Formation in Aqueous Solutions

The kinetics and mechanism of mackinawite formation in aqueous solutions at low temperatures has been studied by Rickard.[220] The mechanism involves two competing reactions involving aqueous $H_2S$ and $HS^-$. The rate laws for both reactions are consistent with Eigen−Wilkins mechanisms[228] where the rate is determined by the exchange between water molecules in hexaqua iron(II) sulfide outer sphere complexes, $Fe(H_2O)_6^{2+}\cdot H_2S$ and $Fe(H_2O)_6^{2+}\cdot HS^-$, and the inner sphere complexes, $FeH_2S\cdot(H_2O)_5^{2+}$ and $Fe(SH)\cdot(H_2O)^{5+}$. The subsequent nucleation of FeS is fast. There is no observable lag phase and, as discussed above, it is probable that aqueous FeS clusters, with the same structures as the fundamental structural elements in mackinawite, are involved.

The rate of formation of $FeS_m$ is therefore described by two competing reactions, one with $H_2S$ and one with $HS^-$. For the $H_2S$ reaction, the overall reaction can be written

$$Fe^{2+} + H_2S \rightarrow FeS_m + 2H^+ \qquad (20)$$

The rate law is

$$\partial c_{FeS_m}/\partial t = k_1\{Fe^{2+}\}\{H_2S\} \qquad (21)$$

where $\{H_2S\}$ and $\{Fe^{2+}\}$ are the formally dimensionless $H_2S$ and $Fe^{2+}$ activities, which are represented on a moles per liter scale for practical convenience, and $k_1$ is the rate constant where $\log k_1 = 7 \pm 1$ L mol $^{-1}$ s $^{-1}$.

Rickard[220] showed that the reaction involving $HS^-$ resulted in the formation of an intermediate complex, $[Fe(SH)_2]$, which then condenses to $FeS_m$. The lack of thermodynamic stability of $[Fe(SH)_2]$ is consistent with the data on iron sulfide complexes discussed above.

The two competing mechanisms involved in FeS precipitation mean that the rate is pH dependent. The rate of the $H_2S$ pathway becomes equal to and greater than that of the $HS^-$ pathway as $[S(-II)]_T$ reaches $10^{-5}$ M or less under near-neutral conditions. In sulfide-rich environments (i.e., with micromolar or greater S(−II) concentrations), the rate of sulfide removal is 2 orders of magnitude greater in neutral to alkaline solutions than in acid environments. By contrast, in sulfide-poor systems, the rate is greater in neutral to acid conditions.

As discussed above, it is possible that the major reactive iron phases involved in $FeS_m$ formation in marine environments are iron hydroxides. As we show, it is possible that the reactive phases include mixed $Fe^{II}Fe^{III}$ hydroxides related to the green rust group. However, at present it is still generally assumed that iron(III) oxyhydroxides, probably in the form of nanoparticulate goethite, are the main phases. Little work has been reported on the sulfidation of the green rusts, although this reaction was noted in 1969.[209] In contrast, the kinetics and mechanism of the reaction between goethite and sulfide have been reported.[229−231] The product of this reaction is $FeS_m$ and colloidal sulfur. The rate is dependent on pH, $[S(-II)]_T$, and the surface area of the goethite, and the kinetics are consistent with the formation of a sulfide complex at the oxyhydroxide surface followed by electron transfer between the sulfide and Fe(III). Sulfide free radicals are proposed to be formed, which would react with Fe(III) to form elemental sulfur, the Fe(II) then reacting with the S(−II) to form $FeS_m$, as in the Rickard kinetics described above. Biber et al.[232] showed that the reaction kinetics are affected by organic and inorganic species, with phosphate being particularly important.

The key reaction in the formation of $FeS_m$ from aqueous solutions is the reaction between Fe(II) and S(−II), independently of whether the reactive iron phase is hexaqua Fe(II) directly or iron(III) (oxy)hydroxide. As discussed with respect to the reduction of sulfate, the form of the Fe involved in the reaction with S(−II) to form $FeS_m$ is influenced by the prevalence of anaerobic dissimilatory Fe(III) iron-reducing prokaryotes (FeRP) in the sediment column.[233−240] Many of the Fe(III)-reducing organisms are closely phylogenetically related to sulfate-reducing bacteria and some species of the Geobacteraceae reduce S(0). The iron-reducers and sulfate-reducers may be part of a tight ecology, since the acetate used by the FeRP is a common product of some strains of SRP.

Kostka and his associates showed that the Fe(III) reducers not only reduced iron(III) oxyhydroxides but also were able to reduce iron(III) sheet silicates.[241−244] Kostka and Nealson[245] showed that the Fe(III) reducers could also reduce the Fe(III) in magnetite. The significance of these observations is that magnetite and the Fe sheet silicates are usually classified as poorly reactive or unreactive iron phases.[42−44] As with the SRP, these organisms bring a sophisticated armory of enzymatic catalysts to bear on marine Fe chemistry such that, counterintuitively, Fe equilibrium in the presence of FeRP may be more nearly attained.

The net results of the ubiquity of FeRP and their close association with SRP in marine sediments is that the process of formation of iron sulfides like $FeS_m$ in marine sediments may not involve a reaction with solid Fe minerals like goethite but may include direct reactions between hexaqua Fe(II) formed by FeRP and sulfide produced by SRP.

### 5.7. Kinetics and Mechanism of Mackinawite Dissolution in Aqueous Solutions

The rate of $FeS_m$ dissolution has been investigated by Pankow and Morgan[246] who showed a first-order dependence on $H^+$ concentration in acid solutions and a constant $H^+$ concentration independent rate in neutral to alkaline solutions. These kinetic data are consistent with the solubility data of Rickard[178] discussed above, which demonstrated that in neutral to alkaline solutions, $FeS_m$ solubility was dominated by $FeS^0$ in a pH-independent reaction whereas, in more acid solutions, the solubility was determined by the activities of $Fe^{2+}$ and $H_2S$.

The rate equation in systems with no added Fe or S can be expressed as

$$-\partial FeS_m/\partial t = k_1[H^+] + k_2 \quad (22)$$

where $k_1 = 0.18 \pm 0.06$ cm min$^{-1}$ and $k_2 = (1.9 \pm 0.9) \times 10^{-9}$ mol cm$^{-2}$ min$^{-1}$ and the rate is expressed in units of mol cm$^{-2}$ min$^{-1}$. Simple inspection of eq 22 shows that the $H^+$ concentration independent rate dominates the dissolution at pH > 5.3, which is consistent with the solubility data of Rickard.[178] The rate in most low-temperature, natural aqueous solutions such as seawater is therefore given by

$$-\partial FeS_m/\partial t = k_2$$

Pankow and Morgan[246] expressed the rate of dissolution in solutions containing Fe and S in terms of the function $(1 - c/c_s)$ where $c$ is the concentration of Fe(II) and S(−II) in solution and $c_s$ is the concentration at equilibrium with $FeS_m$. This is a version of the classical $(1 - \Omega)^n$ function for dissolution reactions[247] where $\Omega$ is the degree of supersaturation. Pankow and Morgan[246] assumed that $n = 1$. Then eq 22 becomes

$$-\partial FeS_m/\partial t = k_2(1 - \Omega) \quad (23)$$

The maximum rate of $FeS_m$ dissolution occurs far from equilibrium where $\Omega$ is small. Pankow and Morgan's[246] data suggest that this rate approaches $3 \times 10^{-7}$ mol m$^{-2}$ s$^{-1}$. The specific surface area for $FeS_m$ has been established by Ohfuji and Rickard[194] to be 380 m$^2$ g$^{-1}$. This suggests that $FeS_m$ dissolves at a rate of up to $10^{-4}$ mol s$^{-1}$. The data show that $FeS_m$ reaches equilibrium rapidly with dissolved Fe and S. In order for $FeS_m$ to be preserved for any length of time, $\Omega \rightarrow 1$.

Pankow and Morgan[246] found that the Arrhenius energy for $k_1$ was 28 kJ mol$^{-1}$ and that for $k_2$ 30 kJ mol$^{-1}$. Within the uncertainties of the measurements, these are very similar and within the range expected from transport-controlled reactions. The observation implies that the rates of the surface chemical reactions involved in $FeS_m$ dissolution are so fast that the rate-limiting factor is diffusion of the components away from the surface. The rate law (eq 23) suggests that the rate close to equilibrium will become very slow and the rate-controlling reaction may change. The rate of $FeS_m$ dissolution under these conditions has not been investigated, however, and the current data refer to dissolution far from equilibrium.

## *6. Iron Thiospinel, Greigite*

Greigite is the thiospinel of iron, $Fe_3S_{4g}$. Skinner et al.[248] originally defined greigite from a tertiary lacustrian sequence

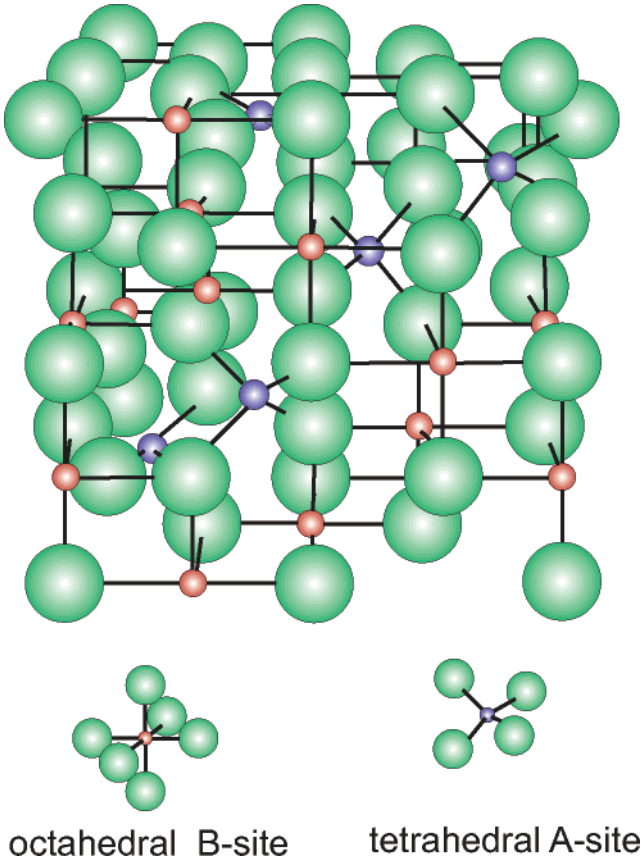


**Figure 30.** Greigite structure. Greigite is an inverse spinel, $A(AB)_2S_4$ where $Fe^{II}$ atoms occur in tetrahedral A-sites and mixed $Fe^{III}$ and $Fe^{II}$ occur in the octahedral B-sites. Modified from ref 1, Copyright 2005, with permission from Elsevier.

in California. Earlier Polushkina and Sidorenko[224] described an iron thiospinel and named it *melnikovite* after a ferromagnetic iron sulfide reported in 1912 by Doss[249] from the estates of Count Melnikoff. Unfortunately, Doss described *melnikovite* as a magnetic variety of $FeS_2$. Ramdohr[250] used the term *melnikovitic pyrite* for a black iron sulfide mixture found in some hydrothermal ore deposits. Rickard[209] showed that *melnikovitic pyrite* was a mixture of pyrite, mackinawite, greigite, and some iron oxyhydroxides. Because of the confusion surrounding the term *melnikovite*, the International Mineralogical Association approved *greigite* as the official name for the thiospinel of iron.

## 6.1. Greigite Structure

Greigite is the sulfur analogue of magnetite and has a similar inverse spinel structure (Figure 30). The unit cell of greigite has $a = 9.876$ Å and consists of eight $Fe_3S_4$ moieties. Eight Fe atoms occur in tetrahedral A-sites and 16 in octahedral B-sites. In the spinel structure, this arrangement would reflect the formula $AB_2S_4$ where A = Fe(II) and B = Fe(III) giving the overall formula for greigite, $Fe^{II}Fe^{III}{}_2S_4$. However, molecular orbital[251] calculations suggested that the Fe in the octahedral B-sites is mixed $Fe^{III}$ and $Fe^{II}$. This would tend to an inverse spinel structure, $A(AB)S_4$, and may suggest nonstoichiometry in greigite.

The greigite structure can be regarded as a cubic, close-packed array of S atoms linked by smaller Fe atoms. This arrangement shows a remarkable congruity with the cubic, close-packed S array of mackinawite, which was first pointed out by Yamaguchi and Katsurai.[252] Projections of both

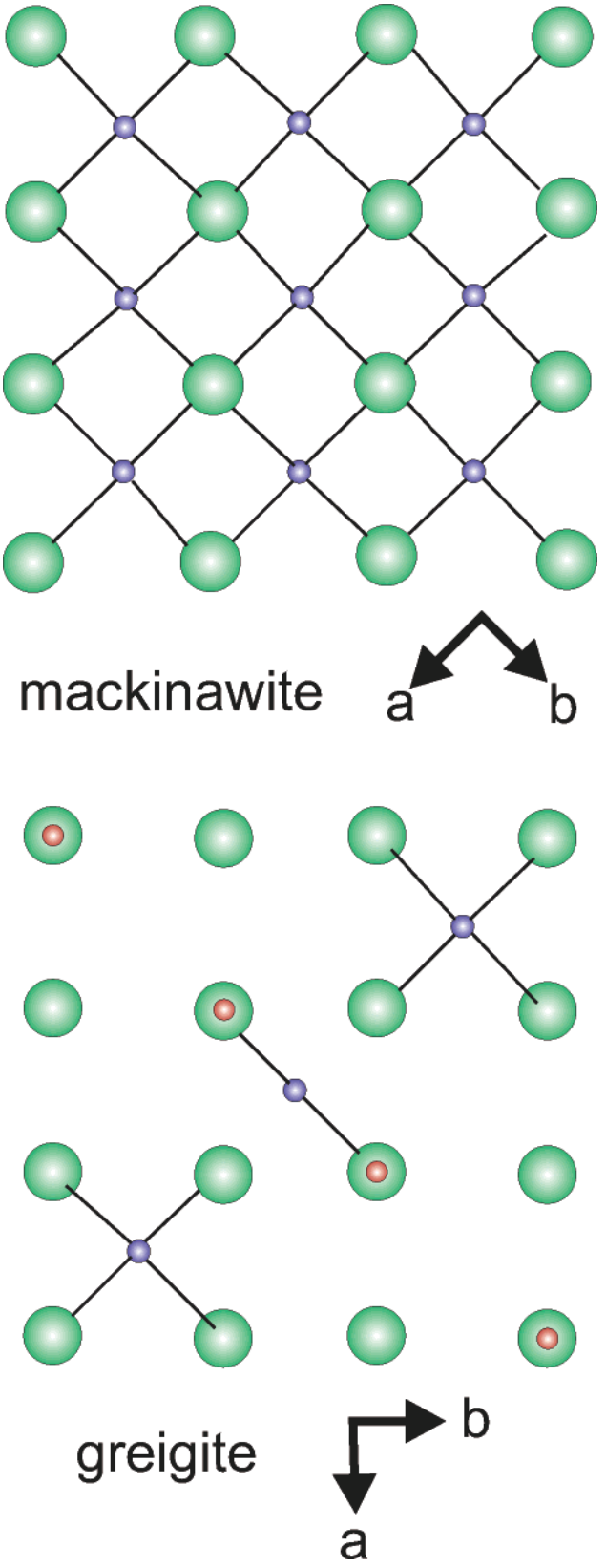


**Figure 31.** Homology of the mackinawite and greigite structures (based on Lennie et al.[211]) Projections of both structures onto (001) emphasize the similarity in the close-packed cubic arrays of S -atoms in both minerals. Modified from ref 1, Copyright 2005, with permission from Elsevier.

structures onto (001) emphasize the similarity in structural arrangements (Figure 31). The implication is that the transformation of mackinawite to greigite is essentially a

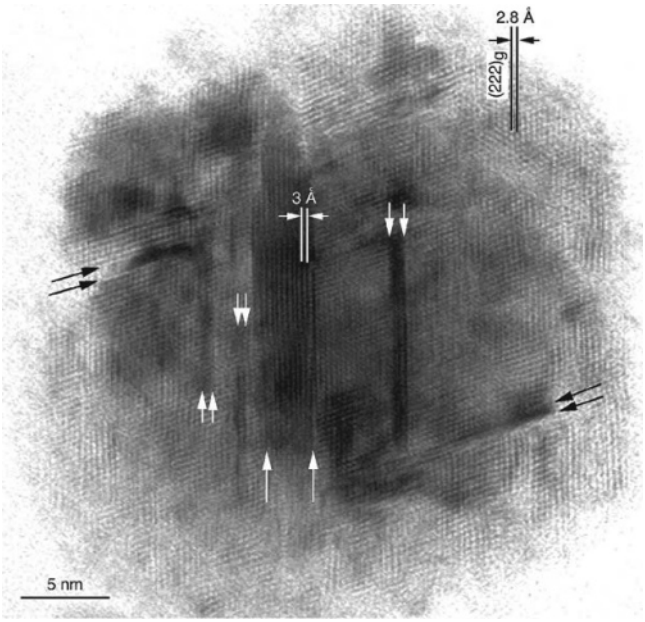


**Figure 32.** High-resolution transmission electron micrograph of a greigite grain showing relict mackinawite interlayers made by Posfai et al.[253] The grain is from a bacterial magnetosome. The arrows delimit bands several atomic layers in thickness parallel to (222), which retain relict mackinawite structural elements. The cubic-closed packed S array is continuous across the interface between the two materials. Reprinted with permission from *Science* (http://www.aaas.org), ref 253. Copyright 1998 American Association for the Advancement of Science.

rearrangement of Fe atoms in a close-packed, cubic array of S atoms. The rearrangement is caused by the oxidation of two-thirds of the mackinawite Fe(II) to greigite Fe(III), where the Fe(III) acquires an octahedral coordination. The transformation involves a reduction in the volume of the cubic, closed-packed S array of 12% in the transformation.[211] This is consistent with greigite being more stable than mackinawite.

The homology of the mackinawite and greigite structures was originally suggested by Yamaguchi and Katsurai[204] and Lennie et al.[211] High-resolution electron microscopy of the transformation (Figure 32) has neatly confirmed the crystallographic considerations regarding the structural congruity of mackinawite and greigite originally suggested by Yamaguchi and Katsurai[252] and Lennie et al.[211] The HR-TEM study does bring up one worrying aspect about the dependence on XRD analyses to determine mackinawite and greigite. Figure 32 shows mackinawite interlayers within a greigite crystal. At these dimensions, it is doubtful whether the mackinawite interlayers would be detected by conventional XRPD, although Yamaguchi and Katsurai[252] assigned the asymmetry of the {200} greigite XRPD peak to $FeS_m$ contamination. The problem is not simply a matter of concentration but also of the size and lack of continuity of the mackinawite layers. It is presently not easy to detect relict mackinawite within greigite. The result is that greigite analyses are prone to uncertainties due to the presence of $FeS_m$ in the structure within concomitant effects on both compositional and solubility analyses.

## 6.2. Greigite Composition

The composition of greigite is not well-constrained. There have been few recent reports of total analyses, mainly because of the difficulty of separating greigite from related iron sulfides and (oxyhydr)oxides and the difficulties of sufficiently accurate S analyses on small amounts of material. Skinner et al.[248] originally reported $Fe_{3.00}S_{4.00}$. Polushkina and Sidorenko,[224] in contrast, gave the composition as ranging from $Fe_{2.83}S_4$ to $Fe_{3.11}S_4$. Some reports have been presented using electron beam methods to analyze greigite or greigite-containing particles. The problem here is that the analyses at best provide Fe/S ratios with an uncertainty that would not preclude nonstoichiometry and totals are difficult to obtain. Spender et al.[254] suggested that greigite was nonstoichiometric because Mössbauer spectra did not yield the expected intensity ratio of 1:2 of the spinel A and B sites. B-site vacancies would lead to nonstoichiometry. Dekkers et al.[255] and Posfai et al.[256] noted that this effect could be enhanced by storage of greigite samples but note that nonstoichiometry could explain the lack of any low-temperature transition in greigite analogous to the Verwey transition in magnetite. The suggestion that the Fe in the octahedral sites contain mixed Fe(III) and Fe(II)[251] again might suggest at least a propensity for nonstoichiometry. Rickard and Morse[1] concluded that greigite probably does display some degree of nonstoichiometry.

Greigite has been reported to contain small amounts of Cu, Co, and Ni. However, Posfai et al.[256] reported that mackinawite and mackinawite−greigite mixtures contained significant Cu but an apparently pure greigite crystal contained little Cu. The amounts of Cu are not listed here because the analytical precision was necessarily limited in these analyses. However, as Posfai et al.[256] point out, mackinawite from the high-temperature monosulfide solid solution association can incorporate large concentrations of Cu into its structure. The solid-state transformation of mackinawite to greigite would therefore tend to include varying amounts of inherited Cu in transitional stages. However, it is still not clear whether greigite can contain significant (e.g., >1 wt %) Cu in its structure.

The valence electrons in greigite are localized. Analogous thiospinels of Co, Ni, and mixed thiospinels of Cu and Co and Fe and Ni have delocalized valence electrons. Vaughan and Craig[213] suggested that this is the reason that there is no stable solid solution between greigite and Co, Ni, and Cu thiospinels. This would limit the amount of Cu, Ni, and Co that could be contained in the greigite structure.

## 6.3. Greigite Solubility

The net reaction of greigite with mineral acids can be written

$$Fe_3S_4 + 6H^+ = 3Fe^{2+} + 3H_2S + S(0) \qquad (24)$$

The reaction shows elemental sulfur being produced at a ratio of 1 mol of S(0) for each mole of $Fe_3S_4$ digested. Cornwell and Morse[222] found that this accorded with what they observed in the laboratory. They found that reaction with cold 1 N HCl, cold 6 N HCl, cold 6 N HCl + $SnCl_2$, or hot 6 N HCl resulted in visually complete digestions of greigite but they only recovered 75% of the S(0). Complete recoveries (i.e., 93−100%) were only possible in the presence of a strong reducing agent such as Sn(II) or Ti(III). Filtration of the digestion and treatment with Cr(II) resulted in recovery of a further 25% S, strongly suggesting that the missing S is in the form of S(0).

The problem with the purity of the synthetic greigite also affects the measurement of the solubility of greigite in

**Table 10. Recalculation of Berner's[225] Experimental Measurements of the Total $Fe^{2+}$ Concentration in Equilibrium with Greigite at 25 °C Using Thermodynamic Data Cited in the Text[a]**

| pH | $[Fe^{2+}]$ | $\gamma Fe^{2+}$ | $\{Fe^{2+}\}$ | log {HS−} | log $K$ | $\Delta G_f^\circ(Fe_3S_4)$, kJ mol$^{-1}$ | $\Delta G_f^\circ(Fe_3S_4)$, kcal mol$^{-}$ | Berner, kcal mol$^{-1}$ |
|---|---|---|---|---|---|---|---|---|
| 2.93 | $1.30 \times 10^{-2}$ | 0.5082 | 0.0066 | −5.0490 | −12.90 | −308.62 | −73.76 | −69.60 |
| 2.92 | $1.10 \times 10^{-2}$ | 0.4996 | 0.0055 | −5.0590 | −13.20 | −310.33 | −74.17 | −70.00 |
| 2.97 | $1.20 \times 10^{-2}$ | 0.5258 | 0.0063 | −5.0090 | −12.72 | −307.59 | −73.52 | −69.30 |
| 2.93 | $1.20 \times 10^{-2}$ | 0.5138 | 0.0062 | −5.0490 | −12.99 | −309.13 | −73.88 | −69.70 |
| 2.99 | $9.50 \times 10^{-3}$ | 0.5156 | 0.0049 | −4.9890 | −12.93 | −308.79 | −73.80 | −69.60 |
| 2.95 | $9.60 \times 10^{-3}$ | 0.5102 | 0.0049 | −5.0290 | −13.17 | −310.16 | −74.13 | −69.90 |
| 2.92 | $1.10 \times 10^{-2}$ | 0.4996 | 0.0055 | −5.0590 | −13.20 | −310.33 | −74.17 | −70.00 |
| 4.01 | $8.30 \times 10^{-5}$ | 0.9139 | 0.0001 | −3.9690 | −12.24 | −304.85 | −72.86 | −68.70 |
| 4.04 | $7.30 \times 10^{-5}$ | 0.9051 | 0.0001 | −3.9390 | −12.24 | −304.85 | −72.86 | −68.70 |
| | | | | **average** | | | | |
| | | | | | **−12.84** | **−308.30** | **−73.68** | **−69.50** |

[a] The $Fe^{2+}$ activity coefficient, $\gamma Fe^{2+}$, is calculated from Berner's data. The calculated standard free energy for greigite, $\Delta G_f^\circ(Fe_3S_4)$, is also listed in kcal mol$^{-1}$ and compared with Berner's original value.

mineral acids. Cornwell and Morse[222] used Wada's[257] recipe for preparing greigite by boiling $FeS_m$ with 5 mL of polysulfide solution overnight. They noted that aging of greigite in solution for 1 week decreases its dissolution in weak acids. This is in accord with TEM observations, which suggest that mackinawite continues to transform to greigite on storage. Cornwell and Morse[222] concluded that it was not possible to separate greigite from pyrite via acid digestions. Allen and Parkes[223] used Berner's[225] recipe for synthesizing greigite. They found recoveries of 34% ± 12% in cold 6 N HCl and 88% ± 4% in hot AVS digestions. With $CrCl_2$ added, the resulting recoveries were 91% ± 24% and 78% ± 21%, respectively. The worrying aspect of these results is not only the deviations from 100% recovery but also the magnitude of the standard deviations. These imply a considerable lack of reproducibility or uncertainty in the results.

The analysis of greigite in a mixture of iron sulfides remains a primary hindrance to progress on understanding greigite formation. Although a number of analytical protocols have been suggested for mixed iron sulfide analyses, none of these are sufficiently accurate in the presence of greigite.[222,258−264] The problem is that the quantification of greigite dissolution is difficult. Ideally, greigite should dissolve in acid to produce S(−II) and S(0). However, the stoichiometry of this reaction is difficult to control, especially in a mixture including pyrite. In experimental systems, analysis of the Fe(III) contents of iron sulfide mixtures may be possible since greigite is the only common iron sulfide containing Fe(III). However, this is precluded in natural systems because of the presence of Fe(III) in a number of associated Fe minerals.

The solubility of greigite has only been measured once, by Berner.[225] Berner synthesized greigite by bubbling $H_2S$ through an aerated $FeSO_4$ solution at 80−90 °C for around 45 min. Berner assumed that the system was in equilibrium with rhombic sulfur, although this was not identified. Using this assumption, the solubility could be calculated from the reaction

$$Fe_3S_4 = 3Fe^{2+} + 3S^{2-} + S^0 \qquad (25)$$

where $S^0$ is rhombic sulfur. Berner took Maronny's[76] value for $pK_2(H_2S)$ of 13.9 and reported the solubility in terms of $\Delta G_f^\circ$ using free energy values from Garrels and Christ.[85] His original value for $\Delta G_f^\circ(Fe_3S_{4g})$ was −69.4 ± 0.7 kcal mol$^{-1}$ (i.e., −290.4 kJ mol$^{-1}$). We recalculate this value from Berner's original listing of analyses of total dissolved $Fe^{2+}$ in equilibrium with greigite (Table 10) and using Berner's original activity coefficients for $Fe^{2+}$ calculated from his data. The reaction is rewritten in terms of $HS^-$, in order to avoid the uncertainty in $pK_2(H_2S)$,

$$Fe_3S_4 + 3H^+ = 3Fe^{2+} + 3HS^- + S^0 \qquad (26)$$

and the thermodynamic data used are listed in this paper. The result is that the free energy of formation of greigite is −308.30 kJ mol$^{-1}$ and log $K$ for reaction 26 is −12.84. This result compares with Berner's original result of −290.4 kJ mol$^{-1}$, suggesting that greigite is a little more stable than originally supposed. An alternative value recalculated from Berner's measurement of −273.8 kJ mol$^{-1}$ has been published,[101] but the way that this value was recalculated was not shown and the authors appear to have used the erroneous NBS $\Delta G_f^\circ(Fe^{2+})$ value as discussed above. This value would suggest a substantial decrease in greigite stability.

The problem is that it is difficult to synthesize pure greigite. Berner used XRPD methods to demonstrate that the product was mainly greigite, but subsequent high-resolution electron microscopic analyses of greigite precipitates have commonly shown that a varying amount of $FeS_m$ often occurs in greigite particles. Since mackinawite is more soluble than greigite, the effect would have been to increase the apparent solubility of greigite. The suggested greigite solubility based on Berner's original measurement is therefore likely to be too high, and the actual solubility of greigite is probably less than these numbers. This means that greigite is more stable in the Fe−S−$H_2O$ system than the solubility measurements would imply.

It is obvious that it is important for understanding of the sedimentary iron sulfur system that greigite solubility be revisited. Severe technical difficulties must be overcome, however. Pure greigite needs to be synthesized, its composition needs to be established, and a means of accurately determining the activities in solution needs to be found.

## 6.4. Reactions To Form Greigite

Greigite was synthesized by Yamaguchi and Katsurai[252] before the material was identified naturally. Since that time a number of recipes have been tried for greigite synthesis (Table 11). The interesting aspect of these syntheses is the varying conditions. Thus elevated temperatures, S(0), and $O_2$ are not necessary for greigite syntheses, although these

**Table 11. Greigite Recipes**

| reactants | $T$ (°C)[a] | comments | ref |
|---|---|---|---|
| $FeS_m$ | 25+ | under TEM beam | 265 |
| $FeS_m$ | 200 | anhydrous | 204 |
| $FeS_m + H_2S(g)$ + aldehydic carbonyl | 40 | aldehydic carbonyl recovered after reaction | 273 |
| $Fe(NH_4)_2(SO4)_2 + Na_2S + S(0)$ | 140 | $Fe(NH_4)_2(SO_4)_2$ injected into $Na_2S$ + S(0) mixture at 140 °C | 255 |
| $Fe(NH_4)_2(SO_4)_2 + Na_2S$ + sodium polysulfide | 100 | pH = 5.8−6.1 | 257 |
| $Fe(NH_4)_2(SO_4)_2 + Na_2S$ | 190 | $FeS_m$ precipitated | 268, 266, 274 |
| $Fe(NH_4)_2(SO_4)_2 + Na_2S$ (pH = 5) | 150 | $FeS_m$ precipitated | 275 |
| $Fe(NH_4)_2(SO_4)_2 + Na_2S$ (pH = 3) | 100 | $FeS_m$ precipitated; $H_2SO_4$ added and product reheated to 80 °C | 275 |
| $FeSO_4 + H_2S(g)$ | 80 | aerated $FeSO_4$ at pH = 3 | 225 |
| $FeS_m \pm H_2S$ (g) | 35−160 | $FeS_m$ freeze-dried and exposed to air | 267 |
| $FeSO_4 \pm Na_2S$ | 25 | pH > 3.4−6.5 | 209 |

[a] Unless otherwise stated, the reactants were mixed at room temperature and heated to around the listed temperature for various periods.

may help in the process. Current work in the Rickard laboratory suggests that greigite may form directly through the reaction between mackinawite and anoxic $H_2O$ (i.e., in the absence of both aqueous $O_2$ and excess S(−II)). The reaction appears to be quite rapid at temperatures somewhat above 70 °C. This observation is consistent with earlier speculations that greigite may have an increased stability in this temperature regime. However, the reaction does not appear to balance at first sight in the absence of an oxidizing agent unless it is autocatalytic.

One factor that seems to be consistent is pH. Thus, Yamaguchi and Wada[268] (p 477) wrote, "It is known that a high concentration of hydrogen ion promotes formation of greigite." The most successful syntheses are carried out in acid pH systems with pH values as low as 3 being used. It does not appear that greigite has ever been reported to form directly from solution. All syntheses of this material involve pre-existing mackinawite, which is metastable with respect to greigite.[225] The observations of the apparent requirement for pre-existing $FeS_m$ and the acid pH are consistent with observations in natural systems where greigite is commonly observed in freshwater sediments, which generally are more acid than marine systems. The pH dependence might be mechanistic or simply reflect enhanced dissolution of $FeS_m$ in more acid environments, giving faster reaction rates and the removal of the $FeS_m$ reactant. However, the kinetics and mechanism of the greigite formation reaction have not been studied in aqueous solutions. Until this is done, the present conclusions about the reaction mechanism must remain somewhat empirical.

Greigite has also been synthesized microbiologically. Freke and Tate[269] reported greigite from SRP enrichment cultures, although Rickard[270] found no greigite in Freke and Tate's samples. They may have oxidized by the time Rickard analyzed them (cf. ref 271), but he found only magnetite and $FeS_m$. Freke and Tate[269] thought the sample contained greigite because it was ferromagnetic and contained Fe and S. The use of SRP enrichment cultures to produce greigite has been promoted by Watson and his group as a possibly means of cleaning up nuclear waste.[272] Rickard[270] synthesized greigite with pure cultures of the SRP *Desulfovibrio desulfuricans*. Posfai et al.[256] described the iron sulfides formed in magnetotactic bacteria. They found both mackinawite and greigite to be common and showed that the greigite developed from a solid-state transformation of mackinawite. Rickard et al.[273] showed that trace amounts of aldehydic carbonyls enable greigite formation from mackinawite and inhibited the formation of pyrite. This work suggests how the bacteria may produce greigite (rather than pyrite) from mackinawite, since low concentrations of aldehydic carbonyls (and by inference, other as yet unknown organic moieties) are involved in key biochemical processes in the form of glyceraldehydes, for example.

Detailed electron diffraction studies[211,256,257,274,275] and high-resolution synchrotron XRD[211] of the mackinawite to greigite transition in anhydrous environments demonstrate that this is a solid-state transformation with a structural congruency between the two phases. Greigite formation requires the oxidation of two-thirds of the Fe(II) of mackinawite to Fe(III), whereas the S(−II) is not oxidized. In contrast, pyrite formation from iron(II) monosulfide requires that the FeS Fe(II) remains unoxidized whereas the S(−II) is oxidized (see below). The pyrite reaction involves a dissolved stage, whereas the greigite reaction is a solid state. The results suggest that the oxidation of $FeS_m$ S(−II) occurs in solution whereas the oxidation of $FeS_m$ Fe(II) occurs in the solid state.

Lennie et al.[211] showed that the greigite XRD reflections were first detected at 100 °C after stepwise heating of mackinawite from room temperature. Transformation was complete after 5 h at 200 °C, and greigite began to decompose at temperature beyond 260 °C. A similar result was found using transmission electron microscopy. In the XRD and electron microscope experiments, no water was present and the atmosphere was the machine vacuum. No other components were present, and no other products were detected. So what happened to the electrons? The reaction stoichiometry, in the absence of any other reactant, would appear to be

$$4FeS_m = Fe_3S_{4g} + Fe(0) \qquad (27)$$

However, $\Delta G_r^\circ$ for this reaction is +84.5 kJ mol$^{-1}$ at 25 °C (see below), and the reaction seems to be thermodynamically improbable. Rickard and Morse[1] discussed the electronic balance of the reaction quantitatively. It appears likely that $O_2$ was involved in the reaction and that it was introduced when the $FeS_m$ was briefly exposed to air. Posfai et al.[256] concluded that the oxidation occurred in the 10 days storage preceding the HR-TEM work. Mullet et al.,[276] for example, found that the surface of mackinawite contained 19 at. % O by XPS analyses and ascribed this to oxidation during sample

handling. Mullet et al.'s mackinawite was prepared in the same manner as that of Lennie et al.,[211] and they described their reactant as 1−2 $\mu$m tabular FeS crystals. Mullet et al. did not report greigite formation, and the 19 at. % surface oxygen that they analyzed would provide insufficient $O_2$ to produce measurable amounts of greigite if modeled as a monolayer on the mackinawite surface. To produce measurable (≥1 wt %) quantities of greigite, some 0.3 wt % of the reactant mackinawite needs to be oxidized *in situ*. The reaction of dry mackinawite with air has been followed by Boursiquot et al.[271] They showed that greigite, sulfur, and iron (oxyhydr)oxides were formed. After 6 months, greigite itself was entirely converted into sulfur and iron (oxyhydr)-oxides. It appears therefore that sample handling in air during the experimentation and analysis is sufficient to provide enough oxidation to account for the formation of greigite reported in several accounts of anhydrous $FeS_m$ reaction chemistry.[101,211] The reaction is accelerated under electron and X-ray beams probably due to damage to the $FeS_m$ lattice under the influence of the beam and then a structural rearrangement to the lower energy state of greigite.

The net stoichiometry of the reaction involving $O_2$ may be written

$$4FeS + 0.5O_2(g) = Fe_3S_{4(greigite)} + FeO^*(s) \quad (28)$$

where $FeO^*_{(s)}$ represents an unspecified (oxyhydr)oxide of iron. The reaction is thermodynamically favored if $\Delta G_f^\circ(FeO^*) < -84.5$ kJ mol$^{-1}$. Since the old NBS $\Delta G_f^\circ$(wüstite) value was around −244 kJ mol$^{-1}$, this seems thermodynamically possible. The mass balance would suggest that the product should be heavier than the initial $FeS_m$ reactant by 0.5 mol of $O_2$ for each mole of $Fe_3S_4$ produced. In mass terms, this is an uncertainty of less than 3 wt % in the analysis, well within the analytical error. In other words, the iron (oxyhydr)oxide produced during the reaction would not necessarily be seen. Lennie et al.[211] checked the Fe/S ratio of the greigite−mackinawite mixture produced by heating the mackinawite at 100 °C. The average Fe/S ratio of seven such mixed grains was 1.00 ± 0.07, which is close to the original composition of the $FeS_m$ reactant. The stoichiometry converts to an analytical uncertainty of around ±2 wt %, or adequate to include sufficient (oxyhydr)oxide to account for the electron balance.

The reaction of anhydrous $FeS_m$ with $O_2$ appears to involve the direct reaction with FeS-$Fe^{II}$ rather than the reaction with dissolved S(−II). The development of significant Fe−Fe bonding in mackinawite compared with the aqueous FeS molecular clusters leads to an apparent oxidation number of 0 for the $FeS_m$-Fe. This suggests the strong possibility of rapid oxidation of the Fe by $O_2$ in the condensed phase. An initial reaction, such as that described in reaction 28, with $O_2$ immediately grabbing electrons from Fe(0) in the mackinawite, as suggested by Lennie et al.,[211] is another way of presenting this reaction. The concern is, of course, that greigite will form artefactually from mackinawite during XRD and TEM analyses.

In contrast, the autoxidation of $FeS_m$ in water to form $Fe_3S_4$ is not thermodynamically favored at 25 °C. All possible iron oxide, hydroxide, and oxyhydroxide products, as listed in Table 6 give rise to a positive $\Delta G_r^\circ$ value for reactions like

$$4FeS_m + 2H_2O = Fe_3S_4 + Fe(OH)_2 + H_2 \quad (29)$$

This means that the $P_{H_2}$ in equilibrium with such reactions is inhibitingly high. For example, in reaction 29, it would be around 10 atm at 25 °C. This is in accord with observations in the Rickard laboratory that $H_2$ is not detected as a product in the apparent autoxidation of $FeS_m$ to form $Fe_3S_4$. Of course, the autoxidation reaction is not precluded at higher temperatures. $FeS_m$ appears to become more rapidly unstable with respect to greigite above ca. 70 °C. This suggests that reactions like reaction 29 may not display linear temperature dependence.

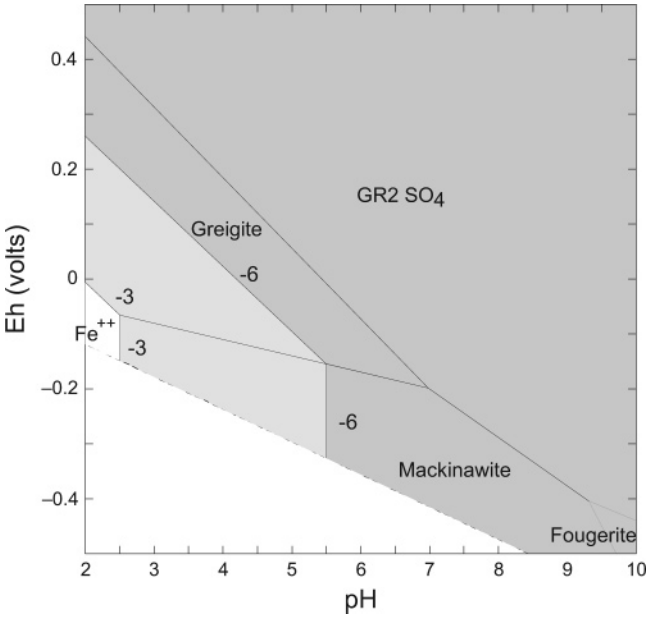


**Figure 33.** pH−Eh diagram showing the mackinawite−greigite boundary at 25 °C, 1 bar total pressure, $\sum\{Fe\}_T = 10^{-3}$, and $\sum\{S(-II)\} = 10^{-3}$ and $10^{-6}$.

The stability relationships between greigite and mackinawite in "seawater" conditions are shown in the form of a pH−Eh diagram in Figure 33. $\{Fe\}_T$ is set at $10^{-6}$, approximating to micromolar Fe concentrations, which are higher than those found in normal seawater. However, at lower $\{Fe\}_T$, greigite stability becomes insignificant, which is consistent with the scarcity of observations of greigite in normal marine sediments. Note also that these data are computed for the recalculated greigite stability data and the remeasured mackinawite stability, which makes greigite more stable than was previously supposed. For example, for the reaction

$$3FeS_m + S^0 = Fe_3S_{4g} \quad (30)$$

$\Delta G_r^\circ = -13.7$ kJ mol$^{-1}$. Thus greigite is stable relative to mackinawite plus sulfur, and in acid conditions at high $\{S\}_T$ where sulfur is stable, greigite will form readily from mackinawite, as is observed. Note that the conversion involves the formation of 1 mol of $Fe_3S_4$ for 3 mol of $FeS_m$. The pH−Eh diagram (Figure 33) is drawn for $\{S\}_T = 10^{-3}$ and $10^{-6}$, equivalent to approximately millimolar and micromolar sulfide concentrations. Greigite replaces mackinawite in more acid systems with higher Eh values. This result is consistent with observations that greigite is most abundant in freshwater systems where such conditions may prevail.

### 7. Iron Disulfide, Pyrite

Pyrite, cubic $FeS_{2p}$, is the most common sulfide mineral in Earth surface environments. It is sometimes said to be

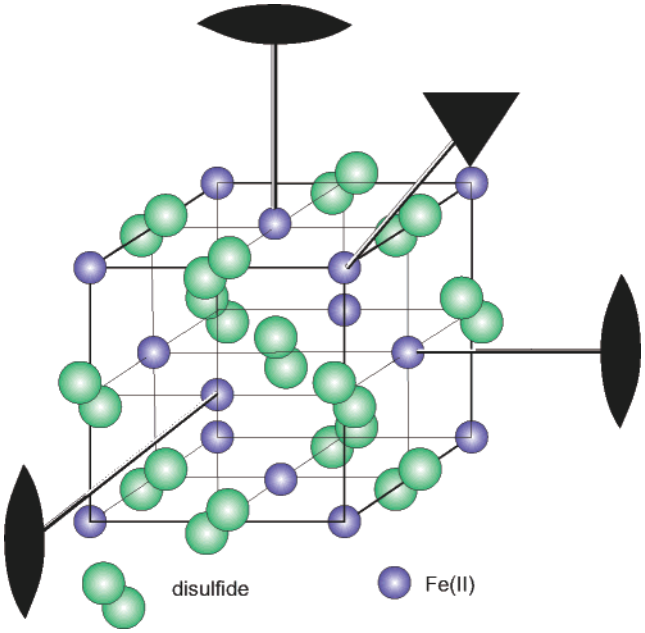


**Figure 34.** Structural elements of pyrite.

the most common sulfide mineral on Earth, but this is doubtful. Pyrrhotite group minerals are common in mantle rocks and meteorites, and it is probable that pyrrhotite group minerals are the most common sulfides in the bulk Earth. However, the abundance of pyrite on the Earth surface has led to it being the target of many pioneering investigations. Thus, pyrite was the first mineral structure determined in 1914 by Bragg[277] with his new X-ray diffraction system. In 1804, Hatchett[278] found the composition of pyrite to be $FeS_2$. In 1815, Bakewell[279] inadvertently synthesized pyrite serendipitously when a mouse got into a jar of ferrous sulfate in his laboratory. Bakewell examined the mouse droppings and discovered that they were covered in pyrite crystals. Allen et al.[280] synthesized pyrite hydrothermally in 1912. Sugawara[281,282] first reported the importance of pyrite in marine sediments, and Berner's[206,217,225,283−285] and Rickard's[209,270] work in the 1960s led to the key role of pyrite in the Earth surface system being fully appreciated.

In the geochemical literature, there is much made of a "controversy" about pyrite formation, especially with respect to its formation in low-temperature environments such as marine sediments. In fact, critical examination of the literature reveals that no such controversy actually exists. The concept is fueled by (1) a misunderstanding of the various concepts of *mechanism* and *process* in some of the geochemical literature; (2) experimental problems with pyrite syntheses, which often require large amounts of components (relative to pyrite solubility) in order to obtain sufficient amounts of product for study; and, of course, (3) the promotion of reports of investigations and grant proposals on the back of the idea that there *is* a controversy and it is about to be resolved.

## 7.1. Pyrite Structure

The structure of pyrite (Figure 34) is well-known. Pyrite is an iron(II) disulfide with a NaCl-type structure. The $S_2^{2-}$ groups are situated at the cube center and the midpoints of cube edges, and the low-spin $Fe^{II}$ atoms ($d^6$, $t_{2g}^6$) are located at the corners and face centers. The arrangement of the disulfide dumbbells is such that the structure, although cubic, has a relatively low symmetry, space group *Pa*3. The structure has 3-fold axes along the ⟨111⟩ directions and 2-fold axes along the ⟨100⟩ directions. The 2-fold symmetry means that the [100], [010], and [001] zone axes (equivalent to the *a*, *b*, and *c* crystallographic axes) are crystallographically not interchangeable with each other by a simple 90° rotation as in simple cubes. One result of this structure is that pyrite, along with several other minerals, exhibits chirality. Thus Guevrement et al.[286] demonstrated that there are significant differences in the sensitivity of pyrite to oxidation of the (100) and (111) planes. This chirality of pyrite has been theoretically exploited in the involvement of pyrite in the adsorption of organic molecules and, consequently, in prebiotic syntheses implicated in the origins of life.[287] However, this idea was challenged by Pontes-Buarque et al.[288] who argued that Stern-layer modulation of surface charge, acetate adsorptive behavior and the requirement for divalent cations in the attachment of organic key molecules, make such chiral-discriminator character of pyrite unlikely in this context.

Bither et al.[289] first presented a molecular orbital (MO) interpretation of the pyrite structure, which has been further described by Tossell et al.,[290] Luther,[291] and Rickard et al.[170] The MO and frontier molecular orbital (FMO) calculations have been shown to have significant implications for a fundamental explanation of pyrite properties and in predicting both bulk and surface reactions.[52,292−294]

## 7.2. Pyrite Composition

Kullerud and Yoder[295] originally suggested that the composition of pure pyrite is stoichiometric $FeS_2$. They concluded that deviations from stoichiometry were caused by analytical uncertainties or the presence of traces of other elements in the material. Ellmer and Hopfner[296] used theoretical arguments and a critical review of stoichiometry measurements to show that pyrite has a very narrow homogeneity range (<1 at. ‰). Thomas et al.[297] also concluded that pyrite is a stoichiometric semiconductor with a homogeneity range ≪0.5 at. %.

Pyrite displays both p-type and n-type semiconductivity,[298] which results from trace amounts of other elements in the structure. For example, Oertel et al.[299] were able to synthesis n-type pyrite by doping pyrite with 0.3 at. % Co. Pyrite analyses commonly show the presence of trace and minor elements,[300] and this is to be expected in view of the solid solution ranges possible between pyrite and other disulfide minerals.

## 7.3. Pyrite Solubility

The solubility of pyrite in water at ambient temperatures is not measurable as expected for an Fe(II) low-spin $t_{2g}^6$ electron configuration. Pyrite solubility data are derived from heat capacity measurements of the formation of pyrite from its elements at higher temperatures. The equilibrium solubility product of pyrite, $K^*_{1sp,pyrite}$, in aqueous solutions is usually given by the eqs 31, 32, and 33

$$FeS_2 + H^+ = Fe^{2+} + HS^- + S^0 \qquad K = 10^{-14.2} \qquad (31)$$

$$H^+ + HS^- = H_2S \qquad K = 10^{7} \qquad (32)$$

$$FeS_2 + 2H^+ = Fe^{2+} + H_2S + S^0 \qquad K = 10^{-7.2} \qquad (33)$$

According to Emerson et al.,[179] $K_{sp}$(pyrite; 25 °C, $I = 0$) $= 10^{-16.4}$, recalculated from data collated by Robie et al.,[301] which were based on original measurements by Grønvold and Westrum[302] and Toulmin and Barton.[303] These measurements are independent of the errors in the earlier NBS value of $\Delta G_f^\circ(Fe^{2+})$, discussed above, since they were derived for the reaction

$$Fe^0 + S^0{}_2(g) = FeS_2 \quad (34)$$

Toulmin and Barton used the Stull and Sinke[304] value for $\Delta G_f^\circ(S^0{}_2(g))$ of 19.13 kcal mol$^{-1}$, which compares closely with the Cox et al.[84] value of 79.7 ± 0.3 kJ mol$^{-1}$ recommended by Nordstrom and Munoz.[305] However, the Emerson et al. value for $K^*_{1sp,pyrite}$ is affected by the erroneous NBS $\Delta G_f^\circ(Fe^{2+})$ value. Correcting for this leads to $K^*_{1sp,pyrite} = 10^{-14.2}$ for reaction 31. At pH = 7, then the $\{H_2S\}\{Fe^{2+}\}$ product in the $S^0$ stability field is $10^{-21.2}$.

Congruent dissolution of pyrite involves the disulfide ion, $S_2{}^{2-}$. Previously, the stabilities of $S_2(-II)$ species were only imperfectly understood, and therefore the congruent dissolution of pyrite

$$FeS_{2p} = Fe^{2+} + S_2{}^{2-} \quad (35)$$

has not generally been used to describe pyrite solubility. However, Harmandas et al.[306] suggested $K_{sp}$(pyrite) $= 8.51 \times 10^{-26}$ for this reaction. This assumes an equilibrium constant for the reaction

$$S(0) + H_2S = S_2{}^{2-} + 2H^+ \quad (36)$$

of $10^{-15.6}$, which compares with $10^{-18.5}$ according to the Kamyshny et al.[78] polysulfide data set. Recalculation according to the Kamyshny polysulfide data set gives $10^{-24}$ for the congruent dissolution of pyrite.

The relative stability of $S_2(-II)$ species according to the Kamyshny data set has interesting implications regarding the thermodynamics of pyrite formation in low-temperature aqueous systems like marine sediments and anoxic basins. The dominant polysulfide species in the pH range of most natural waters is $HS_2{}^-$, and this is the third most abundant sulfide species in this region after $HS^-$ and $H_2S$. We can therefore consider the reaction

$$FeS_2 + H^+ = Fe^{2+} + HS_2{}^- \quad (37)$$

for which log $K = -13.84$. This suggests that at pH = 7, log $\{Fe^{2+}\}\{HS_2{}^-\} = -20.97$ and that at log $\{Fe^{2+}\} = -9$, log $\{HS_2{}^-\} = -11.97$. That is, in nanomolar $Fe^{2+}$ concentrations, just picomolar $HS_2{}^-$ is required to precipitate pyrite. We can relate $\{HS_2{}^-\}$ to $HS^-$, for example, directly through

$$HS^- + S^0 = HS_2{}^- \quad (38)$$

for which log $K = -1.76$. This suggests that log $\{HS^-\}$ in equilibrium with picomolar $HS_2{}^-$ is $-10.21$. That is, less than 1 nM dissolved sulfide is necessary to precipitate pyrite in solutions with nanomolar dissolved Fe.

The implications of these very small quantities of sulfur species required to precipitate pyrite are considerable in both experimental and natural systems. In an experimental system with high total sulfide, at least at the millimolar level, the purity of the reagent with respect to $HS_2{}^-$ specifically, but $S^0$ species generally, would need to be greater than analytical grade usually available to investigators. The sulfide reagent would need to contain less than 6.5 ppm S(0) species. Another way of looking at it is to consider a 100% pure sulfide reagent and consider how much of an electron acceptor, like $Fe^{3+}$ or $O_2$, would be required to produced the minimum amount of $HS_2{}^-$ required to precipitate pyrite. In the case of an $Fe^{2+}$ reagent, the limiting concentration of $Fe^{3+}$ required would be determined by the stoichiometry of equilibria like

$$2Fe^{3+} + H_2S = 2Fe^{2+} + S(0) + 2H^+ \quad (39)$$

That is, the $Fe^{3+}$/S(0) ratio is 2:1. This implies that the $Fe^{2+}$ reagent used would need to contain less than 10 ppm in order for the disulfide not to be present in sufficient quantities for pyrite to precipitate. As a codicil, it might be noted that the $Fe^{3+}/Fe^{2+}$ ratio in any solution at equilibrium is determined by

$$Fe^{3+} + e^- = Fe^{2+} \quad (40)$$

for which Nordstrom and Munoz[305] recommend log $K = 13$. Simple inspection suggests that at all Eh values above water breakdown, enough $Fe^{3+}$ will be present at equilibrium in an $Fe^{2+}$ solution to accept sufficient electrons from S(−II) to produce enough S(0) to precipitate pyrite.

A similar calculation can be made for oxygen. Experimental oxygen control is limited by the lower limit of quantitative analysis of $O_2(g)$, since measurements of dissolved $O_2$ in sulfide solutions are currently constrained by technical problems. The most precise $O_2(g)$ controls in sulfide experimentation have been achieved in the Rickard laboratory, with $O_2(g)$ levels maintained at less than 1 ppmv, the lower limit of measurement. As can be seen from the calculations with respect to $Fe^{3+}$, this level of $O_2(g)$ is easily sufficient to produce enough S(0) to precipitate pyrite under all reported experimental Fe and S(−II) concentrations. Current work in the Rickard laboratory examined pyrite formation in the presence of <1 to 100 ppmv $O_2$ and found no increase in pyrite formation. The role of $O_2$ may be limited to high concentrations in conditions where S(0) forms from S(−II) oxidation and because it is the presence of S(0) that enhances pyrite syntheses through kinetic, rather than equilibrium thermodynamic, effects.

In the natural environment, of course, there are adequate quantities of electron acceptors to produce the minimum $HS_2{}^-$ concentrations require for pyrite formation, even in the low Fe contents of normal marine systems.

From the equilibrium thermodynamic viewpoint, there is no problem with the observation that pyrite forms in most Earth surface environments, including marine systems. Pyrite is the stable phase in systems with even submicromolar concentrations of S(−II) since (a) its solubility product is so low and (b) the relatively high stability of $S_2(-II)$ means that the pyrite solubility product is exceeded in all reasonable experimental and natural Fe- and S(−II)-containing environments. In fact, pyrite has a significant stability even in more oxic environments where $\{SO_4{}^{2-}\} > \{S(-II)\}$. S(−II) species, and therefore pyrite, continue to have a significant activity into the $SO_4{}^{2-}$-dominated region.

The resultant pH−Eh diagram for pyrite stability in "seawater", as discussed above, is shown in Figure 35. To those of us brought up on Garrels and Christ,[85] the diagram is somewhat unfamiliar. Pyrite has an extensive stability

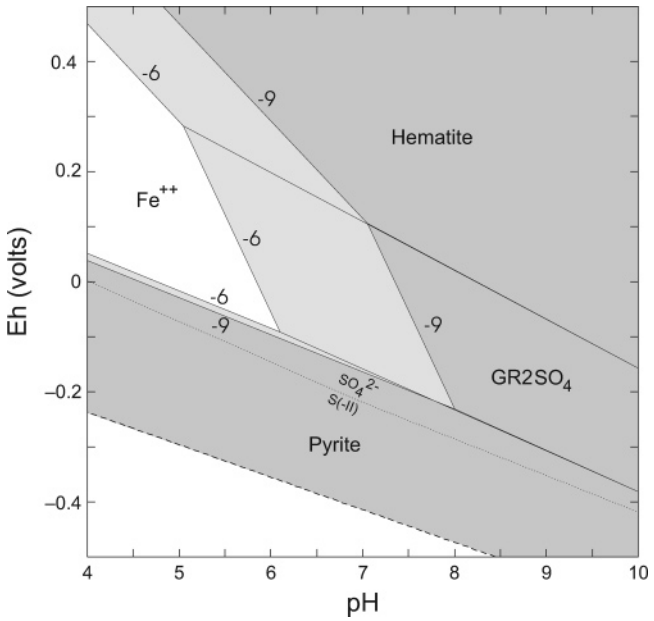


**Figure 35.** Pyrite stability in seawater at 25 °C, 1 bar total pressure, and $\sum\{Fe\} = 10^{-6}$ and $10^{-9}$ (indicated by −6 and −9 on diagram). The boundary for $\{SO_4^{2-}\}/\{S(-II)\} = 1$ is shown for reference.

region over pH 2−10, both above and below the $SO_4^{2-}/S(-II)$ boundary, which is often taken as marking the upper limit of "reduced" systems, as discussed above. In this computation, the iron polysulfide complexes ($FeS_4$, $FeS_5$, $Fe_2S_4^{2+}$, and $Fe_2S_5^{2+}$) are suppressed since the GWB program would force an artificially high relative stability for these species relative to pyrite. As discussed above, these complexes only have a significant stability at very high total iron and sulfur activities where rhombic sulfur is stable (see Figure 24).

Note that with the revised $\Delta G_f^\circ(Fe^{2+})$ and $\Delta G_f^\circ(S_n^{2-})$ values, pyrite is stable with respect to both pyrrhotite and troilite in these systems. Pyrrhotite and troilite have no stability regions at 25 °C in aqueous solution relative to pyrite, which is consistent with these minerals being rare to absent in marine sediments.

The upper boundary of pyrite stability is limited by the stability of $GR2SO_4$ under seawater sulfate concentrations. The stability zone of $GR2SO_4$ is still an estimate, as indicated above. Its extent on this diagram is partly caused by the lack of inclusion of $Fe(OH)_3^-$, for which we have no modern data. Including the classical Garrels and Christ[85] numbers for $Fe(OH)_3^-$ in the computation leads to an extensive stability field replacing $GR2SO_4$ in alkaline systems.

The pyrite stability field extends into the area where $\{SO_4^{2-}\} \geq \{S(-II)\}$. Near to this redox boundary, the calculated IAP in equilibrium with pyrite changes extremely rapidly. We can see this with reference to Figure 12, where the concentrations of polysulfide species increase rapidly near the redox boundary. This means that at any given total dissolved {Fe(II)}, the relative saturation state of the system with respect to pyrite will be extremely sensitive to the system Eh. Butler and Rickard[307] noted that the change could be as much as $10^{14}$ within an Eh variation of 50 mV over a wide range of pH. The Eh in natural sulfidic systems is mainly controlled by the S(−II)/S(0) couple near this redox boundary,[308] which means that the Eh is largely, though of course not wholly, controlled by sulfide activity.

The Fe−S system in low-temperature aqueous solutions includes many solid phases. Apart from the stable phase, pyrite, the metastable phases mackinawite and greigite are also observed in natural environments. The reason these metastable phases are observed is, of course, that the formation of the stable phase, pyrite, is kinetically hindered. If equilibrium were instantaneous, neither phase would be seen. As discussed below, one of the key processes in determining the rate of formation of pyrite is pyrite nucleation. Spontaneous pyrite nucleation requires extremely large supersaturations, so the steep IAP gradient near the redox boundary may affect whether pyrite nucleates rapidly in a particular sedimentary environment. The effect is significant in that supersaturations with respect to pyrite vary over very small regions of pH−Eh space in this region.

The result is that (1) pyrite formation varies over extremely small distances in a sedimentary or aquatic environment due to local spatial heterogeneities and (2) metastable phases, such as mackinawite and greigite, may be preserved for geologically significant time periods, especially within the lower part of the pyrite stability field where pyrite IAPs are lower and vary less in pH−Eh space.

## 7.4. Pyrite Formation

Many of the problems associated with pyrite formation reported in the geochemical literature center on confusing kinetics with thermodynamics. The equilibrium thermodynamics of pyrite formation appear to be consistent with the observations of the pyrite distribution in marine systems. However, the fact that thermodynamically there is enough $HS_2^-$ to account for pyrite formation in marine waters says nothing about the mechanism of pyrite formation nor, indeed, of how and whether it will occur.

The confusion in the geochemical literature is often expressed in terms of writing balanced equations for pyrite formation and then claiming that these represent conflicting pyrite-forming processes or mechanisms. It is obvious that a virtually infinite number of balanced reactions may be written that include pyrite as a product with different reactants and products.[1] The choice of reactants and products in these equations depends on what the investigator is attempting to describe. None of these balanced reactions are wrong in the sense that, ultimately, at equilibrium the product pyrite will be formed. However, they do not represent reaction mechanisms.

Rickard[309] pointed out that Berner's[285] original overall reaction for sedimentary pyrite formation,

$$FeS_m + S(0) = FeS_{2p} \quad (41)$$

could not describe a mechanism since S(0) is in the form of $S_8$, which would make this an impossible multimolecular reaction step. Berner himself was quite aware of the distinction and viewed his equation as summarizing an overall process. Likewise, the balanced reaction cited by Neretin et al.[262] and ascribed to Wilkin and Barnes,[310]

$$2FeS_m + {}^1/_2H_2O + {}^3/_4O_2 = FeS_{2p} + FeOOH \quad (42)$$

is not a mechanism because it involves 3.25 molecules, which makes it statistically improbable and, anyway, the fractions of molecules as written are, of course, mechanistically impossible. Wilkin and Barnes[310] described this as a pathway. They were pointing out that, in the absence of excess sulfur, $FeS_m$ will dissolve and, since the solubility of $FeS_{2p}$ is far less than that of $FeS_m$, $FeS_{2p}$ will be produced (eq 43).

$$2FeS_m + 2H^+ = FeS_{2p} + Fe^{2+} + H_2 \qquad (43)$$

The involvement of phases such as $O_2$ and FeOOH are merely there as suggested electron donors and acceptors in order to provide an overall reaction balance.

The mechanism is a molecular process normally derived from studies of the kinetics of pyrite formation and the derived rate law. The mechanism is involved in all possible pyrite-forming reactions in aqueous solutions no matter what reactants and products are chosen. The rate law itself describes the slowest molecular step in the process. The rate-controlling molecular mechanism formally involves a transition state complex. However, in experimental studies of heterogeneous kinetics such transition state complexes may not be formally accessible or defined. In the case of pyrite formation, the kinetic evidence described below demonstrates that an aqueous [FeS] reaction intermediate is produced in the rate-controlling reaction. However, as has been repeatedly demonstrated,[311] this [FeS] reaction intermediate is not equivalent to $FeS_m$.

Table 12 summarizes experimental syntheses of pyrite. Work prior to 1935 was reviewed in some detail by Mellor,[203] and further listings were reported by Schoonen and Barnes[328] and Wei and Osseo-Asare.[171] We have restricted our summary to experiments at typically <100 °C and in aqueous solutions. Because of the interest in pyrite in material science, as a possible solar cell material, for example, there are a large number of published reports of syntheses in nonaqueous solvents, at high temperatures, or both. Table 12 is a summary of the reactions described but needs to be treated with caution and the original reports should be read in detail. One problem is that $FeS_2$ also describes the pyrite dimorph, marcasite, and the synthesis of pyrite needs to include XRD confirmation of the product. Furthermore, the product is rarely 100 wt % pyrite but also contains various amounts of reactants and other iron sulfide products.

In reality the various Fe salts used appear to be largely irrelevant: Fe(II) and Fe(III) are mostly dissociated in these systems. Experimentally, the use of Mohr's salt, $Fe(NH_4)_2(SO_4)_2$, is recommended since this is more resistant to oxidation than simple iron(II) sulfates, chlorides, and nitrates. The reasons for this are unknown. Except in the case of Harmandas et al.,[306] all the reactions with Fe salts were supersaturated with respect to $FeS_m$, and because of the kinetics, $FeS_m$ can be assumed to have been precipitated, even when this is not reported. The experimental systems used are overwhelmingly of the batch reactor type and the reactant concentrations are therefore necessarily in the millimolar to molar range, often much greater than would normally be encountered in natural systems. The reaction processes therefore often involve the reaction of a dissolved FeS species, nanoparticulate $FeS_m$, or both with the solution.

In order to overcome this, a series of reactions have been carried out using variously defined FeS precipitates as reactants, rather than the less well-defined *in situ* precipitate. Obviously, for well-defined experiments, especially kinetic studies, the FeS reactant needs to be both well-characterized and reproducible. Freeze-dried $FeS_m$ has been used as a defined reactant,[54] for example, and the process of freeze-drying has been shown to arrest the development of $FeS_m$.[189] The development of this material continues when it is placed back in solution.

These systems with an FeS reactant appear to have been mostly undersaturated with respect to $FeS_m$ since excess Fe was not added, and the $FeS_m$ therefore dissolved in the course of the experiments. However, as noted above, nanoparticulate $FeS_m$ is sensitive to oxidation and to the medium in which it is handled. The problem here is that the material has to be carefully defined in order that the experiments may be reproduced. The Cardiff laboratory has contributed to overcoming this problem by sending synthetic samples of reactants to other laboratories worldwide on request.

One of the effects of the prior precipitation of $FeS_m$ is that the actual reactant concentrations of dissolved Fe and S(−II) are not easily controlled. Opening systems to air or using apparently oxidized $FeS_m$ also makes the reactant materials difficult to define. A similar discussion is applicable to the sulfur reagents. We define $H_2S$ where this is introduced as a gas, but it should be noted that this normally required a counterion to maintain solution pH and this is generally $Na^+$. Thus there is little chemical difference between this and $Na_2S$ or NaHS, which are basically solutions of $H_2S$ in NaOH and are mainly dissociated.

In the case of polysulfide reactants, rapid equilibration occurs in solution providing a spectrum of polysulfide stoichiometries, even if a well-defined polysulfide reagent is used in the first place. The best that can be attained is dominance of a particular species under specific physicochemical conditions, as noted above. In each case, the reaction between iron(II) and polysulfides appears to have been oversaturated with respect to $FeS_m$, and this is therefore precipitated rapidly in the experiments. The minimum S(−II) concentrations in rapidly equilibrated aqueous polysulfide systems occur in the presence of excess $S_8$. However, even here the dominant dissolved S species are S(−II), as discussed above. It has been shown that $Fe^{2+}$ reacts directly with polysulfides to form $FeS_m$ and S(0).[280,285,311,328] Even in systems apparently undersaturated with respect to $FeS_m$, $FeS_m$ still forms locally in the reaction kettle and then dissolves.[51,54,309,311,328] Schoonen and Barnes[328] did not observe pyrite formation in such systems, although they did not observe pyrite formation in oversaturated systems either, and this is probably a result of the very short reaction time in these experiments.

Mechanistically it has been demonstrated that pyrite formation in low-temperature aqueous solution involves the formation of a dissolved [FeS] transition intermediate[51,309,311] and that the suppression of such intermediates can inhibit pyrite formation.[273] This raises an immediate experimental problem in that Rickard et al.[273] showed that trace amounts of aldehydic carbonyl were sufficient to suppress pyrite formation. This means that the reaction systems need to be very clean with respect to aldehydic carbonyls, which are widespread in a number of key biochemical pathways; it also implies that other trace organics might also have similar effects. The possible effects of trace contaminants, including microorganisms, in low-temperature experimental sulfide systems have not been investigated. It might help explain some of the contradictory and often irreproducible results that have been reported in pyrite syntheses. It would seem certain to have an effect on the distribution of pyrite in natural systems.

Even so, experimentally the main problem appears to be the control of oxidation. The maximum $O_2$ content measured in the Cardiff laboratory for commercial analytical grade $O_2$-free $N_2$ gas was 17 ppmv. Obviously, this was from a bad batch, but even blowing $N_2$ gas with a lower ppmv level of $O_2$ into sulfidic reaction vessels can provide sufficient oxidant to change the system. In the Cardiff laboratory, all reactions

**Table 12. Pyrite Recipes from Reported Abiologic Syntheses of Pyrite in Aqueous Solutions Typically at <100 °C and 1 bar Total Pressure**

| Fe reactants | S reactants | *T* (°C) | pH | comments | ref |
|---|---|---|---|---|---|
| Fe(II)[a] | $H_2S$ | 20[i]−95 | 3−5 | open to air | 283 |
| | | ~25[i] | 7−8 | | 312 |
| | $H_2S + S_8$ | 65 | 6.9, 7.9 | | 285 |
| | | 25[i]−60 | ? | open to air | 218 |
| | $NaHS + S_8$ | 65[i] | 1.5 − 8.8 | | 357 |
| | $Na_2S_n$[g] | 25[i] | 4.4−9.5 | | 209 |
| | $H_2S + Na_2S_4$ | 75[i] | 2.4−7.2 | | 344 |
| | $NaHS + Na_2S_4$ | 25[i] | 7.3−7.6 | | 328 |
| | $Na_2S_2$, $Na_2S_4$, $Na_2S_5$[h] | 25[i], 100 | 5.5−8 | | 311 |
| | $H_2S + Na_2S_2O_3$ | 75[i] | 3.4−6.9 | | 344 |
| Fe(III)[b] | $Na_2S_5$[h] | 25[i] | 5.5 | | 311 |
| | NaHS, $Na_2S$ | | 3.6, 6.5 | | |
| | $H_2S$ | 25[i] | 5.5 | | 313 |
| $FeCO_3$ | cystine | 100 | ? | with humic acids | 314 |
| FeOOH[c] | $H_2S$ | 20−25[i] | 4 | | 283 |
| | | 25[i] | 3.8−6.5 | | 313 |
| | $Na_2S$ | 25[i] | 4.4−7.0 | | 209 |
| | | 25[i] | 6−8 | | 229 |
| | | ? | 7−8.5 | | 231 |
| | $H_2S + S_8$ | ~25[i] | 6.5−7.5 | | 315 |
| $FeS_m$[d] | $S_8$ | 65 | 7 | | 316 |
| | | 60−85 | ? | open to air | 218 |
| | $H_2S + S_8$ | 25[i]−50 | 6−8 | | 309 |
| | $H_2S$ | 70[i] | 6−8 | | 310 |
| | | 25−125 | | | 54 |
| | | 100 | | | 313, 317 |
| | | 60−100 | 6 | | 310 |
| | | 70[i] | 6−8 | open to air | 310 |
| | $H_2S$ + RSH, RSSR, sulfonate | 70[i] | 6−8 | | 310 |
| | $H_2S + Na_2SO_3$, $Na_2S_2O_3$ | 70[i] | 6−8 | | 310 |
| | $Na_2S_n$ | 25[i] | 7 | | 209 |
| ox $FeS_m$[e] | $H_2S$ | 35−160 | ? | | 317 |
| | | 70 | | | 310 |
| $FeS_t$[f] | $H_2S$ | 100 | ? | | 267 |
| $Fe_{1-x}S$[g] | $H_2S$ | 100 | ~7 | | 369 |
| $Fe_3S_{4g}$ | RSH, RSSR, sulfonate | 70[i] | 6−8 | | 310 |
| | | 70[i] | 6−8 | open to air | 310 |
| | $H_2S + Na_2SO_3$, $Na_2S_2O_3$ | 70[i] | 6−8 | | 310 |
| | $H_2S$ | 70[i] | 7.71 | | 310 |
| $FeS_{2p}$ | NaHS | 25[i] | 6.5 | undersaturated wrt $FeS_m$ | 306 |

[a] As $FeSO_4$, $FeCl_2$, or $Fe(NH_4)_2(SO_4)_2$. [b] As $FeCl_3$ or $Fe(NO_3)_3$. [c] As α-FeOOH or unspecified iron(III) (oxy)hydroxide. [d] Precipitated FeS is assumed to be $FeS_m$. [e] $FeS_m$ oxidized in air before reaction with unspecified composition. [f] Troilite. [g] Commercial unspecified pyrrhotite. [h] S(−II) present, see text. [i] Reaction temperature. In all other cases, the reactants were mixed at room temperature and heated to the noted temperature.

are now carried out in anoxic chambers under an inert gas atmosphere, which has been scrubbed for $O_2$ removal with Zr powder in a high-temperature furnace. A further problem, as mentioned above is the analysis of $O_2$ at low levels; conventional methods even in the absence of S compounds have detection limits of >1 ppm, which can constitute a substantial amount of $O_2$ in these systems. It is possible that the $O_2$ contents in natural marine and sedimentary anoxic systems is lower than that routinely attainable in the laboratory, since microorganisms are likely to remove all $O_2$ to an extremely low level.

Careful reading of the original reports is required to establish exactly what S source was added. Thus it might appear that Wilkin and Barnes,[310] for example, used simple $S_8$, polysulfides, or organic sulfur salts as reactants. However, they state (p 4169), "After purging the solution again, the input gas was switched to a 3% $H_2S$ mixture in $N_2$ to maintain a constant partial pressure of hydrogen sulfide." This is not mentioned in their summary table of experimental results, since it is a constant feature of their experiments, and could be missed by the casual reader.

The listed pH of the experiments is merely a guide. In most cases, it is the final pH, and this is often reached within a few hours. The problem is that the reactions generally tend to produce relatively large quantities of acid and buffering in batch systems is normally impractical, since at the concentrations required the buffer itself reacts with the Fe and S reactants.

In most cases, the reactants were added at room temperature and then heated to the temperature listed. Since the precipitation of $FeS_m$ is fast, this means that a $FeS_m$ precipitate was initially formed in the reaction vessel at room temperature and the subsequent, ill-defined mixture was the one involved in the reaction. Of course, the initial reactant could include $Fe_3S_{4g}$ or $FeS_{2p}$, as well as $FeS_m$. Where the reaction as a whole was carried out at the listed temperature, this is noted.

The reaction products have been quantitatively analyzed in very few cases, indeed mostly in the kinetic investigations (e.g., refs 54, 306, and 309) The solid products are usually identified qualitatively by powder XRD, for example, and the product solutions are rarely analyzed at all. This, together with the lack of definition of the actual reactant, is one reason we refer to these reactions as "recipes". Unfortunately, these poorly defined experimental syntheses have formed the basis

for widespread discussions of pyrite formation in marine and sedimentary environments.

Only three mechanisms for pyrite formation have been established, one involving iron(II) and polysulfide,[309,311] one involving FeS(aq) and S(−II),[51,54] and a third for pyrite crystal growth.[306] A problem for the reader is that some of the large numbers of suggested theoretical balanced reactions are written on the bases of experiments or natural observations that report few chemical analyses of the reactants and products and no total analyses of the reactants and products. All these proposed reactions have, at their core, the molecular mechanisms established by Rickard,[309] Luther,[311] Rickard,[54] Rickard and Luther,[51] and Harmandas et al.[306]

### 7.4.1. Mackinawite, $FeS_m$, as a Reactant

As shown in Table 12, a number of Fe reactants have been proposed in pyrite formation. However, $FeS_m$ has been singled out for special mention because (a) it is normally produced initially in experimental syntheses of pyrite and (b) it was formerly believed to be widespread in sediments.[40,101,262,285,310,318−323] Rickard and Morse[1] discuss this in some detail and note that the idea may have partly arisen because of the assumption that HCl-soluble sulfide in modern sediments was equivalent to $FeS_m$.[324] As shown below, $FeS_m$ is involved as a reactant in most experimental syntheses of pyrite because of the demands of the experimental design. However, $FeS_m$ is not generally observed to form in normal marine sediments because the Fe concentration in seawater is usually so low.

In many papers,[40,101,262,285,310−323] mackinawite is referred to as a "precursor" mineral. Of course, $FeS_m$ could be a "precursor" in high Fe systems in the sense that it forms far more rapidly than pyrite. However, it is not a "precursor" in the sense that it is a *necessary* prerequisite for pyrite formation. In fact, there is no reason to suppose that $FeS_m$ is any more of a "precursor" mineral than FeOOH, $Fe_2O_3$, $Fe(OH)_3$, green rust 2, fougerite, or any other Fe phase that may react with sulfide to form pyrite. Certainly, it has been unequivocally demonstrated experimentally and in natural systems that $FeS_m$ does not "transform to pyrite" in the sense of a solid-state transformation. $FeS_m$, where it occurs, dissolves, and pyrite forms from the reaction between dissolved iron and sulfur species to which the products of the $FeS_m$ dissolution reaction contribute. In this sense, $FeS_m$ is no different from any other Fe reactant. In the case of a closed system with no added dissolved Fe or S, the solubility product of $FeS_m$ is far greater than that of pyrite, and pyrite will ultimately precipitate from the products of the dissolution reaction. As shown below, for example, this process is at the core of reaction 42.[310]

The distinction between an imagined solid-state process and the proven dissolution process is more than mere sophistry. Sulfur isotopic compositions of sedimentary sulfides are used as key proxies for investigations of the modern sulfur cycle and its geological evolution. Since the sulfur cycle is intimately related to the global oxygen and carbon cycles, these measurements are central to understanding how the Earth system works. The conventional *crossover* plots (Figure 36) showing the decrease of acid volatile sulfur with sediment depth and the increase of pyrite S with depth do not balance, even if it is assumed that the acid volatile sulfur derives mostly from $FeS_m$. The trace element contents of $FeS_m$ are not incorporated directly into pyrite, as might be the case if a solid-state transformation occurred. As the $FeS_m$ dissolves, its trace element load is released back into solution. The importance of this is that trace elements removed by $FeS_m$ precipitation are not permanently fixed in pyrite. This, of course, has consequences for pollution studies and the use of pyrite trace elements as paleoenvironmental indicators. Since pyrite forms from dissolved species, which may include the products of $FeS_m$ dissolution, the specific location of pyrite formation is not necessarily the same as the site of any original $FeS_m$ precipitate. This means that vertical profiles of sedimentary sulfides are dynamic and cannot be treated in terms of static (closed-system) mass balances of sulfide phases, either chemically or isotopically.

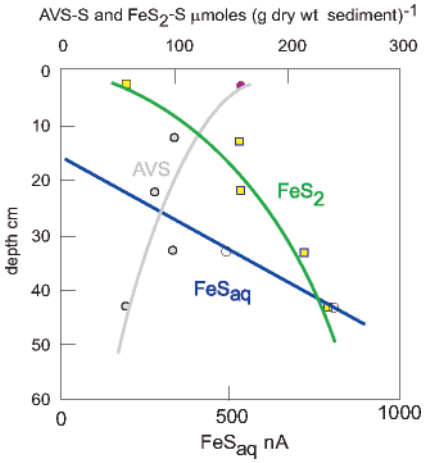


**Figure 36.** A crossover plot compiled from data in Rickard et al.[183] The concentration of acid volatile sulfide (AVS-S) in micromoles per gram dry weight of sediment decreases with depth in a sulfidic sediment, and the concentration of $FeS_{2p}$-S increases with depth. Although widely assumed to suggest that $FeS_m$ transforms to $FeS_{2p}$, in fact it merely shows that metastable $FeS_m$ dissolves and stable $FeS_{2p}$ precipitates, as shown by the increase in FeS(aq) with depth, shown as the current (in nanoamps) of the FeS(aq) voltammetric peak.

Mackinawite solubility in neutral to alkaline solutions is discussed above. Previously, it was supposed that the pH-dependent reaction 15 controlled mackinawite solubility at all pH values. Log $K$ for reaction 15 is around −3.5, which means that $\{Fe^{2+}\}$ in equilibrium with $FeS_m$ at pH = 7 in the presence of millimolar S(−II) is around $10^{-14.5}$, which would imply that $FeS_m$ would precipitate from normal seawater in the presence of millimolar sulfide. In fact, at the neutral to alkaline pH values characterizing many natural aqueous environments, including marine environments, $FeS_m$ stability is constrained by its intrinsic solubility (reaction 18) with log $K = 10^{-5.7}$. Since $[S(-II)]_T = [H_2S] + [HS^-] + [FeS^0]$, $FeS_m$ dissolves at $[S(-II)]_T \leq 10^{-5.7}$ M. At $[S(-II)]_T \geq 10^{-5.77}$ M, it requires $[Fe]_T \geq 10^{-5.7}$ M to produce FeS(aq). As shown above, $FeS_m$ formation is therefore limited to systems with high Fe concentrations. It would not normally be expected to form in normal marine sediments. This in accord with the survey reported by Rickard and Morse,[1] which showed that $FeS_m$ has only once been reported from apparently normal marine sediments.[325] Many of the reports of $FeS_m$ as a precursor to pyrite actually stem from studies of inshore marine and freshwater environments where the Fe content is high compared with normal marine systems. Such environments include the FOAM site, studied by Berner and his co-workers, which had a scrap iron dump, the Black Sea, certain fjords, and the Baltic Sea. Even the open ocean site where mackinawite was reported[325] may have been affected by hydrothermal vent activity. Therefore, mackinawite is not a necessary "precursor" to pyrite formation.

In systems, such as inshore and fresh waters where $[Fe]_T$ is high and $FeS_m$ does form, then it is in equilibrium with relatively high $[Fe]_T$ and $[S]_T$. As reported above, thermodynamically such concentrations are adequate to precipitate pyrite. This is another way of saying that $FeS_m$ is unstable with respect to pyrite. As shown below, the actual mechanism of the reaction to form pyrite involves the dissolution of $FeS_m$ and the precipitation of pyrite.

### 7.4.2. Greigite, $Fe_3S_{4g}$, as a Reactant

The apparent evidence for greigite, $Fe_3S_{4g}$, being involved in pyrite formation appears to have been (1) that $FeS_m$ does transform through a solid-state reaction to greigite, as discussed above and (2) the observations of "magnetic pyrite", from Doss's[249] original report, which appear to derive from intimate mixtures of greigite and pyrite. Bonev et al.,[326] for example, describes pyrite rimming greigite concretions from Black Sea sediments. However, the solid-state transformation of greigite to pyrite has not been demonstrated either experimentally or mechanistically, and it is structurally and chemically improbable. The origin of the "magnetic pyrite" and the intimate mixtures of greigite and pyrite in natural systems is simply that greigite dissolves and pyrite precipitates. We used to call such processes "replacement".

Structurally, all three structures are based on anion cubic close packing (ccp) but whereas mackinawite and greigite show arrays of simple atoms, the pyrite anion ccp is conceptual. It results from a rationalization of the arrangement of the average center points of the $S_2^{2-}$ dumbbells. Thus, while mackinawite can readily transform to greigite through a rearrangement of Fe atoms in a ccp sulfur lattice, pyrite formation requires significant rearrangement of the sulfur lattice. $FeS_m$ precipitated from aqueous solutions at low temperatures is usually nanoparticulate, whereas pyrite is microparticulate; that is the pyrite crystals are normally around 1000 times larger than the $FeS_m$. The pyrite has been demonstrated to form at a distance from $FeS_m$ in experimental systems at a distance defined by the pyrite solubility product. And, of course, pyrite crystals grow. They grow quite rapidly and often to substantial sizes. Pyrite crystal growth has to be a solution process.

Chemically, the formation of $FeS_{2p}$ from $FeS_m$ requires that the $FeS_m$-S is oxidized but the FeS-Fe is not. In the $FeS_m$ to $Fe_3S_{4g}$ transition, the $FeS_m$-Fe is oxidized to Fe(III), whereas the $FeS_m$-S remains unchanged. Pyrite is a low-spin semiconductor with a particularly low unit cell volume,[327] whereas the Fe in greigite and mackinawite is high-spin.

In low-temperature experimental syntheses of pyrite where the initial reactant is a dissolved Fe(II) salt, the solubility product for $FeS_m$ (and $Fe_3S_{4g}$) is almost always exceeded. The reasons for this are technical. In order to synthesize sufficient quantities of pyrite for analysis, the concentration of S(−II) and Fe(II) salts is normally >0.001 M. If the yield of the synthesis is 100% such concentrations would produce around 12 mg of $FeS_2$ per 100 mL of solution. At these Fe(II) and S(−II) concentrations, the $FeS_m$ solubility product is exceeded at all pH values between ca. 4 and 10 at 25 °C. Since the rate of $FeS_m$ precipitation is rapid, $FeS_m$ cannot be avoided in such experiments. One way around this would be to use a continuous flow system, which would permit the gradual accumulation of sufficient quantities of $FeS_{2p}$ for analysis while avoiding $FeS_m$ precipitation. However, there are still some practical problems with this approach. For example, the S(−II) solutions at <0.001 M must be handled very carefully since they are prone to oxidation, and the lower the S(−II) concentration, the greater cryptic oxidation will affect the totals. One benefit of the system is, of course, that if $FeS_m$ precipitation can be avoided, then $Fe_3S_{4g}$ will not form since this is only produced from preexisting $FeS_m$. The use of acidic solutions, where the solubility product of $FeS_m$ is so high that precipitation might be avoided, but where $FeS_{2p}$ is still stable, appears to be precluded because of the formation of marcasite (and possible sulfur) under these conditions. The result of these technical problems has been that nearly all low-temperature pyrite syntheses have, effectively, $FeS_m$, $Fe_3S_{4g}$, or both as a reactant.

### 7.4.3. Pyrite Nucleation and Crystal Growth

Pyrite formation involves two distinct physical processes, nucleation and crystal growth. Whereas pyrite crystal growth, as mentioned above, appears relatively fast, nucleation of pyrite is slow and potentially rate-limiting.[328] Harmandas et al.[306] investigated this by experiments that approached pyrite formation from undersaturation with respect to $FeS_m$ and below the $FeS^0$ stability region. The supersaturation limit, $\Omega^*$, is defined as the supersaturation level up to which a phase can be expected not to precipitate spontaneously. The supersaturation limit can be regarded as the supersaturation level at which pyrite nucleation is relatively fast and not rate-limiting. Harmandas et al. measured $\Omega^*_{pyrite}$ in the presence of pyrite seeds to be $5.7 \times 10^{14}$ (±10%) for reaction 35. Converting this to the solubility reactions in terms of $HS^-$ gives a similar value for $\Omega^*_{pyrite}$. This result is important since it means that at $\Omega^*_{pyrite} < 10^{14}$, the rate of pyrite nucleation determines the rate of pyrite formation. At $\Omega^*_{pyrite} > 10^{14}$, the rate of pyrite crystal growth is the rate-limiting process, and this feature was exploited by Harmandas et al. in their experimental investigation of pyrite crystal growth kinetics.

Rickard et al.[329] investigated the supersaturation limit for pyrite in the presence of an organic substrate and found that $\Omega^*_{pyrite}$ was some 3 magnitudes lower, around $10^{11}$. This result suggests that the supersaturation necessary for spontaneous nucleation of pyrite is substrate dependent.

At 25 °C, the solubility of $FeS_m$ written in terms of $\{Fe^{2+}\}$-$\{H_2S\}$ (eq 16) at pH 7 is $10^{-10.5}$. The solubility of pyrite written in terms of $\{Fe^{2+}\}\{H_2S\}$ (eq 33) at pH 7 is $10^{-21.2}$. The supersaturation with respect to pyrite in an aqueous solution at 25 °C at pH 7 in the presence of $FeS_m$ is thus $10^{10.7}$. This is similar to $\Omega^*_{pyrite}$ in the presence of active surfaces like organic substrates.

The result suggests that systems that contain $FeS_m$ are close to the pyrite supersaturation limit and small supersaturations with respect to $FeS_m$ will cause pyrite to nucleate spontaneously. It may also infer that $FeS_m$ provides an active surface that enhances pyrite nucleation, a suggestion that would be consistent with the observations of many experimentalists. In other words, the presence of $FeS_m$ in experimental and environmental pyrite-forming systems is neither happenstance nor because of some requirement for $FeS_m$ as a precursor in pyrite formation. The reason is that at the supersaturations required to initiate rapid pyrite nucleation, the system will tend to be saturated with respect to $FeS_m$.

### 7.4.4. Polysulfide-Controlled Pyrite Reaction Kinetics: The Bunsen Reaction

In 1847, Bunsen originally reported that FeS reacted with polysulfide to form pyrite.[330] This work has been largely forgotten, although it was well-known toward the end of the 19th century.[331] The process has been described in the modern geochemical literature as the polysulfide pathway. However, conventional chemical procedures would suggest that the reaction should be described under the name of its discoverer and the reaction should be more correctly referred to as the *Bunsen Reaction*.

Rickard[309] showed that the rate of pyrite formation increases with increased polysulfide concentration. That is, the rate-controlling step in pyrite formation involves a reaction between an iron species and polysulfide. This is unsurprising in view of the equilibrium thermodynamic background to pyrite formation discussed above. Rickard found that the rate of pyrite formation is first order with respect to polysulfide and second order with respect to $FeS_m$ surface area. He expressed the rate equation as

$$\partial[FeS_{2p}]/\partial t = kA_{FeS_m}{}^2 A_{S(0)}\{S(-II)\}_T\{H^+\} \quad (44)$$

where $A_{FeS_m}$ and $A_{S(0)}$ are the surface areas of $FeS_m$ and S(0), respectively, in square centimeters, $\{S(-II)\}_T$ is the total dissolved sulfide activity, and $\{H+\}$ is the hydrogen ion activity. The kinetics show that pyrite formation from $FeS_m$ involves a solution reaction, as originally reported by Bunsen. The Arrhenius energy for the reaction is consistent with this: it is relatively high showing that the rate-controlling step is a chemical reaction and not transport-controlled (e.g., diffusion). Rickard concluded that pyrite formation occurred through the reaction between hexaqua $Fe^{2+}$ and polysulfide.

The rate law (eq 44) is complex and includes the rate of formation of polysulfides from the reaction between S(0) and S(−II). Kamyshny et al.[86] examined the kinetics of equilibration of dissolved polysulfides and showed that the reaction rate was rapid and that equilibration between polysulfide species in solution was fast. The kinetics of the reaction between $S_8$ and S(−II) were originally reported by Hartler et al.[332] and revisited by Boulegue and Michard.[72] Hartler et al.[332] found that the rate was first order with respect to total sulfide in the presence of polysulfide and possibly second order with respect to S(−II) in the absence of polysulfides. They found that the Arrhenius energies for both reactions are low and the reactions are probably mainly diffusion controlled. The rate is not affected significantly by $OH^-$, which suggests that the rate of dissolution is mainly independent of pH. Boulegue and Michard[72] found that the rate of dissolution of $S_8$ is first order with respect to $HS^-$. The problem with these transport-controlled reactions is that they are sensitive to the small variations in the nature of the reactant sulfur through the surface area dependence and dependence of the relative solution velocity with respect to the particle surface. Sjöberg and Rickard[333] showed that even the reaction vessel shape can affect kinetics of transport-controlled reactions. Rickard[309] investigated the reaction under conditions where transport was not rate-controlling, and thus, the rate of sulfur dissolution in the pyrite-forming system that he investigated appears to be relatively fast and equilibration was approached.

The second-order dependence on $FeS_m$ means that $FeS_m$ is involved in more than one rate-determining reaction, and the first-order dependence on $\{H^+\}$ at constant S(−II) suggest that the $FeS_m$ dissolution is involved in the rate-determining step. The rate of $FeS_m$ dissolution has been investigated by Pankow and Morgan[246] as discussed above. Their data show that $FeS_m$ reaches equilibrium rapidly with dissolved Fe and S. The rate of pyrite formation is slow relative to the rate of dissolution of $FeS_m$, and thus $FeS_m$ acts as a continuous source of dissolved Fe and S components for pyrite formation.

Rickard[309] suggested that the mechanism involved an aqueous FeS reaction intermediate, which was attacked by nucleophilic polysulfides with formation of $FeS_2$. The basic mechanism could be illustrated with respect to $S_5^{2-}$ by the sequence

$$Fe^{2+} + S(-II) \rightarrow [FeS] \qquad \text{rapid} \quad (45)$$

$$[FeS] + S_5^{2-} \rightarrow FeS_2 + S_4^{2-} \qquad \text{rate-controlling} \quad (46)$$

where [FeS] is an aqueous iron(II) sulfide reaction intermediate. The kinetics of the [FeS] formation involves an Eigen−Wilkin substitution reaction[220] and the rates are limited by the water-exchange rate for $Fe(H_2O)_6^{2+}$. Thus, with $HS^-$,

$$Fe(H_2O)_6^{2+} + HS^- = Fe(H_2O)_6{\cdot}HS^+ \quad (47)$$

$$Fe(H_2O)_6{\cdot}SH^+ = FeSH{\cdot}(H_2O)_5^+ + H_2O \quad (48)$$

and with $H_2S$,

$$Fe(H_2O)_6^{2+} + H_2S = Fe(H_2O)_6{\cdot}H_2S^{2+} \quad (49)$$

$$Fe(H_2O)_6{\cdot}H_2S^{2+} = FeH_2S{\cdot}(H_2O)_5^{2+} + H_2O \quad (50)$$

Both $FeSH{\cdot}(H_2O)_5^+$ and $FeH_2S{\cdot}(H_2O)_5^{2+}$ are expected to achieve rapid equilibration with species like $FeS^0$ and $FeSH^+$ depending on pH, as discussed above. The Eigen−Wilkins process is significant because the rate is more-or-less independent of the nature of the incoming anion and essentially cation specific. Thus, since under most natural systems S(−II) is more abundant than $S_n$(−II), the [FeS] intermediate is more likely to form rather than a [$FeS_n$] intermediate.

Generally, for $S_n$(−II), where $n \leq 2$ the most stable species is protonated and where $n \geq 3$ the more stable species are unprotonated. Luther[292] reviewed $S_n$(−II) nucleophilicity. The relative nucleophilicity of the species follow the energies of the HOMOs of the $S_n$(−II) species. Longer chain polysulfides are more nucleophilic than shorter chain polysulfides. The nucleophilicity varies in the sequence $S_5^{2-} > S_4^{2-} > HS^- > HS_2^- > S_3^{2-} > H_2S$. Note that longer chain $S_n^{2-}$ species are actually more nucleophilic than $HS^-$, and $HS_2^-$ is less nucleophilic than $HS^-$. This means that, although $HS_2^-$ may be the most abundant polysulfide in many environmentally significant pH regimes, it is less nucleophilic than $HS^-$ and likely to react more slowly.

These FMO considerations are interesting because they help explain why the addition of excess rhombic sulfur in a sulfide solution is a preferred route for the rapid syntheses of pyrite at low temperatures. As shown in Figure 11, the dominant $S_n$(−II) species in the $S_8$ stability field are species with $n \geq 5$. These longer chain polysulfides are the most nucleophilic species, and thus their relative abundance is expected to enhance the rate of the rate-controlling reaction in pyrite formation, the nucleophilic attack on the [FeS]

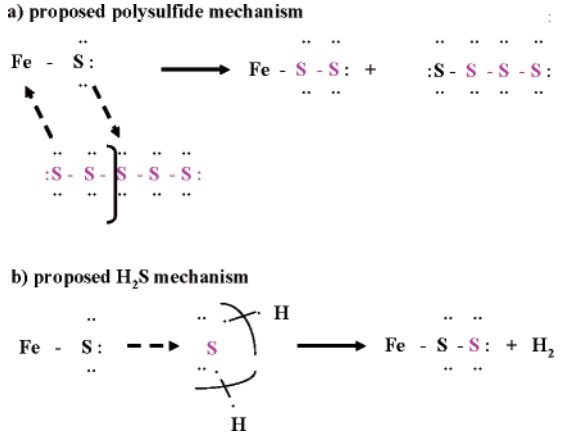


**Figure 37.** Proposed pyrite formation mechanisms from soluble FeS and (a) polysulfides and (b) hydrogen sulfide. Sulfur isotope data support these mechanisms.

reaction intermediate. Luther[311] reacted pure $S_n^{2-}$ solutions with Fe(II) and independently reproduced the kinetics found by Rickard.[309] Figure 37a shows the proposed mechanism, which indicates that the $FeS_{2p}$ formed should have all S atoms from $S_n^{2-}$ species. Butler et al.[334] confirmed this isotopically.

### *7.4.5. Sulfide Controlled Reaction Kinetics: The Berzelius Reaction*

The sulfide-controlled reaction to form pyrite stems from an original observation by Berzelius,[335] which was largely forgotten in the 20th century. It was revisited in reports by Wikjord et al.[336] and Huber and Wächtershauser[337] that $H_2S$ reacted with iron(II) monosulfide to form pyrite. The Berzelius reaction is

$$FeS + H_2S \rightarrow FeS_{2p} + H_2 \quad (51)$$

where FeS was originally undefined but subsequently referred to as pyrrhotite[337] or mackinawite.[54]

Reaction 51 is thermodynamically favorable at low temperatures ($\Delta G_r^\circ = -26.9$ kJ mol$^{-1}$, 25 °C, 1 bar total pressure where FeS = $FeS_m$) using the revised $\Delta G_f^\circ(FeS_m) = -98.22$ kJ mol$^{-1}$ and other data as listed above. Thus any discussions about its significance in the natural environment must solely be dependent on the kinetics. As discussed below, the kinetics of pyrite nucleation are characteristic of a sparingly soluble salt and quite sensitive to catalysis. It has become popular in some parts of the geochemical literature to sideline this reaction to higher temperature environments or late stage sedimentary processes, with little reason. In fact, as discussed below, the reaction is central to some of the most exciting developments in Fe−S chemistry at the present time.

The Berzelius reaction is a special case of the Bunsen reaction where the $S_n(-II)$ species has $n = 1$ and the more stable form is protonated. It is important since S(−II) species are involved in all reported aqueous syntheses of pyrite. As noted above, the FMO sequence for $S_n(-II)$ species suggests that $HS^-$ is less nucleophilic than $S_n(-II)$ where $n > 3$. $H_2S$ is less nucleophilic than all the species listed since the HOMO for $H_2S$ is relatively stable (ca −10 eV).[52] In contrast, the LUMO for $H_2S$ is around −1.1 eV,[52] and therefore $H_2S$ is a good electron acceptor (i.e., oxidizing agent). The mechanism of the reaction between Fe(II) and $H_2S$ to form $FeS_2$ thus again involves [FeS] as a reaction intermediate, but in this case, $H_2S$ does not substitute for [FeS]−$S^{2-}$ in a nucleophilic attack but is involved in a redox reaction resulting in the oxidation of [FeS]−$S^{2-}$ to $S_2^{2-}$. In both reactions, FeS is a nucleophile, but in the polysulfide pathway, it is also an electrophile because higher order and more nucleophilic polysulfides can bind to the Fe(II) in FeS.

Rickard[54] and Rickard and Luther[51] demonstrated that the kinetics of this reaction involved a rate-controlling step involving $H_2S$. They showed that the mechanism involved the formation of an inner sphere complex (Figure 37b) between [FeS] and $H_2S$ followed by electron transfer between S(−II) and H(I) to produce $S_2$(−II):

$$[FeS] + H_2S \rightarrow [Fe{-}S{\rightarrow}SH_2] \rightarrow FeS_2 + H_2 \quad (52)$$

where [Fe−S→$SH_2$] is a reaction intermediate. In this reaction, $H_2S$ acts as an oxidizing agent with respect to [FeS]. Butler et al.[334] confirmed this mechanism isotopically. They demonstrated that the $\delta^{34}S$ of the product $FeS_{2p}$ from the reaction equaled a 1:1 mixture of the $\delta^{34}S$ of the reactant $FeS_m$ and $H_2S$. The rate equation for the $H_2S$ mechanism is

$$\partial[FeS_{2p}]/\partial t = k[FeS_m][H_2S] \quad (53)$$

where $[FeS_m]$ is the molar concentration of $FeS_m$ (applicable because the reactant $FeS_m$ had a comparable initial surface area in all experiments), $[H_2S]$ is the molar concentration of $H_2S$, and $k$ is the rate constant.[54]

Butler et al.[334] noted that the so-called "iron loss pathway" (eq 43) reported by Wilkin and Barnes[310] was actually a modification of the $H_2S$ reaction mechanism. The reaction stoichiometry proposed by Wilkin and Barnes (but not actually analytically demonstrated) was the sum of two well-established reactions:

$$FeS_m + 2H^+ = Fe^{2+} + H_2S \quad (15)$$

$$FeS_m + H_2S = FeS_{2p} + H_2 \quad (51)$$

$$2FeS_m + 2H^+ = FeS_{2p} + Fe^{2+} + H_2 \quad (43)$$

Butler et al.[334] noted that the reaction of $FeS_m$ ($\delta^{34}S = 2.8‰$) and $H_2S$ ($\delta^{34}S = 3.3‰$) by these processes would produce pyrite with an isotopic composition close to that of the reactant $FeS_m$ (and $H_2S$), as observed by Wilkin and Barnes.[310]

### *7.4.6. Relative Rates of Pyrite Formation*

The rate laws for low-temperature pyrite formation in aqueous solutions have been established for pure inorganic systems. The major application of these laws is to elucidate the mechanisms of the pyrite-forming reactions and thereby inform various pyrite-forming processes, such as stable isotope fractionations or toxic element sequestration in sulfidic systems. The rate laws therefore provide a baseline for pyrite-formation rates in natural systems. As discussed above, the actual rates in natural systems can be affected by trace chemical catalysts and inhibitors[273] and by organisms, especially microorganisms. The effect of microorganisms in the natural low-temperature sulfide system is to bring the systems closer to equilibrium. As discussed in section 2.1, for example, the inorganic sulfate−sulfide system is not reversible in low-temperature sulfidic environments because of the recalcitrant kinetics of inorganic sulfate reduction. Reversibility is achieved through the activities, for example, of sulfate-reducing prokaryotes. The effect of microorganisms

is therefore to increase the rates of reactions through catalytic effects of their biochemical pathways. This means that the experimentally measured rates of low-temperature inorganic systems may not describe the rates in any particular natural system. The rates derived from inorganic kinetic studies provide a sort of baseline rate, which may be locally enhanced depending, particularly, on the makeup the local microbial ecology.

As noted above, some workers have limited the Berzelius reaction to higher temperature systems and have assumed that this reaction is far slower than the Bunsen reaction. In fact there is very little reason for this, and those reports do not include calculations of the relative rates under the conditions addressed. As shown above, in most pyrite-forming experimental systems involving polysulfides and in all normal natural environments, the pyrite-forming environment includes both polysulfides and sulfides, as shown thermodynamically above. So both reactions occur in natural sulfidic environments.[338] In the presence of $FeS_m$, the rate is dependent specifically on the concentration of $H_2S$ on the one hand and polysulfides, especially the longer chain species with $n = 4$ or 5, on the other. Therefore, the concentration of polysulfides or $H_2S$ will be rate-limiting. In systems undersaturated with respect to $FeS_m$, the concentration of Fe(II) may become rate-limiting depending on the sulfide or polysulfide concentrations. We can ignore this situation initially in considering the relative rates of polysulfide and $H_2S$ reactions in sulfur-limited systems.

The concentration of both polysulfide and $H_2S$ are pH dependent at similar total sulfide loadings. Thus the $H_2S$ concentration increases as the pH approaches <7, and the polysulfide concentration, as a fraction of the total sulfide, increases as the pH becomes more alkaline. Butler et al.[334] considered the relative rates of these reactions under experimental conditions ($FeS_m$ present and $P(H_2S) = 0.03$ atm). They showed that, under these conditions, pyrite would form at a rate of $\sim 2 \times 10^{-8}$ mol $L^{-1}$ $s^{-1}$ at pH = 7 and 25 °C through the $H_2S$ reaction. In the presence of excess S(0) under the same conditions, the polysulfide mechanism would produce pyrite at a rate of $\sim 8 \times 10^{-11}$ mol $L^{-1}$ $s^{-1}$, or about 2 magnitudes slower than the $H_2S$ reaction.

The Bunsen reaction also becomes more significant near the S(−II)/$SO_4^{2-}$ redox boundary where polysulfides may become important dissolved sulfur species. Thus in a natural marine sulfidic system with a pronounced redoxcline and an alkaline pH (~8.1), the polysulfide concentration may limit the rate of pyrite formation initially. As the system becomes more reduced and acidic (pH→7), the $H_2S$ reaction may become rate-limiting.

Rickard and Morse[1] combined the rate eqs 44 and 51 to produce a master equation for the rate of pyrite formation, which includes the polysulfide and $H_2S$ mechanisms,

$$\partial[FeS_{2p}]/\partial t = k_{H_2S}[FeS_m][H_2S] + k_{S_n(-II)}[FeS_m]^2[S(0)][S(-II)]_T[H^+] \quad (54)$$

In this formulation $k_{H_2S}$ and $k_{S_n(-II)}$ are the experimentally measured rate constants for the $H_2S$ and polysulfide reaction, respectively. The surface area of $FeS_m$ and S(0) in the Bunsen reaction has been assumed to be directly proportional to the concentrations of total FeS (including both $FeS_m$ and FeS(aq)) since they can be approximated as standard materials and the intrinsic solubility of $FeS_m$ (eq 18) is assumed to represent a zero-order process. We have also assumed that $[S(-II)]_T \approx \{S(-II)\}$ and $[H^+] \approx \{H^+\}$ compared with the original formulation as the errors propagated by these assumptions are well within the uncertainties of the calculations.

Equation 54 reveals that the second term becomes very small as [S(0)] becomes relatively insignificant, and the rate is entirely determined by $[FeS_m]$ and $[H_2S]$. Rickard and Morse[1] calculated the abiologic rates of pyrite formation for a typical total dissolved sulfide concentration in anoxic aquatic and sedimentary systems of between 1 μM and 1 mM, which, at pH = 8, is equivalent to between 0.1 μM and 0.1 mM $H_2S$. Typical sedimentary concentrations of acid volatile sulfide lie between 1 and 100 μmol $gdw^{-1}$ of sediment. Assuming all acid volatile sulfide is in the form of $FeS_m$ (a limiting assumption for which there is little actual evidence[1]) and with a porosity of >90%, this is equivalent to 1 and 100 μmol of $FeS_m$/L of wet sediment. In this system, where [S(0)] = 0 at 25 °C, and with $k = 10^{-4}$ mol $L^{-1}$ $s^{-1}$, the rate of pyrite formation is then between $10^{-11}$ and $10^{-6}$ μmol (L of wet sediment)$^{-1}$ $s^{-1}$ or $10^{-2}-10^{3}$ μmol of $FeS_{2p}$ (L of wet sediment)$^{-1}$ $a^{-1}$. Converting back to dry weight terms, this is equivalent to $3 \times 10^{-4}$ to $3 \times 10^{1}$ μmol of $FeS_{2p}$ $gdw^{-1}$ $a^{-1}$. At pH = 7, for the same conditions, $[H_2S]$ is between 0.5 μM and 0.5 mM, and the rate of pyrite formation $1.5 \times 10^{-3}$ to $1.5 \times 10^{2}$ μmol $FeS_{2p}$ $gdw^{-1}$ $a^{-1}$.

As the $H_2S$ concentration approaches 0 in alkaline sulfidic environments (e.g., pH > 8), the first term in eq 54 becomes very small, and the rate is dependent on S(0) and S(−II) concentrations and pH. As discussed above the [S(0)][S(−II)] term in eq 54 actually describes the rate of formation of polysulfides.

The application of eq 54 to sedimentary conditions is not straightforward since it depends on knowledge of both the concentration of S(0) and $FeS_m$ in the sediment and does not take into account the potential catalytic effects of microorganisms on the system. To illustrate the relative abiologic rates, we consider the case where the concentrations of S(0) and $FeS_m$ are of the same magnitude. The rate of pyrite formation for the polysulfide mechanism under the same environmental conditions as for the $H_2S$ mechanism, except that S(0) is present in equal molar quantities to FeS, then ranges between $10^{-2}$ and $10^{-11}$ μmol of $FeS_{2p}$ $gdw^{-1}$ $a^{-1}$. This is between $10^{-4}$ and $10^{-8}$ times slower than the $H_2S$ mechanism in the absence of S(0). Even accepting considerable errors in the estimate of $FeS_m$ and S(0) concentrations, the differences are so great that the polysulfide mechanism is relatively slow except under conditions where S(0) is present in significant concentrations. Thus, although the rate of pyrite formation may be described mainly by the kinetics of the Bunsen reaction initially near the redox cline, pyrite is actually formed relatively slowly by this process, at least in abiologic systems. However, the microbial ecology of the anoxic/oxic boundary in sulfidic environments includes sulfur-disproportionating microorganisms, which are closely involved in sedimentary pyrite formation in this part of the system. Isotopic evidence[338] shows that pyrite forms at similar rates through both the polysulfide and $H_2S$ processes during bacterial sulfur disproportionation, with total rates up to $10^5$ times faster than the purely inorganic process would suggest. The nature of the catalytic processes enabled by these organisms is unknown. However, it is associated with extremely large sulfur isotope fractionations, and the bacteria leave the pyrite with this signature. The effect of microorganisms on the kinetics is a reflection of their effect

on the thermodynamics of aqueous sulfide systems discussed above. Microorganisms bring low-temperature sulfide systems closer to equilibrium. In other words, they increase the reaction rates.

In iron-limited systems, the rate is controlled by the concentration of Fe(II). In eq 54, this is expressed as [FeS]. Obviously as the Fe(II) concentration approached zero, eq 54 shows that the rate of pyrite formation tends to zero. The effect of Fe limitation is greater on the polysulfide reaction since the second term in eq 54 shows a second-order dependence on [FeS]. As Fe(II) becomes limiting therefore, in the presence of equal concentrations of $H_2S$ and $S_n(-II)$, the sulfide reaction will dominate the pyrite formation rate.

### 7.4.7. Kinetics of Pyrite Crystal Growth

Pyrite "formation" or "precipitation" consists of two processes: (1) nucleation, which is slow and requires relatively high supersaturations, catalytic effects of active surfaces, or both or added trace components, and (2) crystal growth, which is relatively rapid and occurs through the reaction between $Fe^{2+}$ and $S_2(-II)$. The equilibrium data discussed above shows that the disulfide species $HS_2^-$ is present in sufficient concentrations in any experimental or natural S(−II) solution to account for pyrite formation. The experimental systems were saturated with respect to $FeS_m$, and the resultant $FeS_{2p}$ was produced by reaction between $FeS^0$ and sulfur species. This is demonstrated by the observations that (a) the mechanism involves a solution reaction and (b) the suppression of $FeS^0$ led to the inhibition of $FeS_{2p}$ formation.[273] Homogeneous nucleation in solution is unexpected at the best of times, and homogeneous nucleation of relatively insoluble salts like $FeS_{2p}$ is unlikely. Harmandas et al.[306] showed that the pyrite surface itself could act as a catalyst to allow rapid nucleation of $FeS_{2p}$ such that the rate-controlling reaction was crystal growth. In order to achieve this relatively rapidly, Ω needs to be in excess of $10^{14}$ at 25 °C and pH = 6.5.

As discussed above, experimental studies of pyrite formation have been limited by technical problems in probing the system at dissolved Fe and S values that would be below saturation with $FeS_m$. However, Harmandas et al.[306] achieved this, and produced measurable amounts of $FeS_{2p}$, using a constant pH system and pyrite seed crystals. The reactants were hexaqua $Fe^{2+}$, added in the form of $Fe(NH_4)_2(SO_4)_2$, and S(−II) added as NaHS. The pH was maintained at 6.5 and the temperature at 25 °C. The relative saturation with respect to pyrite was calculated according to the reaction

$$Fe^{2+} + S_2^{2-} = FeS_{2p} \quad (55)$$

It is unclear how $\{S_2^{2-}\}$ was calculated. Polysulfide stability constants were not listed in their Table 1, and they merely note (p 1252), "Computations of the relative supersaturation were done considering within the equilibria the presence of disulfide ions." They measured the rate of pyrite crystal growth, $R_p$, and showed that it fitted the semiempirical equation

$$R_p = ks\Omega_p^{\,n} \quad (56)$$

where $n = 3.5 \pm 0.5$, $k$ is the growth rate constant, and $s$ is a function of the active growth sites on the crystal seeds. The rate of pyrite crystal growth is given in units of mol $m^{-2}$ $s^{-1}$, which varied from $2.3 \times 10^{-8}$ to $2.1 \times 10^{-7}$ at $\Omega_p$ between $1.1 \times 10^7$ and $2.4 \times 10^7$. The rate law and high value for $n$ suggest a surface diffusion controlled growth mechanism, which is expected for sparingly soluble salts. Harmandas et al. reported that a similar order was found for the spontaneous precipitation of $FeS_{2p}$ at 80 °C. It is therefore quite clear that pyrite crystals grow quite rapidly from a reaction involving $Fe^{2+}$ and $S_2(-II)$ and that there is no requirement for a $FeS_m$ intermediate in the reaction.

Pyrite has also been synthesized from undersaturation with respect to $FeS_m$ or $FeS^0$ within plant cells.[329,339] In these experiments, initially precipitated $FeS_m$ in the open outer xylem cells was shown to dissolve, and $FeS_{2p}$ formed in the closed interior parenchyma cells. As described above, calculations based on these experiments[329] show that organic surfaces provide an enhanced catalytic effect compared with a pyrite surface, with lower Ω values being needed to produce pyrite rapidly. It therefore appears that pyrite can nucleate from the reaction between hexaqua $Fe^{2+}$ and $S_2(-II)$ in the presence of an active surface. It is possible that other iron sulfides, such as $FeS_m$ and $Fe_3S_{4g}$ provide a similar role. Certainly the intimate association observed between $FeS_{2p}$ and $Fe_3S_{4g}$ in some natural settings would support this proposition.

## 8. Other Iron Sulfides

We have considered the chemistry of the main iron sulfides in marine systems above. However, as shown in Table 1, a number of other iron sulfides occur in nature and have been synthesized in the laboratory. In the following, we briefly consider these phases.

### 8.1. Cubic $FeS_c$

Cubic $FeS_c$ is the Fe equivalent of sphalerite, cubic ZnS. It mainly forms as a product of the reaction of $H_2S$ with metallic Fe. It was first identified by de Médicis[340,341] and Takeno et al.[342] It is a corrosion product in the Girdler sulfide process of heavy-water extraction.[343] $FeS_c$ is formed at <92 °C, pH = 2−6, from the aqueous reaction between Fe(0) and S(−II).[344] At >92 °C, troilite ($FeS_t$) and $FeS_m$ form. At pH > 6, $FeS_m$ forms. $FeS_c$ is metastable with respect to $FeS_m$ and $FeS_t$ and converts to these phases at room temperature in hours to days. Murowchick and Barnes[344] note that the reactants and products detected in the reaction suggest that $FeS_c$ forms through competitive reactions between metallic Fe and S(−II) and aqueous $Fe^{2+}$ and S(−II) with the evolution of $H_2$ gas. The reason for the formation of this phase is not understood. The sphalerite structure of $FeS_c$ includes $Fe_4S_6^{2-}$ subunits and thus $[Fe_4S_6(H_2O)_4]^{2-}$ clusters may be necessary solution precursors by analogy with the ZnS system.[345] As discussed above, the common form of aqueous FeS clusters is $Fe_nS_n$, which are directly related to the basic structural moiety of $FeS_m$. The formation of $FeS_c$ may not therefore be enabled in most FeS solutions. The limitation of $FeS_c$ formation to lower pH may be related to the changing nature of the aqueous FeS clusters in more acid solutions as discussed above. Interestingly, one recipe for forming large, micrometer-sized (everything is relative), $FeS_m$ crystals is through the electrochemical reaction between Fe(0) and S(−II). It may be that the presence of a $FeS_c$ template permits these larger $FeS_m$ crystals to form in contrast to the nanoparticulate material produced through the direct solution reaction. $FeS_c$ has not been found in nature and present

evidence, including its short lifespan and relationship with metallic Fe, makes this unlikely.

## 8.2. Troilite, $FeS_t$, and the Pyrrhotite Group

Pyrrhotite has only been reported once in sediments and troilite has not been reported.[1] The pyrrhotite occurrence was as an overgrowth on magnetite from the Sea of Japan.[346] This association may suggest a higher temperature source. Neal et al.[347] reported monoclinic pyrrhotite formed on hematite surfaces after 6 months exposure to sulfate-reducing bacteria although this phase has not been identified in similar experimental studies with these organisms.[101,270,348] Likewise, Farina et al.[349] described the formation of pyrrhotite in intracellular granules of magnetotactic bacteria, but Posfai et al.[256] found no evidence for pyrrhotite in these organisms. So the jury is out. There is no doubt that pyrrhotites have been observed experimentally in low-temperature aqueous systems with and without various types of bacteria. However, the process of formation is not understood and does not seem to be readily reproducible. Of course, the consequence of pyrrhotites being formed in these systems would be that these minerals might yet be formed more often in marine systems.

The pyrrhotite group includes a number of FeS phases based on the NiAs structure displaying various superstructures caused by ordered vacancy geometries in the nonstoichiometric composition. Two basic subgroups are observed: the hexagonal pyrrhotites, which tend to be iron-rich with compositions centering around $Fe_{10}S_{11}$, and the monoclinic pyrrhotites, which tend to be less iron-rich with compositions generally around $Fe_7S_8$. Monoclinic pyrrhotites tend to be stable relative to the hexagonal forms at temperatures less than around 200 °C. Troilite, $FeS_t$, is the stoichometric end-member phase.

Although $Fe_{1-x}S$ and $FeS_t$ are stable relative to $FeS_m$, they are rarely observed in marine systems. The reason is shown in the pH−Eh diagram (Figure 35). In low-temperature aqueous solutions, pyrite is the stable phase. As discussed above, the relative stability of the $HS_2^{2-}$ species in sulfidic solutions combined with the low solubility of pyrite makes this phase unavoidable in terms of equilibrium thermodynamics. If $FeS_t$ and $Fe_{1-x}S$ are to be produced in these systems, some kinetic factors, such as the inhibition of pyrite nucleation and the catalysis of $FeS_t$ and $Fe_{1-x}S$ formation, must be involved. We noted above, for example, that $FeS_t$ may be produced through the reaction between acidic aqueous S(−II) solutions and Fe(0) either directly >92 °C or through a $FeS_c$ intermediary. However, the predominance of pyrite in aqueous equilibrium systems does not explain why $FeS_m$, in particular, forms in place of $FeS_t$ or $Fe_{1-x}S$. The explanation for this is, as discussed above, the identity of the $FeS_m$ structural moiety with the $Fe_2S_2$-type aqueous clusters. The topology of the $FeS_t$ structure is complex with both $Fe_2S_2$ and $Fe_3S_3$ rings.[350] Taylor[351] noted that a trimeric precursor $Fe_3S_3$ may be required for the nucleation of $FeS_t$. $Fe_3S_3$ rings have not been identified in aqueous FeS solutions although their occurrence is not precluded. A kinetic explanation may be consistent with the conflicting reports of pyrrhotite syntheses in low-temperature aqueous solutions reported above.

## 8.3. Smythite, Rhombohedral $Fe_9S_{11s}$

Smythite, rhombohedral $Fe_9S_{11s}$,[352] was originally thought to be a greigite polymorph, $Fe_3S_{4s}$.[353] The revised formulation is equivalent to $Fe_{3.27}S_4$. However, Fleet[354] suggested on structural grounds that the ideal formula was $Fe_{13}S_{16}$, which would bring it close to $Fe_{3.25}S_4$. The problem is that the natural materials on which the composition is based normally include various amounts of Ni and, as discussed above with respect to $FeS_m$ and $FeS_p$, this lends a degree of uncertainty to the composition. It was originally synthesized by Rickard[355] and is a pure member of the Fe−S system. The synthesis was confirmed some 28 years later by Furukawa and Barnes.[356] Rickard noted the coincidence between the rhombohedral structure of $Fe_9S_{11s}$ and that of siderite, $FeCO_3$, and suggested that the material was formed by an epitactic reaction. In nature, $Fe_9S_{11s}$ is usually found associated with rhombohedral carbonates. However, it is also found in pyrrhotites, where it is generally Ni-rich and appears to be produced through exolution on rapid quenching.[354,356] Furukawa and Barnes[356] found that the upper temperature limit of $Fe_9S_{11s}$ formation through the reaction with siderite was 53 °C and the pH needed to be >6. These conditions appear to be possible in some marine, or at least estuarine, environments, but $Fe_9S_{11s}$ has not yet been reported from these systems.

## 8.4. Marcasite, Orthorhombic $FeS_{2m}$

Marcasite is the orthorhombic dimorph of pyrite. Its formation remains somewhat of a mystery. Syntheses of $FeS_{2m}$ require pH < 6, and the rate of formation becomes rapid at pH < 4.[357] It has been suggested that the presence of protonated $S_n(-II)$ species, which may dominate in acid solutions as discussed above, is somehow related to its formation.[358] This mirrors an older idea that $FeS_{2m}$ includes H in its structure, but this is not the case. A kinetic study of $FeS_{2m}$ formation would probably help solve the problem.

Marcasite is not found in normal marine sediments, although it is a common constituent of deep ocean hydrothermal vent mineralization. The reason for the lack of marine $FeS_{2m}$ is probably the pH requirements for its formation. $FeS_{2m}$ is a common constituent of ancient marine sediments, however, where it is produced by circulating acidic groundwaters.

## 8.5. Other Iron Sulfides

For completeness, it should be mentioned that a number of other iron sulfides have been reported in the literature. The case of $Fe_2S_3$ has been mentioned above. However, it continues to be reported, most recently as an hexagonal phase within synthetic pyrrhotites.[359] A variety of $FeS_m$ has been reported as a product of a synthetic reaction between ferrihydrite, goethite, or hematite and S(−II) with a *d*-spacing exactly double that of mackinawite.[360] The material is only produced in high NaCl concentrations and its composition appears variable. It is reported to change to $FeS_m$ with time. In this context, it is also worth noting that a variety of alkali iron sulfides are known and have been reported as minerals from highly saline environments. These materials are easily synthesized in low-temperature aqueous systems, have definitive compositions, and are remarkably stable compared with the usual FeS precipitates. It is possible that they may have or have had some role in extreme marine systems in very alkaline microenvironments.

# *9. The FeS System in Biochemistry and for Organic Compound Formation*

Iron−sulfur clusters are agents that affect many biochemical processes as they are the active sites in proteins with

molecular masses starting from about 6000 Da. They are common to most ancient components of living matter and are present in a host of other organisms such as photosynthetic organisms, nitrogen-fixing bacteria, and submitochondrial fractions of mammalian origin.[361] Recently in this journal, Holm and co-workers[362] have reviewed synthetic analogues of iron−sulfur clusters. The main cluster stoichiometries found are $Fe_2S_2(SR)_2$, $Fe_3S_4(SR)_3$, $Fe_4S_4(SR)_4$, and dimers of the latter. In some enzymes containing $Fe_4S_4(SR)_4$ and higher stoichiometries, one or more of the Fe atoms is replaced by another metal (e.g., Ni, Mo, or W).

The $Fe_2S_2$ structure has a core similar to that found in mackinawite whereas the other structures are cubane-like (Figure 19). Most syntheses of FeS clusters are performed in nonaqueous solvents to prevent iron sulfide precipitation. One of the most interesting examples is the formation of the inorganic cluster $[Fe_4S_4(SH)_4]^{2-}$ in nonaqueous solvents[193,363,364] (Figure 19). This is the simplest synthetic analog of a ferredoxin as SH replaces thiol groups (SR). The ferredoxin clusters containing thiols form readily in aqueous solution[193,365] and are examples of self-assembly reactions. Thus they are considered possible starting materials or catalysts for organic compound formation and the origins of life.

In the last 20 years, there has been much interest in the Fe/S system as a strong reducing system, as a catalytic system in the formation of organic compounds necessary for life, and as a geochemical driver for biochemical processes. The hypotheses are grouped in the "iron−sulfur world" concept, an idea that iron sulfides played an extensive role in prebiotic organic syntheses on the early Earth. Two groups have provided detailed theories for the evolution of organic compounds necessary for life using iron−sulfur chemistry. Wächtershäuser and co-workers[366−371] proposed the hydrothermal synthesis of $FeS_2$, which requires acidic conditions, whereas Russell and co-workers[372−375] proposed the hydrothermal synthesis of FeS species but at lower temperatures and under more alkaline conditions. Both processes have FeS species as important components and reactants. Key in both of these hypotheses is how $CO_2$ can be reduced to form organic compounds. A major stumbling block is that the LUMO orbital of $CO_2$ is positive in potential energy (+0.60 eV[376]) and $CO_2$ has a very negative reduction potential (−2.22 V vs SCE[377]). These data indicate that $CO_2$ is not an efficient electron acceptor and requires very strong reducing conditions for its reduction.

## 9.1. Pyrite Formation Proposal

Wächtershäuser[287,366] proposed the hydrothermal synthesis of organic compounds during the inorganic synthesis of $FeS_2$ as a primary pathway. The initial step was the reduction of $CO_2$ to small organic molecules, particularly thiolated methanoic (formic) acid, $HSCH_2OOH$. In the assumed acidic early Earth ocean,[378] sulfur as $H_2S$ would have dominated sulfur speciation,[379] so pyrite formation through the reaction between $H_2S$ and FeS (eq 51) was proposed as a new energy source for the autotrophic origin of life because of the $H_2$ produced. $H_2$ could then be used directly by organisms for growth or for the reduction of $CO_2$, organic compounds, and nitrate.[370] Drobner et al.[369] documented the reaction, and Rickard[54] determined the rate law from 25 to 125 °C with $FeS_m$ as the reactant (eq 51). As noted above, FeS was nonprescriptive, and pyrrhotites were involved in the original hypothesis. However, Schoonen et al.[294] found that direct electron transfer from the valence band of pyrrhotite to the lowest unoccupied molecular orbital of $CO_2$ would not occur.

Since the original proposal, the reaction with FeS and $H_2S$ alone or with NiS present has been shown to produce organic sulfur compounds, but not formate, when $CO_2$ is added to the reaction mixture.[370,371,380,381] In this case, $CO_2$ is converted to OCS and $CS_2$ [by FeS and $H_2S$], which are then further reduced by $H_2$ to form simple organic sulfur compounds such as $CH_3SH$ and $CH_3SSCH_3$, as well as amide bonds when reduced nitrogen is present. $CH_3SH$ is an excellent starting material because CO insertion forms $CH_3(CO)SH$, which is a precursor for acetyl-CoA in the reverse or reductive citrate cycle.[337] Cody[382] reviewed metal sulfides and detailed their potential importance in the origins of metabolism.

The mechanisms for the above reactions are presently unknown but appear to be related to addition of sulfide to $CO_2$ to form the monothiocarbonate ion, $HCSO_2^-$, which can decompose to OCS.[383] The reducing power of the FeS/$FeS_2$ couple to reduce $CO_2$ to formate and simple amino acids was questioned as an important process by Keefe et al.[384] based on experimental data and by Schoonen et al.[294] based on thermodynamic calculations. The latter group demonstrated that with increasing temperature eq 51 has less reducing power and above 250 °C its reducing power is less than that of other mineral assemblages such as quartz−fayalite−magnetite and pyrrhotite−pyrite−magnetite. Thus $CO_2$ reduction to formate is less likely by the $FeS_2$ formation reaction. At the time of the Schoonen et al. study, the thermodynamic argument did not address three relevant points that may permit reduction of $CO_2$ to formate via $FeS_2$ formation.

First, large black smokers (Figure 38A) at hydrothermal vents with temperatures of 360 °C are not the only source of FeS and $H_2S$. In the absence of substantial sulfate in the ancient Earth oceans,[379] it is improbable that large sulfide edifices such as those in the present-day deep oceans could be produced. Even today, diffuse flow hydrothermal fluids,[385−387] which are typically less than 100 °C, release more material volumetrically than that from black smokers at vents. Diffuse flow fluids also contain FeS and $H_2S$.[200]

In addition to diffuse flow systems, small chimneys and beehive diffusers[388] are porous structures (Figures 38B and 39) associated with large black smoker edifices that are formed at significantly lower temperatures than black smokers. Beehive diffusers have been identified as ideal natural reaction kettles for potential prebiotic organic syntheses.[373] One problem with the iron−sulfur world hypothesis for the origin of life is that although all reactions from CO to peptides, for example, have been reproduced in the laboratory,[389] these syntheses were achieved under a wide range of conditions, especially temperature. In this context, beehive diffusers appear to be interesting natural reactors. However, the modern versions are anhydrite cemented[388] and thus unlikely to be formed in a sulfate-limited Hadean ocean. Also, they mix fluids over a steep thermal gradient from hydrothermal temperatures in the interior to deep ocean temperatures of 2 °C at the surface. As suggested by the analyzed structure in Figure 39, the conditions may vary from 3 to 360 °C, from oxidized to reduced, and from acid to alkaline over short distances. The modern day organic chemistry of beehive diffusers has not been investigated and could be an interesting target for research. If similar natural reactors were present in the prebiotic Earth oceans, they

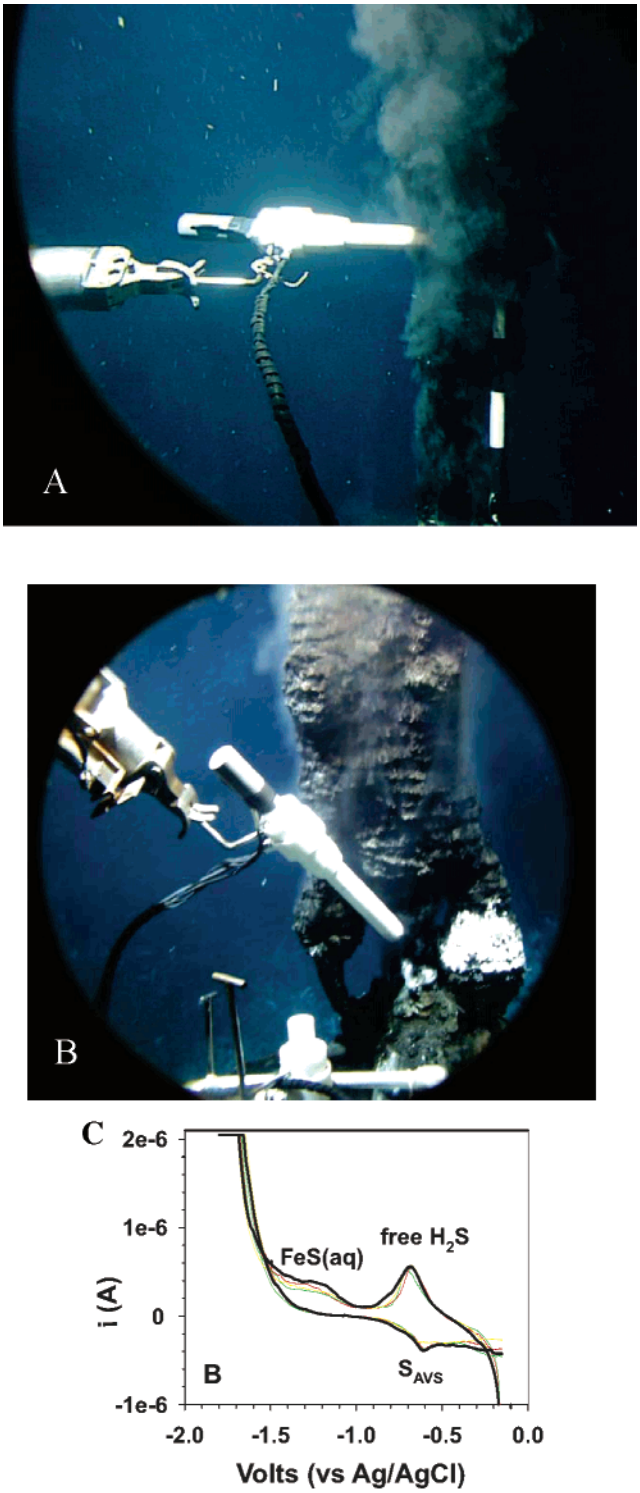


**Figure 38.** (A) Black smoker hydrothermal vent probed by an electrode wand 0.5 m above the vent chimney (≤360 °C) at a depth of 2.5 km on the North East Pacific Rise (9° 50′ N), (B) beehive structure from the North East Pacific Rise (9° 50′ N), and (C) Reproducible cyclic voltammetry scans (1 V/s) taken 0.5 m above the vent orifice (location is the wand tip in Figure 38A) where the temperature was 25 °C and the pH ≈ 6. Only $H_2S$ and FeS(aq) were detected. The total sulfide ($S_{AVS}$) was recovered on the negative scan.

would necessarily have been different from the modern-day examples.

Second, Schoonen et al.[294] assumed that FeS was a solid entity, but Luther and Rickard[166] and Theberge and Luther[173] have shown that there is a soluble form of FeS [FeS(aq)],

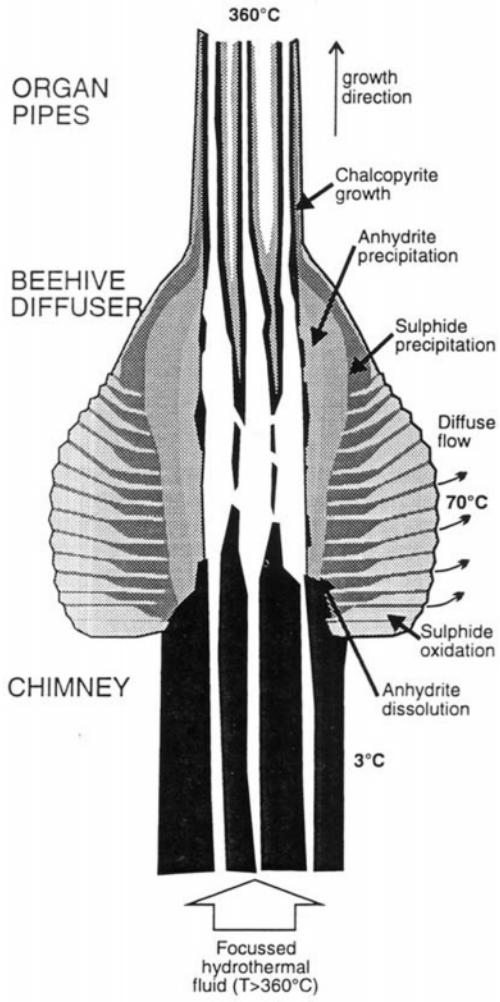


**Figure 39.** Elements of a beehive diffuser from an edifice at Broken Spur (29° 10′ N) from Rickard et al.[388] Reproduced with permission of the Mineralogical Society of Great Britain & Ireland.

which has properties similar to molecular clusters found in ferrodoxins that may enhance the reaction. The Fe in [FeS-(aq)] has facile ligand exchange and the S in [FeS(aq)] has electron-donating capability that permits reaction at the C atom in $CO_2$ to activate $CO_2$. A similar process has been shown in biotin formation from ferredoxin $Fe_4S_4$ clusters.[390] The pH at which all these reactions are performed is probably very critical since the $H_2S/HS^-$ system can interact with $CO_2$ to produce OCS and $CS_2$ on the way to organic compounds.[373] Third, electrochemical reduction of $CO_2$ to formate on pyrite has now been documented.[391]

$CO_2$ reduction is not the only pathway for organic compound formation using the Fe−S system. CO insertion into simple organic molecules has been investigated in subsequent work. Cody et al.[392] suggested the Fe−S system (with CO molecules possibly attached to Fe) as a prime catalyst for the organic synthesis of pyruvate under extreme temperature and pressure. In that work the catalyst was speculated to be $Fe_2(RS)_2(CO)_6$ because of spectroscopic evidence and because it can be converted to $Fe_2(RS)_4S_2^{2-}$. Also, peptides were formed with (Ni,Fe)S surfaces with CO and amino acids, but the structure of the catalyst was not identified.[393] Trapping the catalyst is not an easy task, but spectroscopic techniques can give a clue to the catalyst's identity.[390,392] Clearly more work is needed in this area to better understand reactivity and possible mechanisms. The problem centers on the same dichotomy between equilibrium

thermodynamics and kinetics that has been a continuous thread throughout this review. Equilibrium thermodynamics not only describes the state of the system but is also constrained by the choice of reactants and products. Thus, calculations such as those of Schoonen et al.[294] are unquestionably correct; however, a different result might be obtained with soluble FeS catalysts or intermediates as reactants.

### 9.2. FeS Membrane Proposal

The other proposed use of the FeS system comes from Russell and colleagues.[372−375] In this proposal, life emerged from a redox and pH front about 4.2 Ga ago (Ga = gigaannum or billion years). Here hot alkaline bisulfide-bearing submarine seep waters emerged into the Hadean ocean, which was acidic (due to high $CO_2$ levels), warm, and iron-bearing. At the interface of these two aquatic systems, an FeS colloidal membrane spontaneously formed. This semipermeable membrane contained Ni and acted as a catalytic boundary for the transfer of electrons for the reduction of $CO_2$ to organic acids and anions as well as the hydrogenation and $CO/CO_2$ insertion of other hydrothermal organic primers. Russell views the chemistry of the FeS membrane as a ferredoxin-like material, which may have been the precursor to the use of ferredoxins in living organisms. One of the problems with this idea is that $FeS_m$ does not form large crystals but is commonly nanoparticulate. Filtness et al.[394] synthesized a pure $FeS_m$ "membrane" and found that it behaved more like a permeable reactive barrier than a membrane.

Still the Russell proposal is attractive for several reasons. First, the reaction of $CO_2$ with FeS alone or with $H_2S$ has resulted in OCS, $CS_2$, and organic sulfur compound formation including $CH_3SH$[380] indicating that FeS is a strong reductant. The FeS HOMO (~0.5 eV and near in energy to the LUMO of $CO_2$) is less stable than the $FeS_2$ HOMO.[51,291,294,383] Thus, the HOMO of FeS is an excellent electron-donor orbital and should interact better with all the LUMO orbitals of $CO_2$, OCS, and $CS_2$ in a manner similar to that of Zn−OH in carbonic anhydrase.[395] Second, solid and soluble FeS clusters have high-spin Fe atoms in tetrahedral coordination, and electron transfer is facilitated with this configuration over low-spin and octahedral Fe in $FeS_2$. The high-spin and tetrahedral Fe in FeS clusters permits other metals such as Ni, W, and Mo to replace an Fe atom in the cluster. Known biochemical FeS clusters have similar structural features as those found in mackinawite, greigite, and NiFeS minerals,[373,382] so FeS bubble formation likely resulted in FeS clusters and efficient electron transfer as well. The replacement of a Ni atom for an Fe atom in an FeS cluster[396] has been shown to enhance organic compound formation as has the use of mixed FeS/NiS solid phases.[381,393] Last, the electroreduction of $CO_2$ is catalyzed by $Fe_4S_4$ clusters[397] and can shift the electrode reduction potential for $CO_2$ by about + 0.7 V in nonaqueous solvents. Although Russell's hypothesis was for the Hadean ocean, other interfaces including hydrothermal vents and sediments that show profiles as in Figure 2 are likely places for present day occurrence of this pathway. The beehive structure in Figure 38 is an example of a present day environment that is porous and that fits the requirements of the Russell hypothesis.

These two Fe−S hypotheses indicate that hydrothermal vents, hot springs, sediments, and the sub-seafloor biosphere are ideal chemical sources for FeS clusters, nanoparticles, and solids. Also, these extreme environments are possible systems for the evolution of organic molecules and life since they provide not only Fe−S chemistry but many of the other transition metals that are essential to life in micromolar to millimolar concentrations.[398] There is some exciting chemistry out there.

## 10. Acknowledgments

D.R. acknowledges NERC Grant NRE/L/S/2000/00611. G.W.L. acknowledges support from NSF Grants OCE-0240896 and OCE-0326434. We thank Ovadia Lev for comments on an earlier version of this paper. Reviewing this paper was not a trivial exercise: We thank John Morse and two anonymous referees for their heroic efforts, which did much to improve the manuscript. We thank Mihály Posfai for providing a high-resolution version of his electron micrograph, originally published in *Science* and reproduced in Figure 32.

## 11. References

(1) Rickard, D.; Morse, J. *Mar. Chem.* **2005**, *97*, 141.
(2) Rickard, D.; Luther, G. W., III *Rev. Mineral. Geochem.* **2006**, *61*, 421.
(3) Morse, J. W.; Millero, J.; Cornwell, J. C.; Rickard, D. *Earth Sci. Rev.* **1987**, *24*, 1.
(4) Edmond, J. M.; Measures, C.; McDuff, R. E.; Chan, L. H.; Collier, R.; Grant, B.; Gordon, L. I. *Earth Planet. Sci. Lett.* **1979**, *46*, 1.
(5) Walker, J. C. G. *Mar. Geol.* **1986**, *70*, 159.
(6) Parkes, R. J.; Cragg, B. A.; Bale, S. J.; Getliffe, J. M.; Goodman, K.; Rochelle, P. A.; Fry, J. C.; Weightman, A. J.; Harvey, S. M. *Nature* **1994**, *371*, 410.
(7) Hensen, C.; Zabel, M.; Pfeifer, K.; Schwenk, T.; Kasten, S., Riedinger, N.; Schulz, H. D.; Boetius, A. *Geochim. Cosmochim. Acta* **2003**, *67*, 2631.
(8) Raiswell, R.; Bottrell, S. H.; Albiatty, H. J.; Tan, M. M. *Am. J. Sci.* **1993**, *293*, 569.
(9) Bottrell, S.; Newton, R. J. *Earth Sci. Rev.* **2006**, *75*, 59.
(10) Millero, F. J. *Chemical Oceanography*; CRC Press: Boca Raton, FL, 1996.
(11) D'Hondt, S.; Rutherford, S.; Spivak, A. J. *Science* **2002**, *295*, 2067.
(12) Jorgensen, B. B. *Nature* **1982**, *296*, 643.
(13) Froelich, P. N.; Klinkhammer, G. P.; Bender, M. L.; Luedtke, N. A.; Heath, G. R.; Cullen, D.; Dauphin, P.; Hammond, D.; Hartman, B.; Maynard, V. *Geochim. Cosmochim. Acta* **1979** *43*, 1075.
(14) Reeburgh, W. S. *Annu. Rev. Earth Planet. Sci.* **1983**, *11*, 269.
(15) Howes, B. L.; Dacey, J. W. H.; King, G. M. *Limnol. Oceanogr.* **1984**, *24*, 999.
(16) Mackin, J. E., Swider, K. T. *J. Mar. Res.* **1989**, 47, 681.
(17) Berner, R. A. *Am. J. Sci.* **1982**, *282*, 451.
(18) Berner, R. A. *Principles of Chemical Sedimentology*; McGraw-Hill: New York, 1971.
(19) Murray, J. W.; Jannasch, H. W.; Honjo, S.; Anderson, R. F.; Reeburgh, W. S.; Top, Z.; Friederich, G. E.; Codispoti, L. A.; Izdar, E. *Nature* **1989**, *338*, 411.
(20) Hastings, D.; Emerson, S. *Limnol. Oceanogr.* **1988**, *33*, 391.
(21) Skei, J. M. *Mar. Chem.* **1988**, *23*, 209.
(22) Officer, C. G.; Biggs, R. B.; Taft, J. L.; Cronin, L. E.; Tyler, M. A.; Boynton, W. R. *Science* **1984**, *23*, 22.
(23) Luther, G. W., III; Sundby, B.; Lewis, B. L.; Brendel, P. J.; Silverberg, N. *Geochim. Cosmochim. Acta* **1997**, *61*, 4043.
(24) Revsbech, N. P.; Jorgensen, B. B.; Brix, O. *Limnol. Oceanogr.* **1981**, *26*, 717.
(25) Reimers, C. E.; Fischer, K. M.; Merewether, R.; Smith, K. L.; Jahnke, R. A. *Nature* **1986**, *320*, 741.
(26) Revsbech, N. P.; Jorgensen, B. B.; Blackburn, T. H. *Science* **1986**, *207*, 1355.
(27) Luther, G. W., III; Reimers, C. E.; Nuzzio, D. B.; Lovalvo, D. *Environ. Sci. Technol.* **1999**, *33*, 4352.
(28) Todd, J. F.; Elsinger, R. J.; Moore, W. S. *Mar. Chem. 23*, 393.
(29) De Lange, G. J.; Catalano, G.; Klinkhammer, G. P.; Luther, G. W., III *Mar. Chem.* **1990**, *31*, 205.
(30) Astor, Y.; Müller-Karger, F.; Scranton, M. I. *Cont. Shelf Res.* **2003**, *23*, 125.
(31) Ho, T.-Y.; Taylor, G. T.; Astor, Y.; Varela, R.; Müller-Karger, F.; Scranton, M. I. *Mar. Chem.* **2004**, *86*,89.

(32) Konovalov, S. K.; Luther, G. W., III; Friederich, G. E.; Nuzzio, D. B.; Tebo, B. M.; Murray, J. W.; Oguz, T.; Glazer, B.; Trouwborst, R. E.; Clement, B.; Murray, K. J.; Romanov, A. S. *Limnol. Oceanogr.* **2003**, *48*, 2369.
(33) Gregg, M. C.; Yakushev, E. *Geophys. Res. Lett.* **2005**, *2*, L03604.
(34) Aller, R. C.; Aller, J. Y. *J. Mar. Res.* **1998**, *56*, 905.
(35) Aller, R. C. *Chem. Geol.* **1994**, *114*, 331.
(36) Trouwborst, R. E.; Clement, B. G.; Tebo, B. M.; Glazer, B. T.; Luther, G. W., III *Science* **2006**, *313*, 1955.
(37) Ma, S.; Noble, A.; Butcher, D.; Trouwborst, R. E.; Luther, G. W., III *Estuarine, Coastal Shelf Sci.* **2006**, *70*, 461.
(38) Postma, D.; Appelo, C. A. J. *Geochim. Cosmochim. Acta* **2000**, *64*, 1237.
(39) Canfield, D. E. *Geochim. Cosmochim. Acta* **1989**, *51*, 645.
(40) Canfield, D. E.; Raiswell, R.; Bottrell, S. *Am. J. Sci*. **1992**, *292*, 659.
(41) Kostka, J. E.; Luther, G. W., III *Biogeochemistry* **1995**, *29*, 159.
(42) Larsen, O.; Postma, D. *Geochim. Cosmochim. Acta* **2001**, *65*, 1367.
(43) Postma, D. *Geochim. Cosmochim. Acta* **1993**, *57*, 5027.
(44) Hyacinthe, C.; Bonneville, S.; Van Cappellen, P. *Geochim. Cosmochim. Acta* **2006**, *70*, 4166.
(45) DeLong, E. F. *Nature* **2000**, *407*, 577.
(46) Raiswell, R. T.; Berner, R. A. *Am. J. Sci.* **1985**, *285*, 710.
(47) Bruchert, V. *Geochim. Cosmochim. Acta* **1998**, *62*,1567.
(48) Bruchert, V.; Pratt, L. M. *Geochim. Cosmochim. Acta* **1996**, *60*, 2325.
(49) Ferdelman, T.; Church, T. M.; Luther, G. W., III *Geochim. Cosmochim. Acta* **1991**, *55*, 979.
(50) Gimarc, B. M. *Molecular Structure and Bonding. The Qualitative Molecular Orbital Approach*; Academic Press: New York, 1979.
(51) Rickard, D.; Luther, G. W., III *Geochim. Cosmochim. Acta* **1997**, *61*, 135.
(52) Drzaic, P. S.; Marks, J.; Brauman, J. I. *Gas Phase Ion Chem.* **1984**, *3*, 167.
(53) Radzic, A. A; Smirnov, B. M. *Reference Data on Atoms, Molecules, and ions*; Springer Series in Chemical Physics, Vol. 31; Springer-Verlag: Berlin, 1985; pp 375−438.
(54) Rickard, D. *Geochim. Cosmochim. Acta* 1**997**, *61*, 115.
(55) Trsic, M.; Laidlaw, W. G. *Int. J. Quantum Chem.* **1980**, *XVII*, 969.
(56) Suleimenov, O. M.; Seward, T. M. *Geochim. Cosmochim. Acta* **1997**, *61*, 5187.
(57) Millero, F. J.; Plese, T.; Fernandez, M. *Limnol. Oceanogr.* **1988**, *33*, 269.
(58) Giggenbach, W. *Inorg. Chem.* **1971**, *10*, 1333.
(59) Schoonen, M. A. A.; Barnes, H. L. *Geochim. Cosmochim. Acta* **1988**, *52*, 649.
(60) Pourbaix, M. *Atlas of Electrochemical Equilibria in Aqueous Solutions*; Pergamon Press: Oxford, U.K., 1966.
(61) Goldhaber, M. Sulfur-rich sediments. In *Treatise on Geochemistry*; Mackenzie, F. T., Ed.; Elsevier: Amsterdam, 2004; Vol. 7, pp 257−289.
(62) Seal, R. R., II *Rev. Mineral. Geochem.* **2006**, *61*, 633.
(63) Kohn , M. J.; Riciputi, L. R.; Stajes, D.; Orange, D. L. *Am. Mineral.* **1998**, *83*, 1454.
(64) Ingvorsen, K.; Zehnder, A. J. B.; Jørgensen, B. B. *Appl. Environ. Microbiol.* **1984**, *27*, 1029.
(65) Cypionka, H. In *Sulfate-Reducing Bacteria*; Barton, L. L., Ed.; Plenum: New York, 1995; p 151.
(66) Habicht, K. S.; Gade, M.; Thamdrup, B.; Berg, P.; Canfield, D. E. *Science* **2002**, *298*, 2372.
(67) Canfield, D. E.; Thamdrup, B. *Science* **1994**, *266*, 1973.
(68) Habicht, K. S.; Canfield, D. E.; Rethmeier, J. *Geochim. Cosmochim. Acta* **1998**, *62*, 2585.
(69) Licht, S.; Hodes, G.; Manassen, J. *Inorg. Chem.* **1986**, *25*, 2486.
(70) Müller, A.; Diemann, E. *Adv. Inorg. Chem. Radiochem.* **1987**, *31*, 89.
(71) Meyer, F. H.; Riggs, O. L.; McGlasson, R. L.; Sudbury, J. D. *Corrosion* **1958**, *14*, 109.
(72) Boulegue, J.; Michard, *G. C. R. Acad. Sci. Paris* **1977**, *284C*, 713.
(73) Cloke, P. L. *Geochim. Cosmochim. Acta* **1963**, *27*, 1265.
(74) Cloke, P. L. *Geochim. Cosmochim. Acta* 1**963**, *27*, 1299.
(75) Giggenbach, W. *Inorg Chem.* **1972**, *11*, 1201.
(76) Maronny, G. *Electrochim. Acta* **1959**, *1*, 58.
(77) Teder, A. *Acta Chem. Scand.* **1971**, *25*, 1722.
(78) Kamyshny, A. J.; Goifman, A.; Gun, J.; Rizkov, D.; Lev, O. *Environ. Sci. Technol.* **2004**, *38*, 6633.
(79) Schwarzenbach, G.; Fischer, A. *Helv. Chim. Acta* **1960**, *43*, 1365.
(80) Williamson, M. A.; Rimstidt, J. D. *Geochim. Cosmochim. Acta* **1992**, *56*, 3867.
(81) Bard, A. J.; Parsons, R.; Jordan, J. *Standard Potentials in Aqueous Solution*; Marcel Dekker Inc.: New York, 1985.
(82) Chadwell, S. J.; Rickard, D.; Luther, G. W., III *Aquat. Geochem.* **1999**, *5*, 29.
(83) Chadwell, S. J.; Rickard, D.; Luther, G. W., III *Electroanalysis* **2001**, *13*, 21.
(84) Cox, J. D.;Wagman, D. D.; Medvedev, V. A. *CODATA Key Values for Thermodynamics*; Hemisphere Publishing Corp.: New York, 1989.
(85) Garrels, R. M.; Christ, C. L. *Solutions, Minerals and Equilibria*; Harper & Row: New York, 1965.
(86) Kamyshny, A. J.; Goifman, A.; Rizkov, D.; Lev, O. *Aquat. Geochem.* **2003**, *9*, 291.
(87) Amrani, A.; Kamyshny, A.; Lev, O.; Aizenshtat, Z. *Inorg. Chem.* **2006**, *45*, 1427.
(88) Wagman, D. D.; Evans, W. H.; Parker, V. B.; Halow, I.; Bailey, S. M.; Schumm, R. H. *Selected Values of Chemical Thermodynamic Properties*; NBS Technical Note 270-4; National Bureau of Standards, U.S. Government Printing Office: Washington, DC, 1969.
(89) Wagman, D.; Evans , W. H.; Parker, V. B; Schumm, R. H.; Halow, I.; Bailey, S. M.; Churney, K. L.; Nuttall, R. L. *J. Phys. Chem. Ref. Data* **1982**, *11*, 1.
(90) Latimer, W. M. *The Oxidation States of the Elements and Their Potentials in Aqueous Solutions*; Prentice Hall: New York, 1952.
(91) Randall, M.; Frandsen, M. *J. Am. Chem. Soc*. **1932**, *54*, 47.
(92) Patrick, W. A.; Thompson, W. E. *J. Am. Chem. Soc*. **1953**, *75*, 1184.
(93) Whittermore, D. O.; Langmuir, D. *J. Chem. Eng. Data* **1972**, *17*, 288.
(94) Hoar, T. P.; Hurlen, T. *Proc. Int. Comm. Electrochem. Thermodyn. Kinet., 8th Meet.*, **1958**, 445.
(95) Larson, J. W.; Cerruti, P.; Garber, H. K.; Hepler, L. G. *J. Phys. Chem.* **1968**, *72*, 2902.
(96) Cobble, J. W.; Murray, R. C., Jr. *Faraday Discuss. Chem. Soc*. **1978**, *64*, 144.
(97) Sweeton, F. H.; Baes, C. F., Jr. *J. Chem. Thermodyn.* **1970**, 2, 479.
(98) Tremaine, P. R.; LeBlanc, J. C. *J. Solution Chem*. **1980**, *9*, 415.
(99) Parker, V. B.; Khodkovskii, I. L. *J. Phys. Ref. Data* **1995**, *24*, 1699.
(100) Langmuir, D. *The Gibbs Free Energies of Substancies in the System $Fe-O_2-H_2O-CO_2$ at 25 °C*; U.S. Geological Survey Professional Paper 650-B; U.S. Geological Survey, U.S. Government Printing Office: Washington, DC, 1969.
(101) Benning, L. G.; Wilkin, R. T.; Barnes, H. L. *Chem. Geol*. **2000**, *167*, 25.
(102) Milburn, R. N.; Vosburgh, W. C. *J. Am. Chem. Soc*. **1955**, *77*, 1352.
(103) Soli, A. L.; Byrne, R. H. *J. Solution Chem*. **1996**, *25*, 773.
(104) Byrne, R. H.; Thompson, S. W. *J. Solution Chem*. **1997**, *26*, 729.
(105) Millero, F. J.; Yao, W.; Aicher, J. *Mar. Chem*. **1995**, *50*, 21.
(106) Turner, D. R.; Whitfield, M.; Dickson, A. G. *Geochim. Cosmochim. Acta* **1981**, *45*, 855.
(107) Byrne, R. H.; Yao, W.; Luo, Y.-R.; Wang, B. *Mar. Chem*. **2005**, *97*, 34.
(108) Milburn, R. N.; Vosburgh, W. C. *J. Am. Chem. Soc*. **1955**, *77*, 1352.
(109) Byrne, R. H.; Kester, D. R. *Mar. Chem*. **1976**, *4*, 275.
(110) Byrne, R. H.; Kester, D. R. *J. Solution Chem*. **1978**, *7*, 373.
(111) Baes, C. F., Jr.; Mesmer, R. E. *The Hydrolysis of Cations*; Wiley: New York, 1976.
(112) Daniele, P. G.; Rigano, C.; Sammartano, S.; Zelano, V. *Talanta* **1994**, *41*, 1577.
(113) Byrne, R. H.; Luo, Y.-R.; Young, R. W. *Mar. Chem.* **2000**, *70*, 23.
(114) Biedermann, G.; Chow, J. T. *Acta Chem. Scand.* **1966**, *20*, 1376.
(115) Fox, L. E. *Geochim. Cosmochim. Acta* **1988**, *52*, 771.
(116) Liu, X.; Millero, F. J. *Geochim. Cosmochim. Acta* **1999**, *63*, 3487.
(117) Delany, J, M.; Lundeen, S. R. *The LLNL Thermodynamic Database*; Technical Report UCRL-21658; Lawrence Livermore National Laboratory: Livermore, CA, 1990.
(118) van den Berg, C. M. G. *Mar. Chem.* **1995**, *50*, 139.
(119) Rue, E. L.; Bruland, K. W. *Mar. Chem*. **1995**, *50*, 117.
(120) Wu, J. F.; Luther, G. W., III *Mar. Chem*. **1995**, *50*, 159.
(121) Witter, A. E.; Hutchins, D. A.; Butler, A.; Luther, G. W., III *Mar. Chem*. **2000**, *69*, 1.
(122) Rose, A. L.; Waite, T. D. *Mar. Chem.* **2003**, *84*, 85.
(123) Barbeau, K.; Rue, E. L.; Bruland, K. W.; Butler, A. *Nature* **2001**, *413*,409.
(124) Powell, R. T.; Wilson-Fineli, A. *Aquat. Sci.* **2003**, *58*, **757**.
(125) Rijkenberg, M. J. A.; Fischer, A. C.; Kroon, J. J.; Gerringa, L. J. A.; Timmermans, K. R.; Wolterbeek, H. T.; de Baar, H. J. W. *Mar. Chem.* **2005**, *93*, 119.
(126) Bruland, K. W.; Lohan, M. C. Controls on trace metals in seawater. In *Treatise on Geochemistry*; Elderfield, H. Ed.; Elsevier: Amsterdam, 2004; Vol. 6, pp 23−47.
(127) Luther, G. W., III; Kostka, J. E.; Church, T. M.; Sulzberger, B.; Stumm, W. *Mar. Chem*. **1992**, *40*, 81.
(128) Johnson, K. S.; Gordon, R. M.; Coale, K. H. *Mar. Chem.* **1997**, *5*, 137.
(129) Bruland, K. W.; Orians, K. J.; Cowen, J. P. *Geochim. Cosmochim. Acta* **1994**, *58*, 3171.
(130) Wen, L.-S.; Santschi, P.; Gill, G.; Paternostro, C. *Mar. Chem*. **1999**, *63*, 185.
(131) Tremaine, P. R.; LeBlanc, J. C. *J. Solution Chem*. **1980**, *9*, 415.

(132) Bratsch, S. G. *J. Phys. Chem. Ref. Data* **1989**, *18*, 1.
(133) Trautmann, J.-M. *Bull. Soc. Chim. Fr.* **1966**, *3*, 992.
(134) Hashimoto, K.; Misawa, T. *Corros. Sci.* **1973**, *13*, 229.
(135) Refait, Ph.; Bon, C.; Simon, L.; Bourrié, G.; Trolard, F.; Bessière, J.; Génin, J.-M. R. *Clay Miner.* **1999**, *34*, 499.
(136) Refait, Ph.; Génin, J. M.-R. *Corros. Sci.* **1993**, *34*, 797.
(137) Drissi, H.; Refait; P.; Abdelmoula, M.; Génin, J.-M. R. *Corros. Sci.* **1995**, *37*, 2025.
(138) Ponnamperuma, F. N.; Tianco, E. M.; Loy, T. *Soil Sci.* **1967**, *103*, 374.
(139) Kawano, M.; Tomita, K. *Am. Mineral.* **2001**, *86*, 1156.
(140) Majzlan, J.; Navrotsky, A.; Schwertmann, U. *Geochim. Cosmochim. Acta* **2004**, *68*, 1049.
(141) van der Zee, C.; Roberts, D. R.; Rancourt, D. G.; Slomp, C. P. *Geology* **2003**, *31*, 993.
(142) Loan, M.; Parkinson, G. M.; Richmond, W. R. *Am. Mineral*. **2005**, *90*, 258.
(143) Schwertmann, U.; Friedl, J.; Stanjek, H. *J. Colloid Interface Sci.* **1999**, *209*, 215.
(144) Bakardjieva, S.; Stengl, V.; Subrt, J.; Vecernikova, E. *Solid State Sci*. **2005**, *7*, 367.
(145) Kukkadapuet, R. K.; Zachara, J. M.; Fredrickson, J. K.; Smith, S. C.; Dohnalkova, A. C.; Russell, C. K. *Am. Mineral*. **2003**, *88*, 1903.
(146) Schwertmann, U.; Murad, E. *Clays Clay Miner.* **1983**, *31*, 277.
(147) Schwertmann, U.; Stanjek, H.; Becher, H. H. *Clay Miner.* **2004**, *39*, 433.
(148) Lovley, D. R.; Phillips, E. J. P. *Appl. Environ. Microb.* **1986**, *52*, 751.
(149) Phillips, E. J. P.; Lovley, D. R.; Roden, E. E. *Appl. Environ. Microb.* **1993**, *59*, 2727.
(150) Schwertmann, U.; Cornell, R. M. *Iron Oxides in the Laboratory, Preparation and Characterization*; Wiley-VCH: Berlin, 2000.
(151) Cornell, R. M.; Schwertmann, U. *The Iron Oxides: Structure, Properties, Reactions, Occurrence and Uses;* Wiley VCH: Berlin, 2003.
(152) Bernal, J. D.; Dasgupta, D. T.; Mackay A. L. *Clay Miner. Bull.* **1959**, *4*, 15.
(153) Trolard, F.; Abdelmoula, M.; Bourrié, G.; Humbert, B.; Génin, J.-M. R. *C. R. Acad. Sci. Paris* **1996**, *323*, 1015.
(154) Liu, X.; Millero, F. J. *Mar. Chem.* **2002**, *77*, 43.
(155) Bourrie, G.; Trolard, F.; Genin, J.-M. R.; Jaffrezic, A.; Maitre, V.; Abdelmoula, M. *Geochim. Cosmochim. Acta* **1999**, *63*, 3417.
(156) Bigham, J. M.; Carlson, L.; Murad, E. *Mineral. Mag.* **1994**, *58*, 641.
(157) Croot, P. L.; Laan, P. *Anal. Chim. Acta* **2002**, *466*, 261.
(158) Madigan, M. T.; Martinko, J. M.; Parker, J. *Brock Biology of Microorganisms*, 8th ed.; Prentice-Hall International: London, 1997.
(159) Alldredge, A. L.; Cohen, Y. *Science* **1987**, *235*, 689.
(160) Alldredge, A. L.; Silver, M. W. *Prog. Oceanogr.* **1988**, *20*, 41.
(161) Cutter, G. A.; Krahforst, C. F. *J. Geophys. Lett.* **1988**, *15*, 1393.
(162) Luther, G. W., III; Tsamakis, E. *Mar. Chem.* **1989**, *27*, 165.
(163) Radford-Knoery, J.; Cutter, G. A. *Geochim. Cosmochim. Acta* **1994**, *58*, 5421.
(164) Walsh, R. S.; Cutter, G. A.; Dunstan, W. M.; Radford-Knoery, J.; Elder, J. T. *Limnol. Oceanogr.* **1994**, *39*, 941.
(165) Theberge, S. M., Luther, G. W., III; Farrenkopf, A. M. *Deep-Sea Res.* **1997**, *44*, 1381.
(166) Luther, G. W., III; Rickard, D. *J. Nanopart. Res*. **2005**, *7*, 389.
(167) Buffle, J. *Complexation Reactions in Aqueous Solutions*; Wiley & Sons: New York, 1988.
(168) Dyrssen, D. *Mar. Chem.* **1988**, *24*, 143.
(169) Zhang, J.-Z.; Millero, F. J. *Anal. Chim. Acta* **1994**, *284*, 497.
(170) Rickard, D.; Schoonen, M. A. A.; Luther, G. W., III Chemistry of Iron Sulfides in Sedimentary Environments. In *Geochemical Transformations of Sedimentary Sulfides*; Vairavamuthy, M. A., Schoonen, M. A. A., Eds.; ACS Symposium Series 612, American Chemical Society: Washington, DC, 1995; pp 168−193.
(171) Wei, D.; Ośseo-Asare, K. *J. Colloid Interface Sci.* **1995**, *174*, 273.
(172) Luther, G. W., III; Rickard, D.; Theberge, S. M.; Oldroyd, A. *Environ. Sci. Technol.* **1996**, *30*, 671.
(173) Theberge, S.; Luther, G. W., III *Aquat. Geochem.* **1997**, *3*, 191.
(174) Davison, W.; Phillips, N.; Tabner, B. J. *Aquat. Sci.* **1999**, *61*, 23.
(175) Al-Farawati, R.; van den Berg, C. M. G. *Mar. Chem.* 1**999**, *63*, 331.
(176) Rozan, T. F.; Benoit, G.; Luther, G. W., III *Environ. Sci. Technol*. **1999**, *33*, 3021.
(177) Luther, G. W., III; Glazer, B.; Ma, S.; Trouwborst, R.; Shultz, B. R.; Druschel, G.; Kraiya, C. *Aquat. Geochem*. **2003**, *9*, 87.
(178) Rickard, D. *Geochim. Cosmochim. Acta* **2006**, *70*, 5779.
(179) Emerson, S.; Jacobs, L.; Tebo, B. The behaviour of trace elements in marine anoxic waters: solubilities at the oxygen−hydrogen sulfide interface. In *Trace Metals in Seawater*; Wong, C. S., Boyle, E., Bruland, K. W., Burton, J. D., Goldberg, E. D., Eds.; Plenum: New York, 1983; pp 579−608.
(180) Davison, W. *Geochim. Cosmochim. Acta* **1980**, *44*, 803.
(181) Davison, W. *Aquat. Sci*. **1991**, *35*, 30.
(182) Luther, G. W., III; Ferdelman, T. G. *Environ. Sci. Technol.* **1993**, *27*, 1154.
(183) Rickard, D.; Oldroyd, A.; Cramp, A. *Estuaries* **1999**, *22*, 693.
(184) Olshanskii, Ya. I.; Ivanenko, V. V. *Tr. Inst. Geol. Rudn. Mestorozhd. Petrogr., Mineral. Geokhim., Akad. Nauk SSSR* **1958**, *16*, 14.
(185) DeVitre, R. R. Multimethod Characterization of the Forms of Iron, Manganese and Sulfur in an Eutrophic Lake (Bret, Vaud, Switzerland), Ph.D. Dissertation, University of Geneva, 1986.
(186) Buffle, J.; de Vitre, R. R.; Perret, D.; Leppard, G. G. Combining field measurements for speciation in non perturbable waters. In *Metal Speciation: Theory, Analysis and Application*; Kramer, J. R., Allen, H. E., Eds.; Lewis Publishers Inc.: London, 1988; pp 99−124.
(187) Theberge, S. M. Investigations of Metal-Sulfide Complexes and Clusters: A Multimethod Approach, Ph.D. Thesis, University of Delaware, Lewes, Delaware, 1999.
(188) Davison, W.; Buffle, J.; DeVitre, R. *Anal. Chim. Acta* **1998**, *377*, 193.
(189) Wolthers, M; Van der Gaast, S. J.; Rickard, D. *Am. Mineral.* **2003**, *88*, 2007.
(190) Luther, G. W., III; Theberge, S. M.; Rickard, D. *Geochim. Cosmochim. Acta* **1999**, *63*, 3159.
(191) Luther, G. W., III; Theberge, S. M.; Rozan, T. F.; Rickard, D.; Rowlands, C. C.; Oldroyd, A. *Environ. Sci. Technol.* **2002**, *35*, 94.
(192) Rozan, T. F.; Lassman, M. E.; Ridge, D. P.; Luther, G. W., III *Nature* **2000**, *401*, 879.
(193) Bonomi, F.; Werth, M. T.; Kurtz, D. M. *Inorg. Chem.* **1985**, *24*, 4331
(194) Ohfuji, H.; Rickard, D. *Earth Planet. Sci. Lett.* **2006**, *241*, 227.
(195) Davison, W.; Heaney, S. I. *Limnol. Oceanogr.* **1980**, *25*, 153.
(196) Luther, G. W., III; Glazer, B. T.; Hohmann, L.; Popp, J. I.; Taillefert, M.; Rozan, T. F.; Brendel, P. J.; Theberge, S. M.; Nuzzio, D. B. *J. Environ. Monit.* **2001**, *3*, 61.
(197) Taillefert, M.; Hover, V. C.; Rozan, T. F.; Theberge, S. M.; Luther, G. W., III *Estuaries* **2002**, *25*, 1088.
(198) Luther, G. W., III; Brendel, P. J.; Lewis, B. L.; Sundby, B.; Lefrancois, L.; Silverberg, N.; Nuzzio, D. B. *Limnol. Oceanogr*. **1998**, *43*, 325.
(199) Luther, G. W., III; Gleimers, C. E.; Nuzzio, D. B.; Lovalvo, D. *Environ. Sci. Technol.* **1999**, *33*, 4352.
(200) Luther, G. W., III; Rozan, T. F.; Taillefert, M.; Nuzzio, D. B.; Di Meo, C.; Shank, T. M.; Lutz, R. A.; Cary, S. C. *Nature* **2001**, *410*, 813.
(201) Raiswell, R. *Chem. Geol.* **1976**, *18*, 227.
(202) Coucouvanis, D.; Swenson, D.; Stremple, P.; Baenziger, N. C. *J. Am. Chem. Soc.* **1979**, *101*, 3392.
(203) Mellor, J. W. *A Comprehensive Treatise On Inorganic And Theoretical Chemistry. Vol. 14, Fe (part 3*); Longmans Green: London, 1934.
(204) Lennie, A. R.; Redfern, A. T.; Champness, P. E.; Stoddart, C. P.; Schofield, P. F.; Vaughan, D. J. *Am. Mineral.* **1997**, *82*, 302.
(205) Meyer, F. H.; Riggs, O. L.; McGlasson, R. L. *Corrosion* **1958**, *14*, 109.
(206) Berner, R. A. *Science* **1962**, *137*, 669.
(207) Kuovo, O.; Vuorelainen, Y.; Long, J. V. P. *Am. Mineral*. **1963**, *48*, 511.
(208) Evans, H. T., Jr.; Milton, C.; Chao, E. C. T.; Adler, I.; Mead, C.; Ingram, B.; Berner, R. A. *U.S. Geol. Surv. Prof. Pap.* **1964**, *475-D*, 64.
(209) Rickard, D. *Stockholm Cont. Geol*. **1969**, *20*, 67.
(210) Lennie, A. R.; Vaughan, D. J. Spectroscopic studies of iron sulfide formation and phase relations at low temperatures. In *Mineral Spectroscopy: A Tribute to Roger G. Burns*; Dyar, M. D., McCammon, C., Schaefer, M. W., Eds.; The Geochemical Society: Houston, TX, 1996; Vol. 5, pp 117−131.
(211) Lennie, A. R.; Redfern, S. A. T.; Schofield, P. F.; Vaughan, D. J. *Mineral. Mag.* **1995**, *59*, 677.
(212) Vaughan, D. J.; Ridout, M. S. *J. Inorg. Chem.* **1971**, *33*, 741.
(213) Vaughan, D. J.; Craig, J. R. *Mineral Chemistry of Metal Sulfides*; Cambridge University Press: New York, 1978.
(214) Watson, J. H. P.; Cressey, B. A.; Roberts, A. P.; Ellwood, D. C.; Charnock, J. M.; Soper, A. K. *J. Magn. Magn. Mater.* **2000**, *214*, 13.
(215) Michel, F. M.; Antao, S. M.; Chupas, P. J.; Lee, P. L.; Parise, J. B.; Schoonen, M. A. A. *Chem. Mater*. **2005**, *17*, 6246.
(216) Rickard, D.; Griffith, A.; Oldroyd, A.; Butler, I. B.; Lopez-Capel, E.; Manning, D. A. C.; Apperley, D. C. *Chem. Geol.* **2006**, *235*, 286.
(217) Berner, R. A. *J. Geol.* **1962**, *72*, 293.
(218) Sweeney, R. E.; Kaplan, I. R. *Econ. Geol*. **1973**, *68*, 618.
(219) Ward, J. C. *Rev. Pure Appl. Chem.* **1970**, *175*, 175.
(220) Rickard, D. *Geochim. Cosmochim. Acta* **1995**, *59*, 4367.

(221) Kornicker, W. A. Interactions of divalent cations with pyrite and mackinawite in seawater and NaCl solutions, Ph.D. Dissertation Thesis, Texas A&M University, College Station, TX, 1988.
(222) Cornwell, J. C.; Morse, J. W. *Mar. Chem.* **1987**, *22*, 193.
(223) Allen, R. E.; Parkes, R. J. Digestion procedures for determining reduced sulfur species in bacterial cultures and in ancient and recent sediments. In *Geochemical Transformations of Sedimentary Sulfur*; Vairavamurthy, A.; Schoonen, M. A. A. Eds.; ACS Symposium Series 612; American Chemical Society: Washington, DC, 1995; pp 243−259.
(224) Polushkina, A. P.; Sidorenko, G. A. *Zap. Vseross. Mineral. O-va.* **1963**, *92*, 547 (in Russian).
(225) Berner, R. A. *Am. J. Sci.* **1967**, *265*, 773.
(226) Wolthers, M. *Geochemistry and environmental mineralogy of the iron−sulfur−arsenic system;* Geologica Ultraiectina: Utrecht, The Netherlands, 2003.
(227) Raiswell, R. *Am. J. Sci.* **1982**, *282*, 1244.
(228) Eigen, M.; Wilkins, R. G. *Mechanisms of Inorganic Reactions*; American Chemical Society: Washington, DC, 1965; p 55.
(229) Rickard, D. *Am. J. Sci.* **1974**, *274*, 941.
(230) Dos Santos, A.; Stumm, W. *Langmuir* **1992**, *8*, 1671.
(231) Pyzik, A. J.; Sommer, J. E. *Geochim. Cosmochim. Acta* **1981**, *45*, 687.
(232) Biber, M. V.; Dos Santos, A.; Stumm, W. *Geochim. Cosmochim. Acta* **1994**, *9*, 1999.
(233) Lovley, D. R.; Phillips, E. J. P. *Appl. Environ. Microbiol.* **1988**, *54*, 1472.
(234) Nealson, K. H.; Meyers, C. R. *Am. J. Sci.* **1990**, *290-A*, 34.
(235) Lovley, D. R. *Microbiol. Rev.* **1991**, *55*, 259.
(236) Lovley, D. R. *Annu. Rev. Microbiol.* **1993**, *47*, 263.
(237) Nealson, K. H.; Saffarini, D. *Annu. Rev. Microbiol.* **1994**, *48*, 311.
(238) Lovley, D. R. *Adv. Agron.* **1995**, *5*, 175.
(239) Lovley, D. R.; Anderson, R. T. *Hydrogeol. J.* **2000**, *8*, 77.
(240) Methe, B. A.; Nelson, K. E.; Eisen, J. A.; Paulsen, I. T.; Nelson, W.; Heidelberg, J. F.; Wu, D.; Wu, M.; Ward, N.; Beanan, M. J.; Dodson, R. J.; Madupu, R.; Brinkac, L. M.; Daugherty, S. C.; DeBoy, R. T.; Durkin, A. S.; Gwinn, M.; Kolonay, J. F.; Sullivan, S. A.; Haft, D. H.; Selengut, J.; Davidsen, T. M.; Zafar, N.; White, O.; Tran, B.; Romero, C.; Forberger, H. A.; Weidman, J.; Khouri, H.; Feldblyum, T. V.; Utterback, T. R.; Van Aken, S. E.; Lovley, D. R.; Fraser, C. M. *Science* **2003**, *302*, 1967.
(241) Kostka, J. E.; Stucki, J. W.; Nealson, K. H.; Wu, J. *Clays Clay Miner.* **1996**, *44*, 522.
(242) Kostka, J. E.; Haefele, E.; Viehweger, R.; Stucki, J. W. *Environ. Sci. Technol.* **1999**, *33*, 3127.
(243) Kostka, J. E.; Wu, J.; Nealson, K. H.; Stucki, J. W. *Geochim. Cosmochim. Acta* **1999**, *63*, 3705.
(244) Kostka, J. E.; Dalton, D. D.; Skelton, H.; Dollhopf, S.; Stucki, J. W. *Appl. Environ. Microbiol.* **2002**, *68*, 6256.
(245) Kostka, J. E.; Nealson, K. H. *Environ. Sci. Technol.* **1995**, *29*, 2535.
(246) Pankow, J. F.; Morgan, J. J. *Environ. Sci. Technol.* **1980**, *14*, 183.
(247) Rickard, D. T.; Sjöberg, L. *Am. J. Sci.* **1983**, *283*, 815.
(248) Skinner, B. J.; Erd, R. C.; Grimaldi, F. S. *Am. Mineral.* **1964**, *49*, 543.
(249) Doss, B. *Z. Prakt. Geol.* **1912**, *20*, 453.
(250) Ramdohr, P. *The Ore Minerals and their Intergrowths*; Pergamon: Oxford, U.K., 1969.
(251) Vaughan, D. J.; Tossell, J. A. *Am. Mineral.* **1981**, *66*, 1250.
(252) Yamaguchi, S.; Katsurai, T. *Kolloid Z.* **1960**, *170*, 147.
(253) Posfai, M.; Buseck, P. R.; Bazlinski, D. A.; Frankel, R. B. *Science* **1998**, *280*, 880.
(254) Spender, M. R.; Coey, J. M. D.; Morrish, A. H. *Can. J. Phys.* **1972**, *50*, 2313.
(255) Dekkers, M. J.; Passier, H. F.; Schoonen, M. A. A. *Geophys. J. Int.* **2000**, *141*, 809.
(256) Posfai, M.; Buseck, P. R.; Bazylinski, D. A.; Frankel, R. B. *Am. Mineral.* **1998**, *83*, 1469.
(257) Wada, H. *Bull. Chem. Soc. Jpn.* **1977**, *50*, 2615.
(258) Popa, R.; Kinkle B. K. *J. Microbiol. Methods* **2000**, *42*, 167.
(259) Ulrich, G. A.; Krumholz, L. R.; Suflita, J. M. *Appl. Environ. Microbiol.* **1997**, *63*, 1627.
(260) Fossing, H.; Jorgensen, B. B. *Biogeochemistry* **1989**, *8*, 205.
(261) Canfield, D. E.; Raiswell, R.; Westrich, J.; Reaves, C.; Berner, R. *Chem. Geol.* **1986**, *54*, 149.
(262) Neretin, L. N.; Böttcher, M. E.; Jørgensen, B. B.; Volkov, I. I.; Lüschen, H.; Hilgenfeldt, K. *Geochim. Cosmochim. Acta* **2004**, *68*, 2081.
(263) Zhabina, N. N.; Volkov, I. I. In *Environmental Biogeochemistry and Geomicrobiology, Vol. 3, Methods, Metals, and Assessment*; Krumbein, W. E., Ed.; Ann Arbor Science: Ann Arbor, MI, 1978.
(264) Lyons, T. W.; Werne, J. P.; Hollander, D. J.; Murray, R. W. *Chem. Geol.* **2003**, *195*, 131.
(265) Horiuchi, S. *Z. Anorg. Allg. Chem.* **1971**, *386*, 196.
(266) Uda, M. *Z. Anorg. Allg. Chem.* **1967**, *350*, 105.
(267) Taylor, P.; Rummery, T. E.; Owen, D. G. *J. Inorg. Nucl. Chem.* **1979**, *41*, 595.
(268) Yamaguchi, S.; Wada, H. *J. Colloid Interface Sci.* **1972**, *40*, 477.
(269) Freke, A. M.; Tate, D. J. *Biochem. Microbiol. Tech. Eng.* **1961**, *3*, 29.
(270) Rickard, D. *Stockholm Cont. Geol.* **1969**, *20*, 49.
(271) Boursiquot, S.; Mullet, M.; Abdelmoula, M.; Genin, J. M.; Ehrhardt, *J. Phys. Chem. Miner.* **2001**, *28*, 600.
(272) Watson, J. H. P.; Croudace, I. W.; Warwick, P. E.; James, P. A. B.; Charnock, J. M.; Ellwood, D.C. *Sep. Sci. Technol.* **2001**, *36*, 2571.
(273) Rickard, D.; Butler, I. B.; Oldroyd, A. *Earth Planet. Sci. Lett.* **2001**, *189*, 85.
(274) Horiuchi, S.; Wada, H.; Noguchi, T. *Naturwissenschaften* **1970**, *57*, 670.
(275) Horiuchi, S.; Wada, H.; Moori, T. *J. Cryst. Growth* **1974**, *25*, 624.
(276) Mullet, M.; Boursiquot, S.; Abdelmoula, M.; Genin, J. M.; Ehrhardt, J. J. *Geochim. Cosmochim. Acta* **2002**, *66*, 829.
(277) Bragg, W. L. *Proc. R. Soc.* **1914**, *A89*, 468.
(278) Hatchett, C. *Philos. Trans.* **1804**, *XXI1*, 63.
(279) Bakewell, R. *An Introduction to Geology*; J. Harding: London, 1815.
(280) Allen, E. T.; Crenshaw, J. L.; Johnson, J.; Larsen, E. S. *Am. J. Sci.* **1912**, *33*, 169.
(281) Sugawara, K.; Toyama, T.; Kozawa, A. *J. Earth Sci.* **1953**, *1*, 17.
(282) Sugawara, K.; Toyama, T.; Kozawa, A. *J. Earth Sci.* **1954**, *2*, 1.
(283) Berner, R. A. *J. Geol.* **1964**, *72*, 293.
(284) Berner, R. A. *Mar. Geol.* **1964**, *1*,117.
(285) Berner, R. A. *Am. J. Sci.* **1970**, *268*, 1.
(286) Guevremont, J. M.; Strongin, D. R.; Schoonen, M. A. A. *Am. Mineral.* **1998**, *83*, 1246.
(287) Wächtershäuser, G. *Microbiol. Rev.* **1988**, *52*, 452.
(288) Pontes-Buarque, M.; Tessis, A. C.; Bonapace, J. A. P.; Monte, M. B. M.; De Souza-Barros, F.; Vieyra, A. *An. Acad. Bras. Ciênc.* **2000**, *72*, 317.
(289) Bither, T. A.; Bouchard, R. J.; Cloud, W. H.; Donohue, P. C.; Siemons, W. J. *Inorg. Chem.* **1968**, *7*, 2208.
(290) Tossell, J. A.; Vaughan, D. J.; Burdett, J. K. *Phys. Chem. Miner.* **1981**, *7*, 177.
(291) Luther, G. W. *Geochim. Cosmochim. Acta* **1987**, *51*, 3193.
(292) Luther, G. W. The frontier-molecular-orbital theory approach in geochemical processes. In *Aquatic Chemical Kinetics*; Stumm, W., Ed.; Wiley: New York, 1990; pp 173−198.
(293) Kornicker, W. A.; Morse, J. W. *Geochim. Cosmochim. Acta* **1991**, *55*, 2159.
(294) Schoonen, M. A. A.; Xu, Y.; Bebie, J. *Origins Life Evol. Biosphere* **1999**, *29*, 5.
(295) Kullerud, G.; Yoder, H. S. *Econ. Geol.* **1959**, *54*, 533.
(296) Ellmer, K.; Hopfner, C. *Philos. Mag.* **1997**, *a.75*, 1129.
(297) Thomas, B.; Cibik, T.; Hopfner, C.; Diesner, K.; Ehlers, G.; Fiechter, S.; Ellmer, K. *J. Mater. Sci.* **1998**, *9*, 61.
(298) Agaev, Y.; Emujazov, K. *Izv. Akad. Nauk Turkm. SSR* **1963**, *F12*, 104. (in Russian)
(299) Oertel, J.; Ellmer, K.; Bohne, W.; Rohrich, J.; Tributsch, H. *J. Cryst. Growth* **1999**, *199*, 1205.
(300) Huerta-Diaz, M. A.; Morse, J. W. *Geochim. Cosmochim. Acta* **1992**, *56*, 2681.
(301) Robie, R. A.; Hemingway, B. S.; Fisher, J. R. *U.S. Geol. Surv. Bull.* **1978**, *1452*, 428.
(302) Grønvold, F.; Westrum, E. F., Jr. *Inorg. Chem.* **1962**, *1*, 36.
(303) Toulmin, P., III; Barton, P. B., Jr. *Geochim. Cosmochim. Acta* **1964** *28*, 1903.
(304) Stull, D. R.; Sixee, G. C. *Thermodynamic properties of the elements*; ACS Advances in Chemistry Series 8; American Chemical Society: Washington, DC, 1956.
(305) Nordstrom, D. K.; Munoz, J. L. *Geochemical Thermodynamics*; Blackwell Scientific Publications: Cambridge, MA, 1994.
(306) Harmandas, N. G.; Navarro Fernandez, E.; Koutsoukos, P. G. *Langmuir* **1998**, *14*, 1250.
(307) Butler, I. B.; Rickard, D. *Geochim. Cosmochim. Acta* **2000**, *64*, 2665.
(308) Berner, R. A. *Geochim. Cosmochim. Acta* **1963**, 27, 563.
(309) Rickard, D. *Am. J. Sci.* **1975**, *275*, 636.
(310) Wilkin, R. T.; Barnes, H. L. *Geochim. Cosmochim. Acta* **1996**, *60*, 4167.
(311) Luther, G. W. *Geochim. Cosmochim. Acta* **1991**, *55*, 2839.
(312) Farrand, M. *Miner. Deposita* **1970**, 5, 237.
(313) Roberts, W. M. B.; Walker, A. L.; Buchanan A. S. *Miner. Deposita* **1969**, *4*, 18.
(314) Lambert, I. B. *J. Geol. Soc. Aust.* **1973**, *20*, 205.
(315) Kribek, B. *Miner. Deposita* **1975**, *10*, 389.
(316) Berner, R. A. *Econ. Geol.* **1969**, 64, 383.
(317) Taylor, P.; Rummery, T. E.; Owen, D. G. *J. Inorg. Nucl. Chem.* **1979**, *41*, 1683.
(318) Jørgensen, B. B. *Limnol. Oceanogr.* **1977**, *22*, 814.

(319) Volkov, I. I. *Sulfur Geochemistry of Ocean Sediments* (in Russian); Nauka: Moscow, 1984.
(320) Boesen, C.; Postma, D. *Am. J. Sci*. **1988**, *288*, 575.
(321) Schoonen, M. A. A.; Barnes, H. L. *Geochim. Cosmochim. Acta* **1991**, *55*, 1505.
(322) Lyons, T. W. *Geochim. Cosmochim. Acta* **1997**, *61*, 3367.
(323) Hurtgen, M. T.; Lyons, T. W.; Ingall, E. D.; Cruse, A. M. *Am. J. Sci.* **1999**, *299*, 556.
(324) Aller, R. C. The influence of macrobenthos on chemical diagenesis of marine sediments, Ph.D. Dissertation Thesis; Yale, New Haven, CT, 1997.
(325) Lein, A. Y.; Sidorenko, G. A.; Volkov, I. I.; Shevchenko, A. Y. *Dokl. Akad. Nauk SSSR, Ser. Geol.* **1978**, *238*, 167.
(326) Bonev, I. K.; Khrischev, G.; Neikov, H. N.; Georgiev, V. M. *C. R. Acad. Bulg. Sci.* **1989**, *42*, 97.
(327) Persson, K.; Cedar, G.; Morgan, D. *Phys. Rev. B* **2006**, *73*, 115201.
(328) Schoonen, M. A. A.; Barnes, H. L. *Geochim. Cosmochim. Acta* **1991**, *55*, 1495.
(329) Rickard, D.; Grimes, S. L.; Butler, I. B.; Oldroyd, A. O.; Davies, K. L. *Chem. Geol*. **2007**, *36*, 228.
(330) Bunsen, R. *Ann. Chem. Pharm*. **1847**, *62*, 1.
(331) Van Bemmelen, J. M. *Verh. K. Ned. Akad. Wet., Afd. Natuurkd.* **1886**, *25*, 90.
(332) Hartler, N.; Libert, J.; Teder, A. *Ind. Eng. Chem*. **1967**, *4*, 398.
(333) Sjöberg, E. L.; Rickard, D. *Geochim. Cosmochim. Acta* **1983**, *47*, 2281.
(334) Butler, I. B.; Böttcher, M. E.; Rickard, D.; Oldroyd, A. *Earth Planet. Sci. Lett*. **2004**, *228*, 495.
(335) Berzelius, J. J. *Traité de Chimie. 2*; Didot: Paris, 1845.
(336) Wikjord, A. G.; Rummery, T. E.; Doern, F. E. *Can. Mineral*. **1976**, *14*, 571.
(337) Huber, C.; Wächtershäuser, G. *Science* **1997**, *276*, 245.
(338) Canfield, D. E.; Thamdrup, B.; Fleischer, S. *Limnol. Oceanogr*. **1998**, *43*, 253.
(339) Grimes, S. T.; Brock, F.; Rickard, D.; Davies, K. L.; Edwards, D.; Briggs, D. E. G.; Parkes, R. J. *Geology* **2001**, *29*, 123.
(340) de Médicis, R. *Rev. Chim. Miner*. **1970**, *7*, 723.
(341) de Médicis, R. *Science* **1970**, *170*, 1191.
(342) Takeno, S.; Zoka, H.; Niihara, T. *Am. Mineral.* **1970**, *55*, 1639.
(343) Shoesmith, D. W.; Taylor, P.; Bailey, M. G.; Owen, D. G. *Electrochem. Soc. J.* **1980**, *127*, 1007.
(344) Murowchick, J. B.; Barnes, H. L. *Am. Mineral.* **1986**, *71*, 1243.
(345) Luther, G. W., III; Theberge, S. M.; Rickard, D. *Geochim. Cosmochim. Acta* **1999**, *63*, 3159.
(346) Kobayashi, K.; Nomura, M. *Earth Planet. Sci. Lett*. **1972**, *16*, 200.
(347) Neal, A. L.; Techkarnjanaruk, S.; Dohnalkova, A.; McCready, D.; Peyton B. M.; Geesey, G. G. *Geochim. Cosmochim. Acta* **2001**, *65*, 223.
(348) Herbert, R. B.; Benner, S. G.; Pratt, A. R.; Blowes, D. W. *Chem. Geol*. **1998**, *144*, 87.
(349) Farina, M.; Esquivel, D. M. S.; Debarros, H. *Nature* **1990**, *343*, 256.
(350) Evans, H. T., Jr. *Science* **1970**, *167*, 621.
(351) Taylor, P. *Am. Mineral.* **1980**, *65*, 1026.
(352) Taylor, L. A.; Williams, K. L. *Am. Mineral.* **1972**, *57*, 1571.
(353) Erd, R. C.; Evans, H. T., Jr.; Richter, D. H. *Am. Mineral.* **1957**, *42*, 309.
(354) Fleet, M. E. *Phys. Chem. Miner*. **1982**, *8*, 241.
(355) Rickard, D. *Nature* **1968**, *218*, 356.
(356) Furukawa, Y.; Barnes, H. L. *Geochim. Cosmochim. Acta* **1996**, *60*, 3581.
(357) Schoonen, M. A. A.; Barnes, H. L. *Geochim. Cosmochim. Acta* **1991**, *55*, 1505.
(358) Murowchick, J. B.; Barnes, H. L. *Am. Mineral.* **1986**, *71*, 1243.
(359) Onufrienok, V. V. *Inorg. Mater.* **2005**, *41*, 650.
(360) Ritvo, G.; White, G. N.; Dixon, J. B. *Soil Sci. Soc. Am. J*. **2003**, *67*, 1303.
(361) Beinert, H.; Holm, R. H.; Münck, E. *Science* **1997**, *277*, 653.
(362) Rao, P. V.; Holm, R. H. *Chem. Rev.* **2004**, *104*, 527.
(363) Müller, A.; Schladerbeck, N. H.; Bögge, H. *J. Chem. Soc., Chem. Commun.* **1987**, 35.
(364) Hoyveda, H. R.; Holm, R. H. *Inorg. Chem.* **1997**, *36*, 4571.
(365) Stevens, W. C.; Kurtz, D. M., Jr. *Inorg. Chem.* **1985**, *24*, 3444.
(366) Wächtershäuser, G. *Appl. Microbiol*. **1988**, *10*, 207.
(367) Wächtershäuser, G. *Proc. Natl. Acad. Sci. U.S.A.* **1990**, *87*, 200.
(368) Wächtershäuser, G. *Proc. Natl. Acad. Sci. U.S.A.* **1994**, *91*, 4283.
(369) Drobner, E.; Huber, H.; Wächtershäuser, G.; Rose, D.; Stetter, K. O. *Nature* **1990**, *346*, 742.
(370) Blöchl, E.; Keller, M.; Wächtershäuser, G.; Stetter, K. O. *Proc. Natl. Acad. Sci. U.S.A.* **1991**, *89*, 8117.
(371) Keller, M.; Blöchl, E.; Wächtershäuser, G.; Stetter, K. O. *Nature* **1994**, *368*, 836.
(372) Russell, M. J.; Daniel, R. M.; Hall, A. J.; Sherringham, J. A. *J. Mol. Evol*. **1994**, 231.
(373) Russell, M. J.; Hall, A. J. *J. Geol. Soc., London* **1997**, *154*, 377.
(374) Russell, M. J.; Martin, W. *Trends Biochem. Sci.* **2004**, *29*, 358.
(375) Milner-White, E. J.; Russell, M. J. *Origins Life Evol. Biosphere* **2005**, *35*, 19.
(376) Compton, R. N.; Reinhardt, P. W.; Cooper, C. D. *J. Chem. Phys.* **1975**, *63*, 3821.
(377) Koppenol, W. H.; Rush, J. D. *J. Am. Chem. Soc.* **1987**, *91*, 4429.
(378) Morse, J. W.; Mackenzie, F. T. *Aquat. Geochem.* **1998**, *4*, 301.
(379) Holland, H. D. *The Chemical Evolution of the Atmosphere and Oceans*; Princeton University Press: Princeton, NJ, 1984.
(380) Heinen, W.; Lauwers, A. M. *Origins Life Evol. Biosphere* **1996**, *26*, 131.
(381) Huber, C.; Wächtershäuser, G. *Science* **1998**, *281*, 670.
(382) Cody, G. D. *Annu. Rev. Earth Planet. Sci.* **2004**, *32*, 569.
(383) Luther, G. W., III *Aquat. Geochem.* **2004**, *10*, 81.
(384) Keefe, A. D.; Miller, S. L.; McDonald, G.; Bada, J. *Proc. Natl. Acad. Sci. U.S.A.* **1995**, *92*, 11904.
(385) Baker, E. T.; Massoth, G. J.; Walker, S. L.; Embley, R. W. *Earth Planet. Sci. Lett.* **1993**, *118*, 235.
(386) Elderfield, H.; Schultz, A. *Annu. Rev. Earth Planet. Sci.* **1996**, *24*, 191.
(387) Schultz, A.; Elderfield, H. *Philos. Trans. R. Soc. London, Ser. A* **1997**, *355*, 387.
(388) Rickard, D.; Knott. R.; Duckworth, R.; Murton, B. *Mineral. Mag.* **1994**, *58A*, 774.
(389) Wächtershäuser, G. *Science* **2000**, *289*, 1307.
(390) Ugulava, N. B.; Gibney, B. R.; Jarrett, J. T. *Biogeochemistry* **2001**, *40*, 8343.
(391) Vladimirov, M. G.; Ryzhkov, Y. F.; Alekseev, V. A.; Bogdanovskaya, V. A.; Otroschchenko, V.A.; Kritsky, M. S. *Origins Life Evol. Biosphere* **2004**, *34*, 347.
(392) Cody, G. D.; Boctor, N. Z.; Filley, T. R.; Hazen, R. M.; Scott, J. H.; Sharma, A.; Yoder, H. S., Jr. *Science* **2000**, *289*, 1337.
(393) Huber, C.; Eisenreich, W.; Hecht, S.; Wächtershäuser, G. *Science* **2003**, *301*, 938.
(394) Filtness, M. J.; Butler, I. B.; Rickard, D. *Trans. Inst. Min. Metall., Sect. B* **2003**, *112*, 171.
(395) Rhodes, C.; Riddel, S. A.; West, J.; Williams, B. P.; Hutchings, G. J. *Catal. Today* **2000**, *59*, 443−464.
(396) Qui, D.; Kumar, M.; Ragsdale, S. W.; Spiro, T. G. *Science* **1994**, *264*, 817.
(397) Tezuka, M.; Yajima, T.; Tsuchiya, A. *J. Am. Chem. Soc.* **1982**, *104*, 6834.
(398) Williams, R. J. P.; Frausto da Silva, J. J. R. *The Natural Selection of the Chemical Elements*; Clarendon Press: Oxford, U.K., 1996.

CR0503658